Using pharmacokinetic and pharmacodynamic techniques to optimize dosing of antifungal agents for serious and life-threatening fungal infections

Thesis submitted in accordance with the requirements of the University of Liverpool for the degree of Doctor of Philosophy.

21 July 2017

Laura L. Kovanda

Prelude

Statement of the originality of the work

The work presented in this thesis is my original work. I am extremely grateful for the support and contributions of many of my colleagues around the world that made this work possible. Below I have included the specific contributors for each chapter.

Chapter 3. The rabbit model of invasive pulmonary aspergillosis was designed and conducted by Thomas Walsh, Vidmantas Petraitis, Ruta Petraitiene at Weill Cornell University. The original mathematical model was developed by William Hope. Dr Hope also assisted in the model fitting process and interpretation.

Chapter 4. The clinical trial data was provided by Astellas Pharma Global Development, Inc. The design and concept of the analysis was provided by William Hope. The statistical modeling of the galactomannan data was conducted by Ruwanthi Kolamunnage-Dona. The PK-PD linked mathematical modeling and concept of AUC:EC_{50} was conceptualized and developed by William Hope and Michael Neely. Preparation and interpretation of the results was supported by the co-authors Johan Maertens and Misun Lee.

Chapter 5. The clinical trial data was provided by Astellas Pharma Global Development, Inc. William Hope, Peter Bonate, and Amit Desai guided and assisted in the PPK model development and fitting process. Assistance in the statistical analysis and interpretation was supported by Qiaoyang Lu.

Chapter 6. The clinical trial data was provided by Astellas Pharma Global Development, Inc. Preparation of the model and fitting process was guided and supported by William Hope, Amit Desai, and Peter Bonate. Design of the study and choice of population for analysis and interpretation of results was prepared with contributions from William Hope, Johan Maertens, Francisco Marty, Amit Desai, Christopher Lademacher, and Qiaoyang Lu.

Chapter 7. The clinical trial data was provided by Astellas Pharma Global Development, Inc. Model development and fitting process was directed and supported by William Hope, Peter Bonate, and Amit Desai. Statistical support for the logistic regression was assisted by Amit Desai. Evaluation of the data and interpretation was supported by William Hope, Peter Bonate, Amit Desai, Daniel K. Benjamin, Jr, Antonio Arrieta, David A. Kauffman, P. Brian Smith, Paolo Manzoni, Thomas J. Walsh, and Atsunori Kaibara.

Chapter 8. The clinical trial data was provided by Vical, Inc. Model development and fitting process was guided and supported by William Hope and Pete Bonate. Evaluation of the data and preparation of the analysis was supported by Amit Desai. Conduct and oversight of the study was conducted by Larry Smith, Sean Sullivan, Andrew Hopkins, and other representatives of Vical, Inc.

Signed,

Laura Lynn Kovanda William W. Hope, BMBS, FRACP, FRCPA, PhD

Acknowledgments

It has always been my passion and desire to further my education and career. Just a few short years ago, I would not have believed this momentous day would arrive. My sincere thanks and gratitude go out to the many very talented people that supported and guided me along my journey. I could not have completed this goal without the help, guidance, and support from everyone. The list is long but at the top is William Hope (University of Liverpool). I will always be grateful for the mentorship and confidence he has had in my abilities and I will be forever indebted to William for giving me this unforgettable opportunity. Pete Bonate (Astellas) always opened his doors to help me with my myriad of questions, both big and small. Never missing an opportunity to guide and mentor me through this complex world of PK-PD. Amit Desai (Astellas) was always available to provide support and guidance. Michael Neely (University of Southern California) provided invaluable support and expertise to me along the way.

I am also extremely grateful to Astellas for the financial and overwhelming support for my education. In addition, I would like to acknowledge all of the support from my colleagues and friends at Astellas and the Antimicrobial Pharmacodynamics and Therapeutics at the University of Liverpool.

A special thank you to my mother, Margaret Anne Minneci, sisters, Beth, Amy and Meg, and brother Ross. I love you all and appreciate all you have done to support me throughout my life. Finally, my husband and best friend, Greg. I appreciate your sense of humor and joy of life. You are a great father, husband, and friend. I love you with all my heart. Thank you for supporting me through this process and taking on so much. To my

children, Jake and Nick, I am proud of the men you are becoming. Always remember that nothing worthwhile comes easy. Never stop believing in yourself and always follow your heart and your dreams!

Presentations and Publications of the Related Work

Relevant to the thesis

1. **Kovanda LL**, Desai AV, Hope WW. Prognostic value of galactomannan: current evidence for monitoring response to antifungal therapy in patients with invasive aspergillosis. J Pharmacokinet Pharmacodyn. 2017 Feb 8. doi: 10.1007/s10928-017-9509-1. [Epub ahead of print] Review. PMID: 28181136
2. **Kovanda LL**, Desai AV, Lu Q, Townsend RW, Akhtar S, Bonate P, Hope WW. Isavuconazole Population Pharmacokinetic Analysis Using Nonparametric Estimation in Patients with Invasive Fungal Disease (Results from the VITAL Study). Antimicrob Agents Chemother. 2016 Jul 22;60(8):4568-76. doi: 10.1128/AAC.00514-16. PMID: 27185799 (**Chapter 5**)
3. **Kovanda LL**, Maher R, Hope WW. Isavuconazonium sulfate: a new agent for the treatment of invasive aspergillosis and invasive mucormycosis. Expert Rev Clin Pharmacol. 2016 Jul;9(7):887-97. doi: 10.1080/17512433.2016.1185361. PMID: 27160418
4. **Kovanda LL**, Petraitiene R, Petraitis V, Walsh TJ, Desai A, Bonate P, Hope WW. Pharmacodynamics of isavuconazole in experimental invasive pulmonary aspergillosis: implications for clinical breakpoints. J Antimicrob Chemother. 2016 Jul;71(7):1885-91. doi: 10.1093/jac/dkw098. PMID: 27084921 (**Chapter 3**)
5. **Kovanda LL**, Marty FM, Maertens J, Desai AV, Lademacher C, Engelhardt M, Lu Q, Hope WW. The Impact of Mucositis on Absorption and Systemic Drug Exposure of Isavuconazole. Antimicrob Agents Chemother. 2017 Mar 13. pii: AAC.00101-17. doi: 10.1128/AAC.00101-17 (**Chapter 6**)
6. **Kovanda, LL**, Walsh, TJ, Benjamin, Jr, DK, Arrieta, A, Kaufman, DA, Smith, PB, Manzoni, P, Desai, AV, Kaibara, A, Bonate, PL, Hope, WW. Exposure-Response Analysis of

Micafungin in Neonatal Candidiasis: Pooled analysis of two clinical trials. *Submitted PIDJ, provisionally accepted pending revisions. Revisions submitted 13Jul2017.*

7. Wiederhold NP, **Kovanda L**, Najvar LK, Bocanegra R, Olivo M, Kirkpatrick WR, Patterson TF. Isavuconazole Is Effective for the Treatment of Experimental Cryptococcal Meningitis. Antimicrob Agents Chemother. 2016 Aug 22;60(9):5600-3. doi: 10.1128/AAC.00229-16. PMID: 27324761

Relevant but not for evaluation

1. Desai A, **Kovanda L**, Kowalski D, Lu Q, Townsend R, Bonate PL. Population Pharmacokinetics of Isavuconazole from Phase 1 and Phase 3 (SECURE) Trials in Adults and Target Attainment in Patients with Invasive Infections Due to Aspergillus and Other Filamentous Fungi. Antimicrob Agents Chemother. 2016 Aug 22;60(9):5483-91. doi: 10.1128/AAC.02819-15. PMID: 27381396
2. Petraitis V, Petraitiene R, Moradi PW, Strauss GE, Katragkou A, **Kovanda LL**, Hope WW, Walsh TJ. Pharmacokinetics and Concentration-Dependent Efficacy of Isavuconazole for Treatment of Experimental Invasive Pulmonary Aspergillosis. Antimicrob Agents Chemother. 2016 Apr 22;60(5):2718-26. doi: 10.1128/AAC.02665-15. PMID: 26883703
3. Yamazaki T, Desai A, Han D, Kato K, Kowalski D, Akhtar S, Lademacher C, **Kovanda L**, Townsend R. Pharmacokinetic Interaction Between Isavuconazole and a Fixed-Dose Combination of Lopinavir 400 mg/Ritonavir 100 mg in Healthy Subjects. Clin Pharmacol Drug Dev. 2017 Jan;6(1):93-101. doi: 10.1002/cpdd.282.
4. Andes DR, Reynolds DK, Van Wart SA, Lepak AJ, **Kovanda LL**, Bhavnani SM. Clinical pharmacodynamic index identification for micafungin in esophageal candidiasis: dosing strategy optimization. Antimicrob Agents Chemother. 2013 Nov;57(11):5714-6. doi: 10.1128/AAC.01057-13. PMID: 23959319

Thesis Overview

The aim of this thesis is to describe how the use of pharmacokinetic and pharmacodynamic techniques can provide a better understanding of the optimal use of antimicrobial agents. *In vivo* animal experimental models and clinical PK-PD datasets for three systemically administered antifungal agents, isavuconazonium sulfate (active moiety isavuconazole), micafungin, and VL-2397, are used to accomplish this goal.

Table of Contents

List of Tables

List of Figures

List of Equations

Glossary

ACM	all-cause mortality
ACN	acetonitrile
ALL	acute lymphocytic leukemia
AML	acute myeloid leukemia
AUC	area under the concentration-time curve
BAL	bronchoalveolar lavage
BDG	1,3-β-D-glucan assay
BMI	body mass index
CF	cystic fibrosis
CFU	colony forming units
CHMP	Committee for Medicinal Products and Human Use
CI	confidence interval
CL	clearance
CLSI	Clinical Laboratory Standards Institute
COPD	chronic obstructive pulmonary disease

Cmin	minimum concentration
CMV	cytomegalovirus
CNS	central nervous system
CSF	cerebral spinal fluid
%CV	coefficient of variation
DMSO	dimethyl sulfoxide
DNA	deoxyribonucleic acid
DRC	Data Review Committee
EC_{50}	amount of drug required for half maximal effect
eGFR	estimated glomerular filtration rate
ELISA	enzyme-linked immunosorbent assay
ECV (ECOFF)	epidemiological cut-off value
EMA	European Medicines Agency
EORTC/MSG	European Organization for Research and Treatment of Cancer/Mycoses Study Group
EOT	end of therapy
F	oral bioavailability

FDA	Food and Drug Association
GI	gastrointestinal
GM	galactomannan
GMI	galactomannan index
GVHD	graft versus host disease
HCME	hematogenous *Candida* meningoencephalitis
HPLC	high performance liquid chromatography
HR	hazard ratio
HSCT	hematopoietic stem cell transplantation
IA	invasive aspergillosis
IC	invasive candidiasis
IFD	invasive fungal disease
IgM	immunoglobulin M
IM	invasive mucormycosis
IMD	invasive mould disease
IPA	invasive pulmonary aspergillosis

ISAV	isavuconazole
ITT	intent to treat
i.v.	intravenous
kDa	kilo Daltons
LC/MS/MS	liquid chromatography/mass spectrometry/mass spectrometry
LLOQ	lower limit of quantification
MAD	multiple ascending dose
MDRD	modification of diet in renal disease
MIC	minimum inhibitory concentration
mITT	modified intent to treat
MOA	mechanism of action
ng/mL	nanogram per milliliter
NIH	National Institute of Health
OD	optical density
OR	odds ratio
PCR	polymerase chain reaction

PD	pharmacodynamic
PK	pharmacokinetic
p.o.	per os; oral administration of medication
PPK	population pharmacokinetics
PTA	probability of target attainment
QC	quality control
rDNA	ribosomal deoxyribonucleic acid
SAD	single ascending dose
SD	standard deviation
TFA	trifluoracetate
V	volume in the central compartment
VOC	volatile organic compound
WT	wild-type

Chapter 1 Introduction

Pharmacokinetic (PK)-pharmacodynamic (PD) experiments in the development of the antimicrobial therapy

Pharmacokinetic (PK)-pharmacodynamic (PD) techniques have been developed to answer important questions regarding the proper use of drug therapies. The techniques offer opportunities to optimize the use of antimicrobial compounds. The field continues to broaden providing an enhanced understanding of the amount and duration of a specific compound required to treat an infection. PK-PD is used to increase the likelihood of better patient outcomes, decrease resistance development, and minimize the risk for antibiotic drug development programs because of the better optimization of regimens.

The intrinsic factors that play a role in the ability of a drug to affect an invading pathogen, and ultimately patient outcomes include the dose, duration of therapy, ability of the drug to reach infected tissues, and the mechanism of action (1). Host factors (e.g. immune status) are also significant but independent factors. PK-PD experimental techniques operate by illustrating important relationships between how the body affects the drug (PK) in correlation with how the drug affects the target pathogen (PD).

Regulatory authorities increasingly recognize the importance of PK-PD techniques and require these data are included in marketing applications. As recent as July 2016, the EMA issued the "Guideline on the use of pharmacokinetics and pharmacodynamics in the development of antimicrobial medicinal products" (EMA/CHMP/594085/2015) (http://www.ema.europa.eu/docs/en_GB/document_library/Scientific_guideline/2016/07/WC500210982.pdf). This guidance outlines important deliverables for the applicant

related to PK-PD data. Specifically, the guidance describes the microbiology data required, the need to identify the PD indices and PD targets, the clinical PK data recommended to support the PK-PD analysis, the probability of target attainment (PTA) analysis to support the dosage regimen, and exposure-response analyses. Importantly, the guidance describes the extent to which results from PK-PD analyses can replace clinical data. The FDA does not have guidance that addresses these more contemporary PK-PD issues, although the NIH is seeking to understand these issues further [NIH workshop in June 2017].

Importance of in vivo and in vitro experimental models. Traditionally, experimental models using laboratory animals that mimic human disease have been used to characterize pharmacological efficacy and safety prior to clinical use. In antimicrobial drug development, these experiments have been shown to be highly predictive of the human disease and efficacy (2). These experimental models have brought forth an increasing ability to further explore exposure-response relationships for many drug-bug combinations, specifically, detailing the time-course of drug exposure, penetration of drug to the site of infection and the ultimate antimicrobial effect (1).

More recently, *in vitro* dynamic experimental models such as hollow fiber used primarily for antibacterial work or in vitro dynamic models used for pulmonary infections caused by filamentous fungi have furthered our ability to explore larger dose ranges and a more diverse spectrum of organisms including resistance organisms (3, 4). Treatment of infections caused by *Aspergillus* spp. and rare filamentous fungi, treatment of infections in rare populations with distinct pathogenesis (e.g. neonatal candidiasis) and in difficult to penetrate body sites (e.g. CNS) are difficult to study in clinical trials. A detailed

understanding of exposure-response relationships bolsters the selection of dosage regimens that are safe and effective and increases the likelihood of studying the optimal dose initially. Further, PK-PD data better inform and provide the basis for treatment and prevention of antimicrobial resistance, determination of the requirement for therapeutic drug monitoring, and decision support for establishing in vitro susceptibility breakpoints.

Using Biomarkers in PK-PD: Use of Galactomannan as Prognostic Tool in Invasive Aspergillosis

Invasive aspergillosis (IA) causes significant morbidity and mortality (5, 6). Treatment is complicated by the limited number of antifungal classes and agents, antifungal drug toxicity, an incomplete spectrum of antifungal activity, and increasing incidence of antifungal resistance (7-11). Patient management is complicated. The diagnosis is not always confirmed, which delays treatment, and treatment duration is guided subjectively without information on appropriate duration of therapy. Bedside assessment of response is tough. Lack of specificity in the clinical signs and symptoms, variability in the radiological exams during treatment, which makes the assessment hazy, and clinical response to therapy occurs over weeks-to-months. Ideally, a tool that could be used at the bedside or in a more objective manner to follow response would significantly improve the routine care of patients with IA. In addition, such a tool would significantly enhance the outcome assessment, duration, and cost of clinical trials of new antifungal drugs. The biomarker such as galactomannan (GM) may be an important way clinical trials for invasive aspergillosis can be expedited.

Galactomannan is a polysaccharide present in the cell wall of *Aspergillus* spp., and some other fungi (12). It is released by hyphae, which are the biologically invasive forms

of filamentous moulds. A commercial double-sandwich enzyme-linked immunosorbent galactomannan assay (ELISA) is available to detect *Aspergillus* GM antigen in body fluids. The assay uses a monoclonal IgM obtained from rats following challenge with mycelial extracts from *Aspergillus* spp. (12, 13). It has been successfully used to aide in the speed and accuracy diagnosis of invasive aspergillosis (IA) allowing for earlier recognition of disease compared to conventional methods. Since its implementation in the clinic as a diagnostic tool, GM has been used in experimental models to measure therapeutic response (14-16). Several clinical studies describe the prognostic value of GM (17). A decline in GM or GM negativity has been linked to clinical outcomes, eg, survival or successful clinical response, was reported to correlate in patients that do well (18-21).

Structure and biology of galactomannan. The polysaccharide cell wall component of GM has a branched structure with a linear α mannan that has a repeating mannose oligosaccharide unit [6Manα1-2Manα1-2Manα1-2Manα1] and short chains of β (1,5) galactofuranose residues (12). It is released from fungal hyphae during growth in the extracellular material (i.e. ethanol-precipitable material) as part of the chemical breakdown in the cell as the hyphae grow (i.e. a metabolic event) and not a result of mycelial lysis. Organisms that are known to release GM include *Aspergillus* spp., *Fusarium* spp., *Scedosporium* spp., *Alternaria* spp., *Histoplasma* spp. and *Penicillium* spp. (22-26). GM can be detected in serum and other bodily fluids such as bronchoalveolar lavage (BAL) and cerebrospinal fluid (CSF), and has been used to support a diagnosis of IPA and cerebral aspergillosis, respectively. There are no established cut-offs values for GM from matrices outside of the serum.

Aspergillus releases GM as part of recycling process of the cell wall during hyphal growth. GM measurement is achieved by using sandwich enzyme-linked immunosorbent assay (ELISA), which detects galactomannan antigen via binding to monoclonal antibody and the formation of a monoclonal antibody-galactomannan-monoclonal antibody/peroxidase complex. A spectrophotometer is used to determine the absorbance (optical density; OD) of the samples. Serum samples are considered positive when the GMI (OD) is ≥ 0.5 and negative when < 0.5. GMI has no units and if expressed as a ratio of the OD value of the sample to the OD value of a standard sample containing 1 ng of GM. The test has a lower limit of detection of 1 ng/mL. GM is utilized primarily as a diagnostic test; however, evidence is increasing for its value as a prognostic test.

Relevance of GM in the pathogenesis of IA. The release of GM correlates with the progression of disease and its resolution in experimental models of IA (4). Clear trends are seen when an infection responds to effective therapy. Levels of GM in the serum correspond to the timing of tissue invasion and are an integral measure of the mass of viable invading organisms. GM can be detected as early as 12 hours post inoculation, which corresponds with hyphal invasion as determined using histopathological techniques (4, 27). Serum GM levels continue to increase and eventually reach a plateau as the ELISA assay is saturated and/or there is capacity limitation of fungal growth following exhaustion of available nutrients. BAL GM concentrations are typically high throughout the course of infection in experimental models. Presumably this reflects hyphal growth in the airways and does not necessarily imply invasion. The presence of GM implies the presence of hyphae rather than conidia (the latter do not liberate GM) and in this sense GM provides slightly different information than culture and PCR from

samples from the airways, which may not necessarily distinguish the different fungal morphotypes.

The discordant kinetic profiles of GM in serum and BAL suggest that the GM does not transverse the alveolar-capillary bilayer or other biological barriers to any great extent. Presumably its molecular weight (~20 kDa) (12) prevent transgression even in the context of significant tissue disruption. The appearance of GM in the circulation therefore represents angioinvasion rather than simple diffusion into the bloodstream from contiguous areas of infection.

Early *in vivo* studies suggest that the major pathway for *Aspergillus* GM clearance from the bloodstream is renal excretion and hepatic metabolism based on uptake by macrophage mannose receptors (28). The majority of the renal excretion is rapid, within the first 24 hours. Detection of GM in the urine of patients with IA has been reported (29).

GM is a Complementary Measure of Fungal Burden in Experimental Models of IA. The traditional measure of tissue burden obtained by plating serial dilutions of tissue homogenates to agar does not (in general) provide a useful measure of fungal burden. There are several reasons for this. In some experimental models, sampling at early time-points may not enable conidia (environmental forms) that are used to initiate infection to be distinguished from hyphae (tissue invasive forms). Detection of both morphotypes leads to a positive culture or PCR signal and quantification of fungal burden even though it is only hyphae that are biologically relevant in this situation. An accurate quantification of fungal burden is further complicated by the growth patterns of

Aspergillus, which extends via hyphal elongation with indistinguishable cellular units and additional branching from older and newer segments (30). Tissue homogenization and quantitative counts do not enable an accurate estimate of the fungal biomass. Propagules are either incompletely separated or more vigorous grinding leads to complete hyphal disruption and subsequent fungal death. In either situation $\log_{10}$CFU/g is an inaccurate reflection of the underlying fungal biomass and neither reflects important events in the pathogenesis nor response to antifungal therapy.

Despite these potential limitations, fungal burden ($\log_{10}$CFU/g) from the rabbit model provides a crude, but reliable readout to assess a variety of antifungal agents (with the possible exception of the echinocandins). In this model sampling occurs late in the treatment period and is probably not confounded by the presence of conidia. In other model systems, $\log_{10}$CFU/g is completely non-informative. In any context $\log_{10}$CFU/g is often too imprecise to construct detailed dose-exposure-response relationships.

Other non-culture techniques used to estimate fungal burden in experimental models after infection with *Aspergillus* spp. include polymerase chain reaction (PCR) to measure of the amount of fungal DNA in tissues, or assays that measure the amount of fungal cell wall components such as chitin and 1,3-β-D-glucan. Each method has advantages and limitations (see **Table 1)**.

Table 1 Comparison of Experimental Techniques to Measure *Aspergillus* fungal burden

Method	Description	Advantage	Disadvantage
CFU	Counting of single organisms by plating of serial dilutions of a suspension; using a hemacytometer	Simple, inexpensive	Homogenisation by mechanical dispersion can disrupt the count by breaking the hyphae into smaller pieces causing either fewer viable fragments or increase in viable units
Chitin-assay	Measure of the amount of chitin by KOH extraction and colorimetric assay of an aldehyde derivative of chitosan	Measuring content in hyphae not conidia since chitin is not present in conidia	Does not distinguish between viable and non-viable hyphae, nor viable but ungerminated conidia can go undetected.
PCR	Measure either 18S rDNA (present in the genome in 100 per nucleus) or *FKS1*, single-copy gene	Better accuracy than CFU depending on the tissue especially in the first few days after inoculation	Does not distinguish between viable and non-viable organisms. Use of 18S rDNA can over-estimate fungal burden given the multinucleic nature of *Aspergillus* spp. High cost, complex
Lateral-Flow	Detects the presence of *Aspergillus*-	Rapid detection of the presence *Aspergillus* spp. within	No quantitative details of the amount

Device	specific MAb (JF5) (31)	an immune-chromatographic lateral-flow device. Measure of growing *Aspergillus*	of organisms
Electronic nose	Detects volatile organic compounds (VOCs) using an "electronic nose" which is an artificial olfactory system to discriminate odors using an array of sensors. (32)	Rapid detection of presence of *Aspergillus* spp. in the airways	No quantitative details of the amount of organisms Only pertinent to pulmonary infection

Abbreviations: CFU: colony-forming units; KOH: potassium hydroxide; PCR: polymerase chain reaction; rDNA: recombinant deoxyribonucleic acid

GM and Experimental Pharmacodynamics. GM is increasingly used in pharmacodynamic models of IA to estimate dose-exposure-response relationships. The advantages of this biomarker include a rapid response to antifungal therapy, the fact it is readily quantifiable, the availability of a commercial kit and validation in a variety of model systems. The disadvantages include a relatively narrow dynamic range, relatively high expense, and large inherent variability.

GM as a Clinical Biomarker with Prognostic Value. Clinical evidence supporting the utility of GM as a prognostic tool for patients with IA has steadily accrued over the past two decades. The earliest suggestion that GM might be a valuable biomarker for measuring therapeutic response in patients was established in 1997. However, the general utility of exploiting the prognostic value of GM was initially limited by the relatively high number of false positive results (33). Early case reports describe increasing GMI during treatment in individual patients with poor outcomes. (34-36).

Evidence of GM's Prognostic Value from Case Series and Clinical Studies. The first clinical study conducted early in the use of GM was limited by sparse sampling. However, a trend of increasing GM in patients that subsequently died was evident (33). Subsequently, nine separate studies representing 661 patients and one meta-analysis covering 27 studies and 257 patients that evaluated the utility of GM assay to monitor therapeutic response have been reported. Eight studies largely focused on patients with hematological malignancy, while one included patients with COPD. The studies evaluate responses in patients with proven, probable, possible, or suspected invasive aspergillosis and one study included patients with invasive fusariosis. One study assesses the use of serial GM in pediatric patients and the associated exposure-response relationship. Each

study demonstrates the potential usefulness of serial GM measurements in IA patients by showing that GM generally increases (or does not decline) in patients that fail treatment or ultimately die.

Correlation with traditional measures of response to therapy. Changes in GMI from the time of diagnosis or baseline correlate significantly with various outcome measures including clinical outcome defined by EORTC/MSG criteria at 6 and 12 weeks, mortality at 12 weeks, and with autopsy findings (18-21). The GMI-based outcome proposed from these correlations is defined as GMI negativity (OD < 0.5) for at least 2 weeks after the first positive value without new pulmonary or extra-pulmonary lesions and lack of findings of IA on autopsy (18, 21).

GMI-based outcome criteria. Several outcome measures for GM are possible and include time to GMI negativity, time to a certain percent reduction in GMI, rate of decline (or GM decay), area under the GMI time curve, or time to negativity. However, with these possibilities, a degree or quantification of GMI change aside from negativity has yet to be defined. The only criterion that is currently used is GMI negativity (OD < 0.5) for a period of 2-weeks without pulmonary or extra-pulmonary lesions. An autopsy may be necessary to definitively exclude IA. While this GM outcome provides excellent correlation to clinical measures of response, the average time to negativity in one study was 21 days in patients who ultimately responded to antifungal therapy. An earlier intervention may be preferable (18). The rate of decline of GM (i.e. slope) at 1 week after diagnosis of IA has also been proposed as a surrogate for clinical outcome (i.e. for 6- and 12-week all-cause mortality) based on increasing hazard ratios with each unit increase from diagnosis (37). This GM outcome measure is more practical than the GM outcome

of negativity for 2 weeks duration as it utilizes an early time point and relatively simple calculation to guide response.

Significant increases in GM after each week of therapy are associated with ultimate treatment failure (38-40). Most studies report a strong correlation of survival with decreases GMI (e.g. GMI normalization to readings <0.5) (19, 21). However, at least one study reports that changes from baseline to week 2 are not predictive of 12-week survival (39). The reason is most likely because mortality by 12 weeks is more often driven by underlying co-morbidities as opposed to the fungal infection.

Other fungal biomarkers, such as, the 1,3-β-D-glucan (BDG) assay (Fungitell™), are used in the clinic. BDG detects the cell wall component, (1,3)-β-D-glucan, which is present in most fungi, and therefore, not specific to *Aspergillus* spp. This assay could potentially be used in conjunction with GM as a prognostic tool after IA is diagnosed. However, there is little data available showing correlation to clinical outcome outside of experimental models (27, 41). One study suggests that decline in the mean time-weighted averages of BDG plus GM from baseline to week 2 of therapy is associated with 6-and 12-week survival (40).

Using GM to individualize antifungal therapy. The time course of GM in an individual patient may be affected by antifungal drug exposure (pharmacokinetics), the MIC of the invading fungal pathogen, the immune status of the host, and the underlying high fungal burden (pharmacodynamics). Therapeutic drug monitoring of antifungal agents has traditionally focused on achieving plasma drug exposure targets. The pharmacodynamic responses to antifungal therapy have typically been less formal.

However, GM can potentially be used to guide antifungal therapy at an individual level. The time course of GM may provide a guide as to the intensity of antifungal therapy that is required to achieve a favorable clinical outcome. Patients with high unremitting GM concentrations receiving a standard antifungal regimen should have the dosage increased, the drug changed or a combination of agents used. The necessary mathematical models that explicitly link dosage, plasma drug concentrations and circulating GM provide a way that therapy can be individualized to move the biomarker rather than merely achieving a target plasma concentration, which may not be optimal for the patient.

A further possibility that is enabled by GM is an estimate of the pharmacodynamic targets required for a successful outcome. Traditionally, this pharmacodynamic measure has been the MIC and drug exposure (e.g. AUC) has been optimized with reference to this in vitro measure of potency. A common problem in clinical mycology is that the organism (and therefore the MIC) is not available- it is quite uncommon for patients to have positive cultures. The use of linked PK-PD models with GM as a real-time pharmacodynamic readout provides alternative measures of in vivo potency that can be used to optimize drug exposure. The EC_{50} is the concentration of antifungal drug that is required to induce half maximal antifungal activity. The AUC can be optimized in relation to the EC_{50} to secure a favorable outcome. This idea was explored in a recent relatively small study in pediatric patients receiving voriconazole (42). In these children, an $(AUC:EC_{50})/15.4$ is significantly associated with terminal GMI (GMI value at the end of therapy). When the ratio is > 6, the terminal GM tends to be lower. However, survival did not correlate with the $AUC:EC_{50}$. Further work is ongoing in this area.

PPK Models Can Be Used to Enhance Understanding of PK in Different Populations and Disease States

Rarely when an antimicrobial agent is initially brought to market are the PK data vast enough to understand all possible scenarios, such as those potentially impacting exposures for different infection types ad sites of infection, underlying diseases, and specific patient conditions such as obesity and gastro-intestinal disruption (mucositis). The data that is available focuses on the primary patient population for the initial labeled indications. Therefore, population PK modeling can be used to explore factors impacting exposure in these different populations and explore the PD impact as well.

Isavuconazole

Isavuconazonium sulfate is the water-soluble prodrug of the triazole antifungal agent isavuconazole and is available in cyclodextrin-free intravenous (i.v.) and oral (p.o.) formulations (43). The pharmacokinetics have been characterized from sub-studies embedded in clinical trials (44-47). Many of the pharmacokinetic (PK) analyses initially reported are limited to healthy volunteers and patients treated for IA. There is a paucity of data regarding the population pharmacokinetics (PPK) in patients with a variety of invasive fungal infections, clinical conditions, and underlying diseases. The pivotal clinical trials included more than 400 patients with >60% with hematological malignancies or other conditions that required intensive chemotherapy and the potential for conditions such as mucositis (48, 49). In one of the registration clinical trials, VITAL, the efficacy and safety of isavuconazole was evaluated for treatment of a variety of invasive fungal diseases (IFD), including the treatment of IA in patients with renal impairment and treatment of patients with diseases caused by emerging moulds, yeasts, and dimorphic fungi.

In vitro data for isavuconazole have demonstrated broad-spectrum activity against a variety of fungi, including *Aspergillus* spp., *Candida* spp., Mucorales, *Cryptococcus* spp., and dimorphic and other rare fungi (50). Concentration-dependent antifungal activity has been demonstrated for infections caused by *Aspergillus* spp., *Candida* spp., organisms of the Mucorales order, and *Cryptococcus* spp. (15, 51-54). Isavuconazole demonstrated successful outcomes for patients with IA and IM, with all-cause mortality rates through day 42 of 12.5% and 37.8%, respectively, for these patients. Successful outcomes have also been reported for patients with IA and renal impairment, and for patients with infections caused by *Cryptococcus* spp., dimorphic fungi (such as *Coccidioides* spp., and *Paracoccidioides* spp.), *Fusarium* spp., and *Scedosporium* spp. (49, 55-59). The pharmacokinetics of isavuconazole in these various populations require further characterization to ensure appropriate exposures across different infections, disease types, and specific patient characteristics, such as mucositis.

Micafungin

Another challenging scenario is neonatal candidiasis that represents a disease state with significant morbidity and mortality in premature neonates and infants (60-62). The associated mortality with invasive candidiasis (IC) is three-times higher than that of uninfected infants of similar gestational age and birth weight (63). The disease is characterized by involvement of the central nervous system (CNS), leading to poor subsequent neurodevelopmental outcomes. The specific disease features dictate scrupulous evaluation in the selection of safe and effective antifungal regimens (64-66).

Micafungin plays a significant role in the treatment of IC in both adults and children based on extensive efficacy and safety database (67). It has broad-spectrum anti-*Candida*

coverage and a favorable safety profile (68, 69). To establish the efficacious exposure of micafungin in CNS infections caused by *Candida* spp., micafungin was studied in a well-characterized experimental model of hematogenous *Candida* meningoencephalitis (HCME) (70). PK-PD bridging studies suggest that a neonatal regimen of 10 mg/kg is required for effective treatment of *Candida* infections in the CNS (70-72). These studies were used to justify the choice of this high dose regimen for treatment of neonates with IC. Because of the intrinsic difficulties in conducting neonatal trials and the decrease in the incidence of neonatal candidiasis, large-scale clinical trials are not feasible. For micafungin, there then lacks a good assessment of the exposure-response relationship in patients with higher doses of micafungin in this setting.

VL-2397

Early population PK models are an important step in the assessment of new compounds. Human phase 1 PK and safety clinical trials have recently begun and there is an opportunity to construct a population PK model to characterize the PK for future and for selection of dosage regimens for the next phase of clinical trials. VL-2397 is a natural product isolated from *Acremonium persicinum,* MF-34733. It exhibits potent fungicidal activity *in vitro* and *in vivo* against medically important *Aspergillus* species (73, 74). The intracellular target that is ultimately responsible for antifungal activity is not known (74, 75). The drug is transported into the cell via a siderophore transporter, Sit1. Mammalian cells do not utilize the Sit1 siderophore transporter, which is one potential explanation for differential activity in fungi and animals.

VL-2397 demonstrates rapid and potent *in vitro* fungicidal activity against *Aspergillus fumigatus* (including triazole-resistant *A. fumigatus*), *A. terreus*, *A. flavus*, *A.*

nidulans, Candida glabrata, C. kefyr, Cryptococcus neoformans, and Trichosporon asahii. Limited *in vitro* activity was demonstrated against *Fusarium solani* and does not appear to be active against *A. niger*, *Candida* spp. (with the exception of *C. glabrata*), Mucorales, *Scedosporium apiospermum* and *Fonsecaea pedrosoi*. Live cell imaging shows that VL-2397 stops hyphal elongation from germinated conidia (75). *In vivo*, VL-2397 demonstrated dose-dependent prolongation of survival and reduced fungal burden in the lung of immunocompromised mice with invasive pulmonary *A. fumigatus* (76). VL-2397 represents an exciting new alterative in the anti-*Aspergillus* armamentarium.

Aims

This thesis was prepared to address the following aims:

Aim 1. To utilize a well-established experimental rabbit model of invasive pulmonary aspergillosis (IPA) using serum galactomannan (GM) concentrations as the primary model readout to characterize the PK-PD relationships of isavuconazole against *A. fumigatus*. To validate the readout of the experimental PK-PD model with the clinical findings from the recent phase 3 clinical trial. To define the decrement in GM in the rabbit that is associated with clinically relevant exposure of isavuconazole and for which clinical efficacy has been established. To reflect on the PD basis for establishing an in vitro susceptibility interpretive breakpoint of isavuconazole against *A. fumigatus*. (**Chapter 3**)

Aim 2. To identify an early pattern of GM index (GMI) change that could guide therapeutic decision making for patients increasing the likelihood of survival and successful outcome by analyzing serial GMI from patients treated in a randomized,

double-blind trial (SECURE) in the treatment of IA or other filamentous fungi. To evaluate the PK-PD relationship in a subset of isavuconazole-treated patients that had available isavuconazole plasma concentrations and serial GMI with a goal to identify a drug-exposure target that can be used for individual patients. (**Chapter 4**)

Aim 3. To compare PK characteristics of isavuconazole in a population of patients infected with a variety of fungal pathogens by constructing a PPK model for patients enrolled in the phase 3 VITAL trial, with the goal of comparing PK across the different patient populations to further understand the optimal use of isavuconazole. (**Chapter 5**)

Aim 4. To examine the impact of mucositis on the bioavailability and drug exposure following the administration of oral isavuconazonium sulfate by constructing a population pharmacokinetic model using the plasma concentrations from patients receiving oral isavuconazole in patients with and without mucositis. To use this model to examine bioavailability and the ultimate drug exposure. To consider the potential impact for dosing and therapeutic drug monitoring of isavuconazole in the setting of mucositis. (**Chapter 6**)

Aim 5.To establish preclinical-to-clinical linkages based on predictions from preclinical models in order to prospectively validate the PK-PD relationships. To examined whether reaching the PD target established in preclinical models matters by combining micafungin plasma concentrations from 4 neonatal clinical trials to construct a population pharmacokinetic (PPK) model and then exploring whether increasing micafungin drug exposures resulted in improved clinical outcomes in infants with IC. (**Chapter 7**)

Aim 6. To evaluate the pharmacokinetics of a novel antifungal compound, VL-2397, by constructing a population PK model using plasma concentration data from phase 1 healthy volunteer studies. (**Chapter 8**)

Chapter 2 Experimental Methods

Each chapter includes detailed descriptions of the materials and methods used for the analyses. In this chapter, additional details to describe the over-arching methods are included. In order to not duplicate information in both places, items too specific to generalize are not repeated in this chapter (e.g. *in vivo* model methods in Chapter 3).

Population PK Modeling. For each population pharmacokinetic (PPK) model, the non-parametric estimation in Pmetrics™ (versions 1.3.2-1.5.1, University of Southern CA, Los Angeles, CA, USA) was utilized (77) and fitted to the plasma concentration data (rabbit or patient). The model fitting process included evaluating multiple compartment models with and without lag-time and oral bioavailability terms for compounds administered orally. This process was guided by visual inspection of the plasma concentration-versus-time curves from the observed data. The PPK models established in Chapters 7 and 8 utilized allometric scaling and non-linear techniques, respectively.

The weighting functions were estimated using several different scenarios. Primarily, data were weighted by the inverse of the estimated assay variance from the bioanalytical assay calibration curve. However, in some cases, the weighting was estimated using ADAPT 5 (https://bmsr.usc.edu/software/adapt/ Biomedical Simulations Resource, Los Angeles, CA, USA) or Pmetrics error estimation runs. Specifically, in ADAPT 5, slope and intercept values were estimated using maximum likelihood estimation for each individual. The error estimation run script (i.e. ERRrun) in Pmetrics also allowed for the estimation of the assay error polynomial coefficients directly from the PK data.

In Chapters 3 and 4, linked PK-PD mathematical modeling was performed. In the case of Chapter 3, rabbit plasma concentrations for PK and GMI for PD were modeled simultaneously. In Chapter 4, modeling proceeded in a stepwise fashion because a stable solution could not be obtained when the PK and PD were co-modeled. Therefore, after fitting a model to the PK data, the posterior estimates for each patient were fixed in the data file for each patient so that a solution for the GM could be estimated but still allow for the linked model.

Calculation of area under the concentration-time curve (AUC). The Bayesian posterior estimates for each individual's PK were used to calculate the area under the concentration-time curve (AUC) for each individual. Depending on the study, AUCs were calculated at a certain time point in the dosing interval or the average AUC was calculated. Average AUCs were estimated by dividing the AUC for the entire dosing duration by the total number of days on therapy. In addition, average daily (24 hour) AUCs (AUC_{ave}) were calculated in Pmetrics by simulating the concentration-time profile for the entire dosing period and dividing by the days on therapy.

Model Acceptance Criteria. Acceptance of the final PK and PK-PD models were evaluated by visual inspection of the observed versus predicted values plotted over time after the Bayesian step and the coefficient of determination (r^2) from the linear regression of the observed versus predicted values. Evaluation included inspection of both median and mean posterior predictions. The estimated bias (mean weighted error) and imprecision (adjusted mean weighted squared error) were also considered.

Monte-Carlo Simulations. Mean Bayesian parameter estimates from the fitted model were used to perform Monte Carlo simulations of 1000-5000 patients using Pmetrics. The simulations were used to calculate steady state AUCs within Pmetrics by the trapezoidal rule for each simulated patient. In Chapter 3, the simulations were used to bridge from the rabbit exposure-response data to the humans. In Chapters 4 and 5, the simulations were used to perform PK-PD assessments via inhibitory sigmoid Emax model and probability of target attainment analyses, respectively.

Covariate Assessments. In the population PK modeling process, covariates (intrinsic and extrinsic) were assessed to determine the potential influence on PK parameters. This was accomplished by plotting the continuous covariate against the individual estimates for clearance and volume. Significance was determined after linear regression of the data. If the 95% confidence interval for the slope did not include zero, the impact of the covariate was deemed significant. In the case of Chapter 6, mucositis was evaluated directly after a difference was seen from initial assessment of the observed plasma concentrations in patients with mucositis compared to those without.

Statistical Analyses. Statistical comparisons were performed in MYSTAT 12 (version 12.02; Systat Software, Inc.; http://www.systat.com) and GraphPad Prism versions 6.0h and 7.0h (http://www.graphpad.com). In Chapter 4, the statistical approach was performed in R and described in detail in that chapter. In Chapter 5, the exposure-response analysis was performed by logistic regression in SAS® (version 9.3, SAS Institute Inc., Cary, NC, USA).

Chapter 3 Pharmacodynamics of isavuconazole in experimental invasive pulmonary aspergillosis. Implications for clinical breakpoints

Abstract

Objectives. Isavuconazole, a novel triazole antifungal agent, has broad-spectrum activity against *Aspergillus* spp. and other pathogenic fungi. Isavuconazole exposure-response relationship in experimental invasive pulmonary aspergillosis using galactomannan index (GMI) suppression as a marker of disease clearance was explored.

Methods. The impact of exposure on GMI suppression in persistently neutropenic rabbits treated with isavuconazonium sulfate (isavuconazole-equivalent dosages of 20, 40, or 60 mg/kg q24h, after a 90 mg/kg loading dose) for 12 days was linked using mathematical modeling. Bridging to humans using population pharmacokinetic (PK) data from a clinical trial in invasive aspergillosis was performed using Monte Carlo simulations.

Results. Mean plasma isavuconazole area under the concentration-time curve over MIC (AUC/MIC) (EC_{50}) of 79.65 [95% CI 32.2, 127.1] produced a half maximal effect in GMI suppression. The inhibitory sigmoid E_{max} curve dropped sharply after an AUC/MIC of ≥30 and was near maximum (EC_{80}) at approximately 130. Bridging the experimental pharmacokinetic-pharmacodynamic (PK-PD) target to human population PK data was then used to return to the rabbit model to determine a clinically relevant PD endpoint. The clinical dosing regimen used in the trial would result in a mean GMI of 4.3 (±1.8), which is a 50% reduction from the starting GMI in the experiment.

***Conclusion*.** The clinical trial data results showing the non-inferiority of isavuconazole to voriconazole further support the PK-PD endpoint, thereby demonstrating the usefulness of the rabbit model and its endpoint for isavuconazole and has implications on interpretive breakpoints. Importantly, the analysis supports this model as an important tool for development of antifungal agents.

Introduction

Isavuconazole is a novel broad-spectrum triazole antifungal agent, which is available as the prodrug, isavuconazonium sulfate, in both intravenous and oral formulations, and which was recently approved by the US Food and Drug Administration for the primary treatment of invasive aspergillosis (IA) and mucormycosis in adults (78). IA is a life-threatening disease that causes significant morbidity and mortality in patients who are severely immunocompromised.(5, 6) Isavuconazole is the first agent that has been developed for IA for 12 years. Despite the recent demonstration of non-inferiority of isavuconazole compared with voriconazole, there is relatively little information regarding exposure-response relationships of isavuconazole against *Aspergillus* spp. that are required for a complete understanding of the clinical utility of this agent.

Laboratory animal models that mimic human disease have long been used to characterize pharmacological efficacy and safety prior to clinical use. Importantly, well-designed animal models used in antimicrobial development are generally highly predictive of clinical efficacy (79). Over the past 20–30 years these experimental models have enabled an exploration of the relationship between the time-course of drug exposure, penetration of drug to the site of infection and the ultimate antimicrobial effect (1). The treatment of infections caused by *Aspergillus* spp. and rare filamentous fungi is relatively difficult to study in clinical settings. A detailed understanding of exposure-response relationships underpins the design of antifungal regimens that are safe and effective and enables the right dose to be studied the first time. An understanding of antifungal pharmacokinetic (PK)-pharmacodynamic (PD) properties also provides the foundation for treatment and prevention of antimicrobial resistance, determination of the

requirement for therapeutic drug monitoring, and decision support for establishing *in vitro* susceptibility breakpoints.

Here, we describe the use of a well-established experimental rabbit model of invasive pulmonary aspergillosis (IPA) using serum galactomannan (GM) concentrations as the primary model readout to characterize the PK-PD relationships of isavuconazole against *A. fumigatus*. We were in a unique position of being able to validate the readout of the experimental PK-PD model with the clinical findings from the recent phase 3 clinical trial. We defined the decrement in GM in the rabbit that is associated with clinically relevant exposure of isavuconazole and for which clinical efficacy has been established. We then reflected on the PD basis for establishing an *in vitro* susceptibility interpretive breakpoint of isavuconazole against *A. fumigatus*.

Methods and Materials

Rabbit model of invasive pulmonary aspergillosis. A previously described persistently neutropenic rabbit model of IPA was used (15, 80). Healthy female New Zealand white rabbits (Covance Research Products, Inc., Denver, PA, USA) weighing 2.6 to 3.5 kg were used in the study. Immunosuppression and profound persistent neutropenia (neutrophil concentration of <100 neutrophils/μL) was established by administration of cytarabine (Ara-C) (Cytarabine injection; Zydus Hospira Oncology Private Ltd, Gujarat, India for Hospira, Inc., Lake Forest, IL, USA) at an initial dose of 525 mg/m^2 for 5 consecutive days beginning on day 1 of the experiment and a maintenance dose of 484 mg/m^2 on days 8, 9, 12 and 13 of the experiment. Methylprednisolone (Solu-Medrol®, Pfizer for Pharmacia & Upjohn Co., Division of Pfizer Inc., New York, NY) was dosed at

5 mg/kg on days 1 and 2 (80). Bacterial infection prophylaxis was maintained with antibiotics (ceftazidime, gentamicin, vancomycin) as previously described (80).

Ethics. Rabbits were monitored under humane care and use of standards in facilities, accredited by the Association for Assessment and Accreditation of Laboratory Animal Care International, and according to the guidelines of the National Research Council for the care and use of laboratory animals, and under the approval of the Animal Care and Use Committee of Weill Cornell Medical Center, New York, NY, USA. Rabbits were housed individually and fed *ad libitum*.

Organism and MIC. NIH 4215 (ATCC No. MYA-1163), which is a well-characterized clinical isolate of *A. fumigatus*, was used for all experiments (80). The MICs of voriconazole and isavuconazole against *A. fumigatus* determined using Clinical and Laboratory Standards Institute (CLSI) standard M38-A2 broth microdilution methodology were 0.5 mg/L and 1 mg/L, respectively (81). The MICs were measured in triplicate.

Treatment. Rabbits received either prodrug, isavuconazonium sulfate, at an isavuconazole (BAL4815; active moiety) equivalent dose of 20 (ISAV20), 40 (ISAV40), and 60 (ISAV60) mg/kg/day or were untreated controls. A loading dose of the prodrug equivalent to isavuconazole 90 mg/kg was given on the first day of antifungal treatment to all isavuconazole-treated rabbits. Treatment was initiated 24 h after inoculation and administered orally once daily thereafter for up to 12 days. Multiple outcome variables were analyzed from the model including survival, pulmonary infarct score, lung weight, residual fungal burden (log cfu/g), serum galactomannan index (GMI), bronchoalveolar

lavage (BAL) fluid GMI, and serum (1→3)-β-D glucan levels, as previously described (15).

Herein, we report the results of the isavuconazole-treated animals with a particular focus on the serum GM experiments and PK-PD mathematical modeling, with a brief description of the primary efficacy results. The primary efficacy results from the animal model are published elsewhere (15).

Pharmacodynamic assessment. Blood was collected via the indwelling Silastic catheter at 24 h post-inoculation, just prior to initiation of antifungal treatment and every other day thereafter for determination of the serum GM concentrations. Concentrations were determined by one-stage immunoenzymatic sandwich microplate assay method (the Platelia® *Aspergillus* Enzyme Immunoassay (EIA) (Bio-Rad, Marnes la Coquette, France) (13), and according to the manufacturer's instructions.

Pharmacokinetics. Single-dose PK analyses were conducted in four non-infected rabbits in each dosage group. Time points included pre-dose, 1, 2, 4, 8, 12, 18, 24, and 48 h post-dosing. Multiple-dose PKs were determined in infected animals 7 days post-inoculation. Blood samples were drawn pre-dose and at 1, 4, 8, and 24 h post-dosing. Each blood sample for PK assay was collected in heparinized syringes. Plasma samples were immediately separated by centrifugation at 400 g and stored at -80°C until assayed.

Measurement. Isavuconazole was measured using liquid chromatography/mass spectrometry/mass spectrometry (LC/MS/MS). Samples were prepared by adding 0.1 M paraoxon (10 µL per 1 mL of plasma) to the blank EDTA/K3 and blank Li-heparin rabbit plasma in order to inhibit esterases. Spiking solutions were prepared by serial dilution in

dimethyl sulfoxide (DMSO) and acetonitrile (ACN), 0.05% trifluoracetate (TFA) out of a 2 mg/mL stock solution with a range from 0.5 µg/mL to 500 µg/mL. Calibration samples were performed by spiking 1 µL of each DMSO (or ACN, 0.05% TFA) solution in 99 µL of blank EDTA/K3 plasma. Each sample was then quenched with 300 µL of ACN, 0.05% TFA containing 1 µg/mL of BAL0004815-d4, and pyridooxazinone as internal standards.

After centrifugation, 10 µL of the supernatant was injected into the LC/MS/MS. A similar preparation method was performed for the QC samples; however, blank Li-heparin plasma was used instead of the EDTA/K3 plasma. For the samples, 50 µL of plasma was mixed with 150 µL of ACN, 0.05% TFA containing 1 µg/mL of BAL0004815-d4, and pyridooxazinone as internal standards, then treated like the calibrators. Assay linear range was 0.005 to 4.45 µg/mL and coefficient of variation (%CV) ranged from 1.1 to 10.7%. The lower limit of quantification of the plasma assay was 0.005 µg/mL.

Pharmacokinetic and pharmacodynamic mathematical modeling. Mathematical modeling was performed in a step-wise manner. First, a population pharmacokinetic (PPK) model was constructed using non-parametric estimation in Pmetrics™ software (v1.3.2, University of Southern CA, Los Angeles, CA, USA)(77) and fitted to the rabbit plasma concentration data. The weighting functions were estimated using a combination of ADAPT 5 (https://bmsr.usc.edu/software/adapt/ Biomedical Simulations Resource, Los Angeles, CA, USA) and Pmetrics error estimation runs. Specifically, in ADAPT 5, slope and intercept values were estimated using maximum likelihood estimation for each individual rabbit. In Pmetrics, the error estimation run script (i.e. ERRrun) was used to estimate the assay error polynomial coefficients directly from the data. After establishing

a model that best described the PK data, the GM concentrations were added to the dataset for each individual rabbit. A linked PK-PD model was built using the following set of differential equations:

Equation 1

$$\frac{dX(1)}{dt} = -Ka \cdot X(1)$$

Equation 2

$$\frac{dX(2)}{dt} = Ka \cdot X(1) - \left(\left(\frac{Cl}{V}\right) \cdot X(2)\right) - Kcp \cdot X(2) + Kpc \cdot X(3)$$

Equation 3

$$\frac{dX(3)}{dt} = Kcp \cdot X(2) - Kpc \cdot X(3)$$

Equation 4

$$\frac{dX(4)}{dt} = Kpmax \cdot \left(1 - \left(\frac{\left(\frac{X(2)}{V}\right)^{Hp}}{C50p^{Hp} + \left(\frac{X(2)}{V}\right)^{Hp}}\right)\right) \cdot X(4) \cdot$$

$$\left(1 - \left(\frac{X(4)}{popmax}\right)\right) - ksmax \cdot X(4) \cdot \left(\frac{\left(\frac{X(2)}{V}\right)^{Hs}}{C50s^{Hs} + \left(\frac{X(2)}{V}\right)^{Hs}}\right)$$

The first three equations describe the pharmacokinetics of the drug, (compartment 1, theoretical absorptive compartment for oral administration; 2, central compartment, and 3, peripheral compartment). Cl is the clearance defined, as the amount of drug being cleared from the central compartment over time and V is the volume of the central compartment. Ka is the first order absorption constant, Kcp is the rate of drug moving from the central to peripheral compartment and Kpc is the rate of drug moving from the

peripheral to central compartment. Equation 4 describes the rate of change of the serum GM values. Kpmax represents the maximum rate of production, Hp is the slope function for production, C50p is the amount of drug where there is half maximal production, popmax is the theoretical maximum density of GM, ksmax is the maximum rate of GM suppression, C50s is the amount of drug where there is half maximal suppression, and Hs is the slope function for the GM suppression.

Acceptance of the final model was evaluated by visual inspection of the observed versus predicted values plotted over time after the Bayesian step, the coefficient of determination (r^2) from the linear regression of the observed versus predicted values, as well as, evaluation of the estimated bias and imprecision. After fitting the model to the PK-PD data, the Bayesian posterior estimates for each rabbit were used to estimate the concentration-time profiles for isavuconazole and GMI for each rabbit. Simulations were performed in ADAPT 5. Area under the plasma concentration-time curves (AUCs) were calculated by integration from the simulated concentration-time profiles on the last day of dosing (at steady-state) in ADAPT 5.

Using the simulated isavuconazole AUC values and the GMI at the end of the dosing period for each rabbit, an inhibitory sigmoid Emax model was constructed to establish the pharmacodynamic relationship between exposure (AUC) divided by MIC and response (GMI). The model used is described below:

Equation 5

$$Effect = E_0 - \left(\frac{Emax \cdot \left(\frac{AUC}{MIC}\right)^H}{EC50^H + \left(\frac{AUC}{MIC}\right)^H}\right)$$

E_0 is the baseline level of GM prior to exposure to drug, Emax is the maximum GM value, EC_{50} is a measure of drug potency, and H is the slope factor.

Bridging to humans. To bridge the exposure-response results from the rabbits to humans, a PPK model was constructed using the isavuconazole plasma concentration data from the phase 3 SECURE clinical trial (48). The SECURE (NCT00412893) trial evaluated the efficacy and safety of isavuconazole compared to voriconazole in the treatment of patients with possible, probable or proven IA and other filamentous fungi. Patients that were randomized to isavuconazole received the prodrug, isavuconazonium sulfate, at a dose of 372 mg every 8 h for the first 2 days followed by 372 mg once daily thereafter (equivalent to isavuconazole at a dose of 200 mg (IV) q8h for 2 days, then 200 mg once daily). The option to receive either IV or oral was allowed after day 2. The maximum treatment duration was 84 days. Plasma trough samples were collected on days 7, 14, 42, end of treatment and follow-up for some patients. Serial plasma samples (seven in total) from less than 25 subjects were collected on day 7 (± 1 day) or 14 (+ 1 day) for PK profiling. Overall, 113 patients with isavuconazole concentrations were used for the analysis.

A PPK model using non-parametric estimation was developed in Pmetrics™ (v1.3.2, University of Southern California, CA, USA) (77). The model fitting process included evaluating both two- and three-compartment models with and without lag-time and oral bioavailability terms.

Mean Bayesian parameter estimates from the fitted human model were used to perform Monte Carlo simulations of 1000 patients using Pmetrics. The simulations were

used to calculate steady state AUCs within Pmetrics by the trapezoidal rule for each simulated patient. Using equation 5 above, the effect of AUC:MIC at various MIC values representative of the MIC distribution of isavuconazole for *A. fumigatus* as described by Espinel-Ingroff *et al.* was calculated (82). Total isavuconazole drug levels are used wherever isavuconazole concentration or AUCs are reported unless otherwise specified.

Results

Animal model. Significant reduction of residual fungal burden, lung weights, and pulmonary infarct score was demonstrated in the two highest dosage groups of ISAV40 and ISAV60 compared with untreated controls ($P<0.001$, ANOVA with Bonferroni's correction for multiple comparisons). The highest dose of isavuconazole significantly prolonged survival compared to untreated controls ($P<0.001$, log-rank test). The lowest dosage of ISAV20 also significantly prolonged survival versus untreated controls ($P<0.05$, log-rank test) (15).

Dose-dependent reductions in biomarkers were demonstrated for isavuconazole-treated animals. ISAV40 and ISAV60 dosage groups significantly decreased the GMI during therapy following day 4 compared to increased GMI in the untreated controls ($P<0.01$). **Figure 1** illustrates GMI versus time for the rabbits treated with isavuconazonium.

Figure 1 Galactomannan index (GMI) versus time for each rabbit after administration of isavuconazonium sulfate (all dose groups) Individual lines represent the GMI values over time for each rabbit. The colors clarify the dosage for each rabbit.

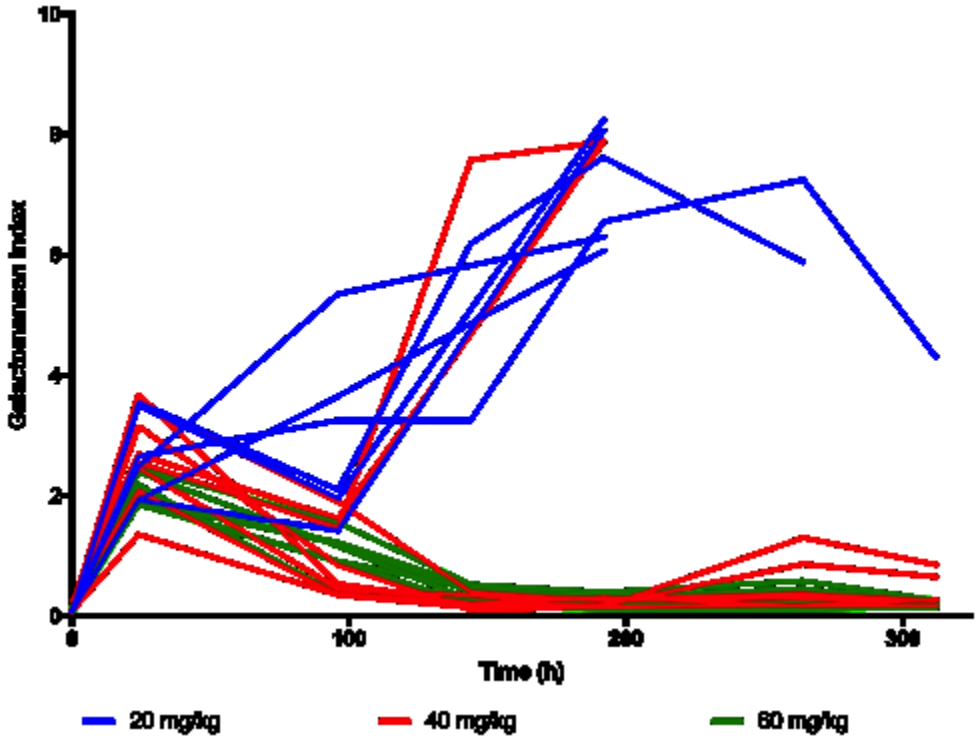

BAL GMI was also significantly reduced in ISAV40 and ISAV60 dosage groups versus untreated controls (P<0.001, ANOVA with Bonferroni's correction for multiple comparisons). Serum (1→3)-β-D-glucan levels were significantly reduced in ISAV40 and ISAV60 compared to untreated controls (P<0.05, ANOVA with Bonferroni's correction for multiple comparisons) (15).

PK-PD modeling. Visual inspection of the raw concentration-time profile of the three isavuconazole dosages suggested linear isavuconazole pharmacokinetics in the rabbit. A

two-compartment model with first-order absorption fit the rabbit plasma isavuconazole drug concentration data well. The fit of the linked PK-PD model was also acceptable based on a coefficient of determination for the observed versus predictive values after the Bayesian step of 0.965 and 0.895 for the PK concentrations and GMI, respectively (**Figure 2**).

Figure 2 Regression plot of observed (y-axis) versus model predicted (x-axis) plots from rabbit isavuconazole population PK (A) and galactomannan index (GMI) (B). Logistic regression of observed versus predicted concentrations. In both figures, the solid line represents the slope of the correlation and the circles and squares are the individual concentrations (values) for plasma (A) and GMI (B), respectively. The coefficient of determination for the observed versus predictive values after the Bayesian step of 0.965 and 0.895 for the PK concentrations (A) and GMI (B), respectively.

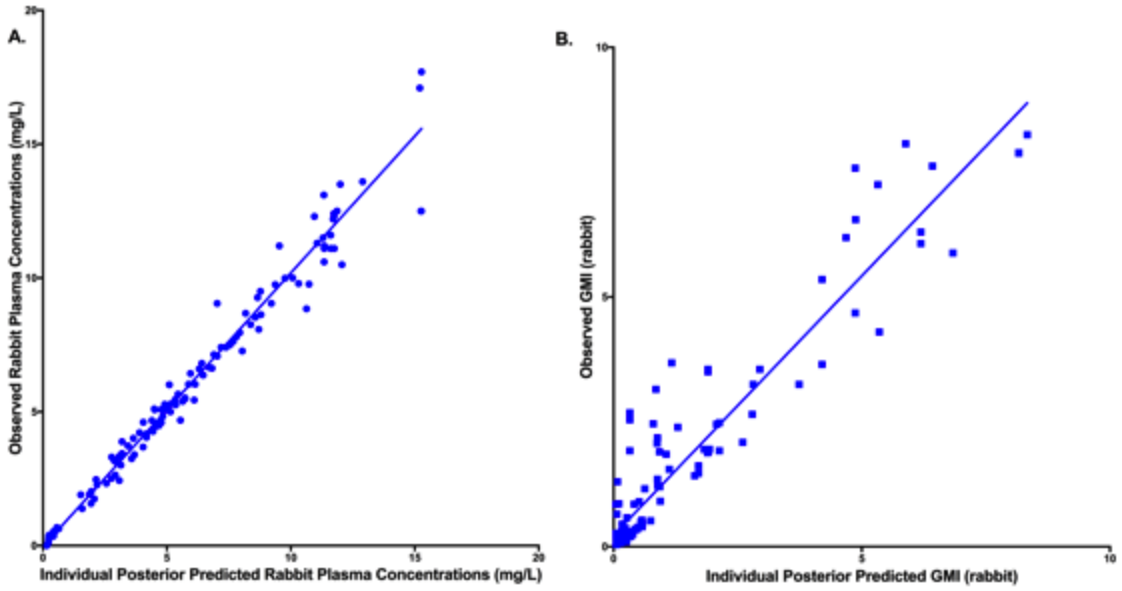

The estimates of bias and imprecision for the rabbit PK were -0.14 and 1.05, and -0.288 and 0.892 for GMI, respectively. Parameter estimates from the final model are summarized in **Table 2**.

Table 2 Mean and standard deviations (SD) values for each parameter estimated from the rabbit population PK-PD linked model

Parameter (units)	Mean	SD
Ka (h^{-1})	20.145	8.842
Cl/F (L/h)	1.108	1.228
V/F (L)	27.911	6.872
Kcp (h^{-1})	5.953	2.498
Kpc (h^{-1})	6.394	2.916
Kpmax (GMI/h)	0.115	0.047
Hp	17.220	4.116
C50p (mg/L)	1.286	1.548
IC (GMI)	0.108	0.053
Ksmax (GMI/h)	0.009	0.002
Hs	12.292	5.029
C50s (mg/L)	0.167	0.127
Popmax (GMI)	6.642	2.324

Abbreviations: SD**,** standard deviation; Ka, first-order rate constant describing the movement of drug from the gut to the central compartment; Cl, clearance from the central compartment; V, volume of the central compartment; F, bioavailability; Kcp, rate of drug moving from central to peripheral compartment; Kpc, rate of drug moving from peripheral to central compartment; Kpmax, maximum rate of GM production, Hp, slope function for production; C50p, amount of drug where there is half maximal production; IC, initial condition of GMI prior to drug exposure; Ksmax, maximum rate of GMI suppression; Hs, slope function for GMI suppression; C50s, amount of drug where there is half maximal suppression; Popmax, theoretical maximum density of GMI.

The exposure-response relationship showed that the GMI responded sharply for AUC:MIC of ≥30 (**Figure 3**). The AUC:MIC that induced the half-maximal effect (EC_{50}) was estimated at 79.65 [95% CI 32.2, 127.1], which resulted in a 50% reduction in GMI. Suppression of GMI was a near maximum (EC_{80}) at an AUC:MIC of approximately 130.

Figure 3 Inhibitory sigmoid Emax curve demonstrating the exposure-response relationship of isavuconazole exposure in terms of the plasma AUC:MIC (x-axis) and the associated terminal GM) value (y-axis). The black squares represent the observed GMI value for each rabbit (+/- SEM). The continuous black line represents the fit of the inhibitory sigmoid Emax model to the data.

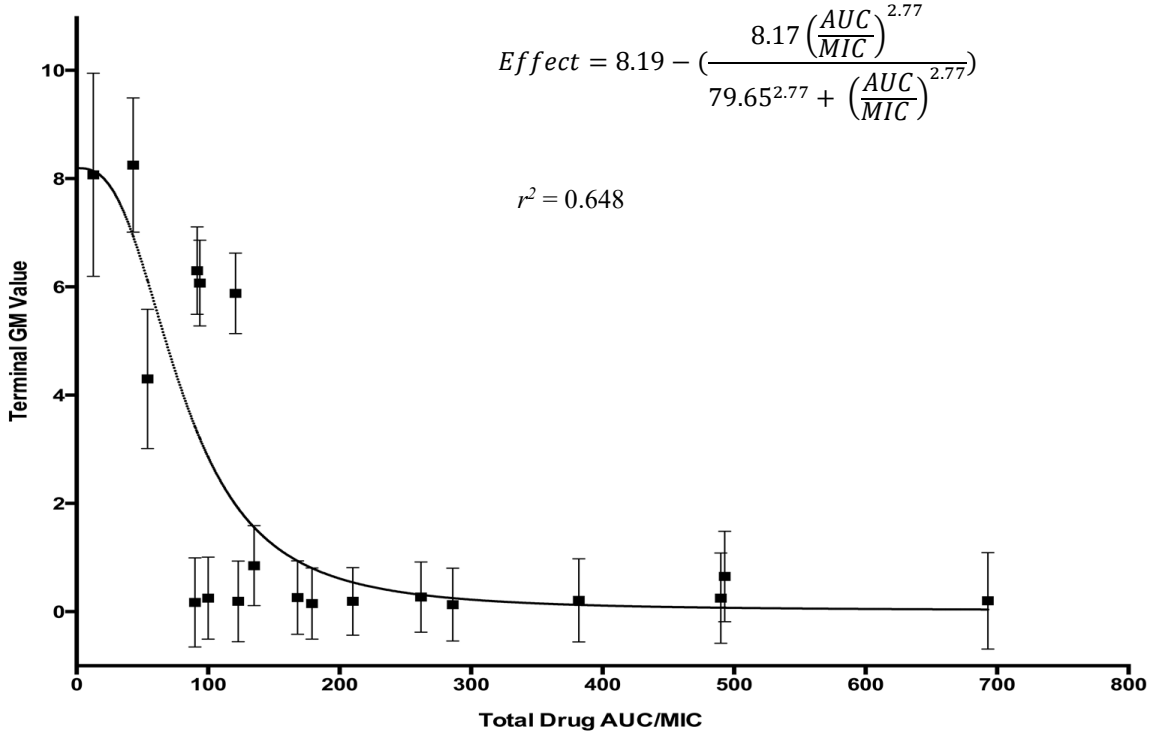

Bridging to humans. Human isavuconazole plasma drug concentrations from the phase 3 SECURE clinical trial in patients with IA or other filamentous fungi were used to

construct a non-parametric PPK model using Pmetrics software (77). A two-compartment model with first order absorption fit the data well with a coefficient of determination after the Bayesian step of 0.877. Visual inspection of the observed versus predicted values was acceptable, as well as, measures of bias and imprecision. The mean parameter estimates from the PPK model for the P3 human plasma concentrations are presented in **Table 3**.

Table 3 Mean and standard deviation (SD) values for each parameter estimated from the human population PK model

Parameter (units)	Mean	SD
Ka (h^{-1})	24.3	16.7
Cl/F (L/h)	2.2	1.1
V/F (L)	398.8	225.2
F (%)	90.2%	20.9%
Tlag (h)	1.5	3.3

SD, standard deviation; PK, Ka, first-order rate constant that describes the movement of drug from the gut to the central compartment (h^{-1}); Cl, clearance (L/h); V, volume of distribution (L); F, bioavailability; Tlag, lag time (h).

Monte Carlo simulations using the mean parameter estimates from the human PPK model were performed. The AUCs for 1000 simulated patients were estimated using the linear trapezoidal rule in the "makeAUC" function within Pmetrics. The mean steady-state AUC ± SD for the simulated population was 82.6 ± 33.0 mg h/L. The corresponding drop in GMI in rabbits receiving human-like exposures of isavuconazole was 4.3 ± 1.8, which closely approximates the EC_{50} for GMI reduction (4.1 GMI units) from the start of the experiment in the rabbits (E_0=8.2).

After Monte Carlo simulations of 1000 patients, the effect of AUC:MIC at different MIC values relevant to the wild-type (WT) MIC distribution of *A. fumigatus* for isavuconazole as tested by CLSI methodology is displayed in **Figure 4**. The figure illustrates the predicted GMI at the end of the experiment given the inherent PK variability in humans as a function of each MIC value following the administration of the regimen of isavuconazonium sulfate that was used in the recent clinical trial.

Figure 4 Frequency distribution of terminal galactomannan values at each MIC value. Monte Carlo simulation of 1000 subjects after exposure to the clinical dosing regimen of isavuconazonium sulfate. The colored bars represent the frequency of each GMI value for an organism at that MIC value after treatment with the standard clinical dosage regimen of isavuconazonium sulfate (372 mg every 8 hours for 2 days, followed by 372 mg once daily thereafter).

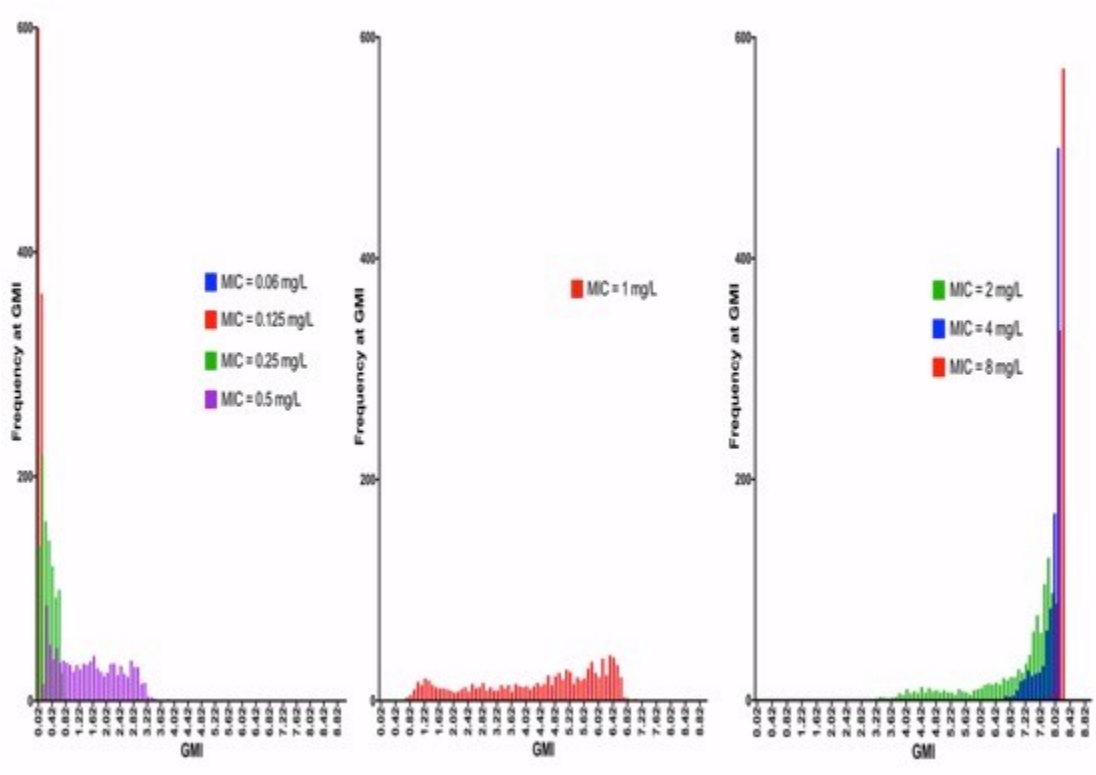

Discussion

Isavuconazole is a novel triazole antifungal agent that is administered as the water-soluble prodrug isavuconazonium sulfate. This novel agent demonstrated non-inferior efficacy (as defined by upper bound of the 95% CI less than the pre-specified 10% non-inferiority margin) compared with voriconazole for all-cause mortality up to day 42 (18.6% versus 20.2%, intent-to-treat population) in the SECURE trial for the treatment of IA and invasive disease caused by other filamentous fungi.

The clinical trial results enable a retrospective validation of the clinical validity of the endpoints used in the experimental PK-PD model. An isavuconazole AUC that has been associated with clinical efficacy that is at least as good as the current standard of care (i.e. voriconazole) induces a 50% reduction in circulating GM concentrations in the persistently neutropenic rabbit model of IPA. Thus, the rabbit model as currently designed produces an "on scale" readout that appears clinically relevant and tractable. These analyses provide a unique opportunity to evaluate the predictive nature of the rabbit model endpoints and further facilitate the use of this model for the future development of new antifungal agents.

The findings in this study also have implications for setting *in vitro* susceptibility breakpoints for isavuconazole against *A. fumigatus*. The recent clinical study (SECURE) clearly suggests that isavuconazole is an effective agent for the treatment of IA. If an assumption is made that the vast majority of isolates in the clinical trial are WT organisms then *A. fumigatus* is considered to be a "good target" for isavuconazole. In the absence of other clinical or PD data, the breakpoint for isavuconazole against *A. fumigatus* is ordinarily set at the epidemiological cut-off value (ECV or ECOFF), which

is ≤1 mg/L (82). There is no evidence from the SECURE study that there is a relationship between MIC and clinical outcome; although the number of patients with a positive culture was too small to enable a definitive analysis. This pharmacodynamic study provides further perspective on the validity of using 1 mg/L as a breakpoint. Without making any assumptions about a GMI cut-off value that defines therapeutic success and failure, **Figure 3** shows the predicted GMI values for patients receiving a standard clinical isavuconazole regimen and infected with isolates with a range of MICs. The histograms in **Figure 4** suggest that a ≥ 50% reduction in GMI is achieved for isavuconazole MICs <1 mg/L. Similarly, GM antigen expression is not suppressed in patients with an MIC ≥2 mg/L. For an MIC of 1 mg/L some patients have suppressed GM antigen expression while others do not. Therefore, an MIC of 1 mg/L may on occasions be difficult to treat and be therefore classified as intermediate to denote the fact that isavuconazole should be used with some caution in this situation.

The PK-PD relationship for isavuconazole against *Aspergillus* spp. has been described for a variety of other experimental designs; however, given the results of the clinical trial, not all appear to predict the clinical response for isavuconazole well. Therefore, it is important to understand the key differences between the models and how those differences may have an impact on the development of a new antifungal drug. Lepak *et al.* used a neutropenic murine model of IPA (51). The model used a diverse group of organisms (10 in total) ranging from WT organisms to organisms with well-characterized *cyp51a* point mutations. In contrast to the current model, primary efficacy was defined by the net stasis in fungal growth as measured by the density of fungal DNA in the lung. The estimated total drug PD target (AUC:MIC_{clsi}) from this experiment was

503. In contrast, Seyedmousavi *et al.* evaluated isavuconazole in a non-neutropenic mouse model of disseminated aspergillosis (83). Similar to the model of Lepak et al, this model utilized both WT and *cyp51a* mutants. However, the primary outcome measure was 14-day survival. The total drug AUC:MIC_{clsi} target associated with 50% survival (EC_{50}) was 10-fold lower and estimated to be approximately 50.

The estimated half-life of isavuconazole in rabbits (17.5 h) is significantly longer than in mice (1–5 h) (51). The difference in half-life between the two animal models could have an impact when estimating the PD target in severe experimental conditions (e.g. profound and prolonged neutropenia). The relative absence of neutrophils combined with long periods of the dosing interval where drug concentrations are beneath a critical threshold may enable fungal regrowth. Progressively higher dosages of isavuconazole are then required to achieve concentrations that prevent fungal regrowth. It is therefore possible that the rapid clearance of drug, the use of dosing intervals (every 12 h) that are many multiples of the half-life and the severe nature of the model conspire to produce an inaccurate estimate of drug exposure that is ultimately required for therapeutic efficacy.

In addition to the animal models described above, an *in vitro* human alveolus model of experimental pulmonary aspergillosis was conducted (84). The total drug AUC:MIC estimated for this system was 11. This lower value probably largely reflects the finding that the model best simulates early (first 24 hours) versus more established disease (>24 hours) (27). The *in vitro* alveolus model also does not reflect the tissue injury, including hemorrhagic infarctions, which may impair penetration of the antifungal agent to the invading hyphae. These factors are important determinants of the drug exposure required to suppress circulating GM antigen concentrations.

Limitations in the reproducibility of GM measurements have been reported. One report describes a meta-analysis of 27 studies where GM was used in the clinic as a surveillance measure for the development of IA. The analysis was done to characterize the performance of the test and also to determine variables that might affect the performance (17). The authors describe sensitivity and specificity values of 0.61 (95% CI, 0.59–0.63) and 0.93 (95% CI, 0.92–0.94), respectively, for the combined proven and probable cases. The sensitivity of the test decreases for solid organ transplant patients and when a reference standard such as EORTC/MSG was utilized. Other studies have reported decreased sensitivity with prior antifungal therapy use (85). These factors are not likely to play a role in the findings presented in this report. Reproducibility due to technical aspects of the assay has also been reported. In 2015, Guigue and colleagues performed a study to identify operational factors that may result in the lack of reproducibility of the GM assay results (86). They found approximately 30% of the positive GM results were not reproducible. To account for this, they suggest retesting the sample and performing serial samples. Given the current study utilizes serial sampling of the rabbit sera, these issues are less likely to impact the current study.

When one considers the possible use of these PD targets in drug development, it is clear that even small differences may have a significant impact on the regimen that is ultimately chosen and the establishment of *in vitro* susceptibility breakpoints. For example, use of the PD target defined in the neutropenic mouse model would have placed the isavuconazole breakpoint in the middle of the WT population (at 0.06 mg/L), which is neither ideal nor consistent with clinical trial findings. A corollary is that a much higher dose would have been predicted to be successful than was ultimately used in the clinical trial. The rabbit model provides “on scale readouts” for isavuconazole and a clinically

relevant model readout of a 50% reduction in GMI. Thus, complete suppression of GM antigen, which may be desirable when treating a patient with IA, is not a relevant consideration for PK-PD bridging studies (in the same way that 100% survival may not be possible or reasonable). Therefore, all the preclinical PK-PD studies for isavuconazole and the subsequent bridging studies provide a salutary lesson in the use of PK-PD models for drug development. Orthogonal reasoning should be applied, models must be stressed, positive controls should be used to benchmark model performance and readouts, and findings should be repeatedly cross-checked.

This study has several limitations. First, only one WT organism of *A. fumigatus* was used in the experimental model. A more diverse group of organisms with a range of MICs including organisms with well-characterized resistance mechanisms would provide a more robust assessment of the exposure-response relationship. Second, the experimental findings as presented are only relevant to CLSI methodology. Third, a small number of terminal GMI values fall in the middle of the curve suggesting that the results could be driven by the majority of values that occur at the extremes of effect or no effect. Nevertheless, this study provides further evidence that GM is a robust clinically relevant biomarker that can be used to characterize the pharmacodynamics of anti-*Aspergillus* agents. A 50% reduction in GMI in this persistently neutropenic rabbit model of IPA correlates well with the results of the phase 3 clinical trial for isavuconazole which provided a foundation to further characterize the PD of new antifungal agents, and the selection of new regimens for study in early-phase clinical trials.

Chapter 4 Pharmacodynamics of Isavuconazole for Invasive Mould Disease: Role of Galactomannan for Real-Time Monitoring of Therapeutic Response

Abstract

Background. The ability to make early therapeutic decisions when treating invasive aspergillosis using changes in biomarkers as a surrogate for therapeutic response could significantly improve patient outcome.

Methods. Cox proportional hazards model and logistic regression were used to correlate early changes in GMI to mortality and overall response, respectively, from patients with positive baseline GMI (≥ 0.5) and serial GMI during treatment from a phase 3 clinical trial for the treatment of invasive mould disease. PK-PD analysis in patients with isavuconazole plasma concentrations was conducted to establish the exposure necessary for GMI negativity at the end of therapy.

Results. The study included 158 patients overall and 78 isavuconazole patients in the PK-PD modeling. By Day 7, GMI increases of > 0.25 units from baseline (3/130 survivors; 9/28 that died) significantly increased the risk of death compared to those with no increase or increases below 0.25 (Hazard Ratio 9.766; 95% CI 4.356, 21.9, $p<0.0001$). For each unit decrease by Day 7 from baseline, the odds of successful therapy doubled (Odds Ratio 2.154, 95% CI 1.173, 3.955). An AUC:EC_{50} of 108.6 is estimated to result in a negative GMI at the end of isavuconazole therapy.

Conclusions. Early trends in GMI are highly predictive of patient outcome. GMI increases by Day 7 could be considered in context of clinical signs to trigger changes in treatment, once validated. Our data suggests this improves survival by 10-fold and positive outcome by 3-fold. These data have important implications for individualized therapy for patients and clinical trials.

Introduction

Invasive fungal diseases caused by *Aspergillus* spp. are a persistent public health problem (87-89). Therapeutic options are few and limited by toxicity, an incomplete spectrum of antifungal activity and acquired drug resistance (7-11). Treatment is initiated when tissue damage is established, usually evidenced by radiographic abnormalities. Assessing the response to therapy at the bedside is difficult. Clinical signs and symptoms are nonspecific and radiological abnormalities may paradoxically deteriorate despite otherwise successful therapy (89). Thus, ways to objectively monitor the response to antifungal therapy and make rational therapeutic choices would significantly improve antifungal stewardship and potentially improve clinical outcomes.

The widespread use of galactomannan (GM) detection and quantification has improved the speed and accuracy of a diagnosis of invasive aspergillosis (IA). Serum GM is often detectable prior to the onset of clinical signs and symptoms of infection (88, 89) and has been used successfully as a surrogate for therapeutic response (14, 15, 90). A decline in GM or GM negativity has been linked to clinical outcomes, eg, survival or successful clinical response, was reported to correlate in patients that do well (18-21). However, interpretive criteria used to direct therapeutic decision-making are lacking.

To identify an early pattern of GM index (GMI) change that could guide therapeutic decision making for patients increasing the likelihood of survival and successful outcome, we analyzed serial GMI from patients treated in a randomized, double-blind trial (SECURE) in the treatment of IA or other filamentous fungi. We also analyzed a subset of isavuconazole-treated patients that had available isavuconazole plasma

concentrations and serial GMI to evaluate the PK-PD relationship with a goal to identify a drug-exposure target that can be used for individual patients.

Methods

Study Design. Patients from the SECURE trial (NCT00412893), a phase 3, randomized, double-blind study comparing isavuconazonium sulfate to voriconazole for the treatment of invasive mould disease caused by *Aspergillus* spp. or other filamentous fungi, were eligible (48). The evaluation of the use of GM as a biomarker was pre-specified as an exploratory objective. Patients from the modified intent-to-treat (mITT; all patients receiving study drug with proven or probable invasive mould infections, as determined by an independent blinded data review committee (DRC)) population who had a positive baseline serum GMI (optical density (OD) ≥0.5) plus one or more post-baseline (>day 7) GMI were included. Patients were eligible for the PK-PD analysis if plasma samples were collected to enable an estimate of isavuconazole plasma exposure.

Eligibility criteria for the main trial are detailed elsewhere (48). Patients randomized to the isavuconazole group received the prodrug, isavuconazonium sulfate, as a loading regimen intravenously (i.v.) over days 1 and 2 at a dose of 372mg (equivalent to 200mg of isavuconazole) every 8 hours, followed by a maintenance dose of 372mg once daily, given either i.v. or orally (p.o.). Voriconazole patients received i.v. 6mg/kg twice daily on day 1 followed by 4mg/kg i.v. twice daily on day 2. From day 3 onwards, voriconazole was administered as an i.v. infusion (4mg/kg twice daily) or orally (200mg twice daily). The patients were treated for up to 84 days.

Outcome Measurements. The primary efficacy outcome measure was all-cause mortality through day 42. Secondarily, overall response at the end of therapy (EOT) as evaluated by the DRC was assessed. Successful overall response was defined as a composite of complete or partial clinical and radiological response, plus a mycological response of eradication or presumed eradication. The response criteria are detailed elsewhere (48).

GM Measurements. Protocol-defined serum samples were drawn at screening, on days 1, 2, 14, 28, 42, 84, and EOT. Samples drawn on an ad hoc basis were included. In total, 1347 GMI values were available with 114 around day 7 (+/-1 day) (see **Figure 5**).

Figure 5 Number of GMI values per day through Day 42 Each bar represents the frequency (number) of GM values available on each day of treatment for the population.

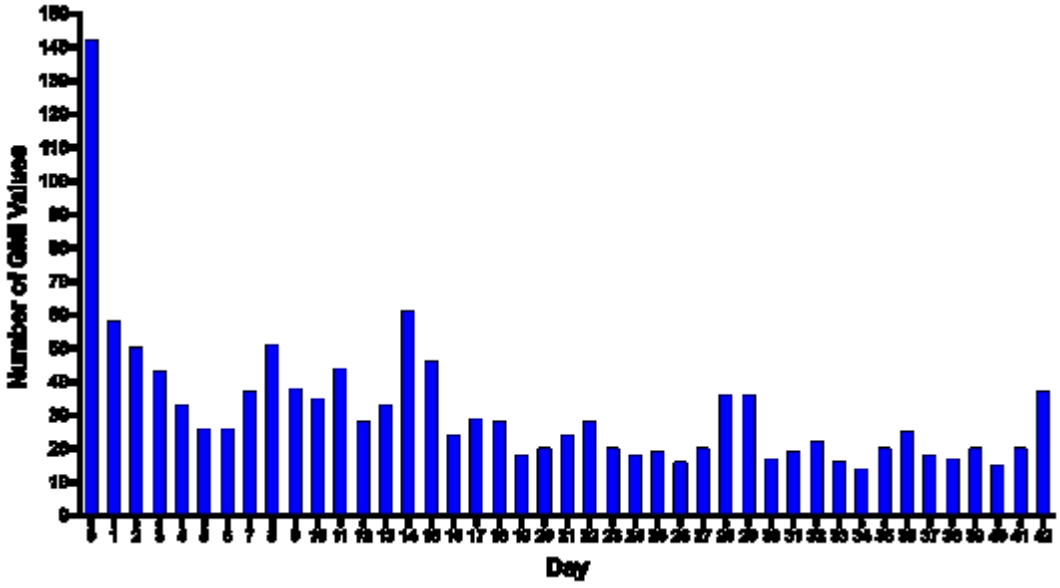

A central laboratory analyzed protocol-defined samples, while ad hoc basis were analyzed locally. Specimens were stored at -20°C until shipped to the central laboratory (Eurofins Global Central Laboratory, Chantilly, VA) and assayed using Platelia *Aspergillus* enzyme immunoassay (EIA) from Bio-Rad Laboratory according to the manufacturer's instructions. The total inter-assay variability, according to the instructions, ranged from 6.8% to 29.2% for samples.

Pharmacokinetics (PK). Blood samples were collected on treatment days 7, 14, 42, and EOT. Collection was targeted 24 h after the start of the infusion or the p.o. dose the previous day (i.e., trough concentration). Full 24-hour profiles were obtained from a subset of 8 patients. After collection, samples were processed immediately and stored at -80°C until shipment to the central research laboratory. Isavuconazole (BAL4815) concentrations in plasma samples were measured retrospectively using a validated LC-MS/MS method as previously described (44). Voriconazole concentrations were not measured.

Pharmacokinetic-Pharmacodynamic Analysis. A population PK-PD model was fitted to the data to describe the relationship between dose, drug exposure and the time-course of GMI. Pmetrics was used for all model fitting (77). Modeling proceeded in a stepwise fashion because a stable solution could not be obtained when the PK and PD were co-modeled. Both 1- and 2-compartment PK models that included an absorptive compartment were initially examined and distinguished (44). The set of differential equations used to describe the change in PK and PD components overtime are as follows:

Equation 6

$$\frac{dX(1)}{dt} = -Ka \cdot X(1)$$

Equation 7

$$\frac{dX(2)}{dt} = \text{RATEIV}(1) + Ka \cdot X(1) - \left(\left(\frac{Cl}{V}\right) \cdot X(2)\right)$$

Equation 8

$$\frac{dX(3)}{dt} = Kpmax \cdot \left(1 - \left(\frac{X(3)}{popmax}\right)\right) \cdot X(3) - Ksmax \cdot \left(\frac{\left(\frac{X(2)}{V}\right)^{Hs}}{EC50^{Hs} + \left(\frac{X(2)}{V}\right)^{Hs}}\right) \cdot X(3)$$

The first 2 equations describe the PK of the drug (compartment 1, theoretical absorptive compartment for oral administration; 2, central compartment). Clearance (CL) is the amount of drug being cleared from the central compartment over time and V is the volume of the central compartment. Ka is the first-order absorption constant. Equation 3 describes the rate of change of the serum GMI values. Kpmax represents the maximum rate of GMI production, popmax is the theoretical maximum density of GMI, Ksmax is the maximum rate of GMI suppression, EC_{50} is the amount of drug where there is half-maximal suppression of GMI, and Hs is the slope function for the GMI suppression.

Acceptance of the final model was evaluated by visual inspection of the observed versus predicted values plotted over time after the Bayesian step and the coefficient of determination (r^2) from the linear regression of the observed versus predicted values. The estimated bias and precision were also considered. After fitting the model to the PK-PD

data, the Bayesian posterior estimates for each patient were used to estimate the concentration–time profiles of both isavuconazole and GMI for each patient. Simulations were performed in ADAPT 5. Isavuconazole and GMI AUCs were calculated by integration from the simulated concentration–time profiles on the last day of dosing (at steady state) in ADAPT 5. In addition, average isavuconazole AUCs (AUC_{ave}) were calculated in Pmetrics by simulating the concentration-time profile for the entire dosing period and dividing by the days on therapy.

The Bayesian posterior estimates for each patient's PK were obtained. These PK parameter values were then fixed for each patient to enable their PD to be estimated. Subsequently, the mean Bayesian posterior estimates were used to calculate the area under the concentration-time curve (AUC) for each patient. The average AUC was calculated by dividing the AUC for the entire dosing duration by the total number of days on therapy. Since MIC was not available, we used a newly described PD index ($AUC:EC_{50}$) to estimate drug exposure in individual patients (42). The EC_{50} is the concentration of drug that causes half-maximal antifungal killing. The relationship between $AUC:EC_{50}$ and the terminal GM was described using an inhibitory sigmoid E_{max} model.

Statistical Analysis. The risk of death through Day 42 over the change in GMI at Day 7 and 14 was estimated using the Cox proportional hazards model. A Goodness of Fit test is used to check the violation of proportional hazards assumption. In this test, if the proportional hazards assumption holds for the covariate (GMI change), then the related Schoenfeld residuals will not be related to event time. The Goodness of Fit test p-values for each model were above 0.05 indicate that the fitted Cox models hold the proportional

hazard assumption. The overall response by EOT was analyzed using a logistic regression model for change in GMI. Not all individuals had GMI measured at each day; therefore, to calculate the above GMI changes, the GMI value of each individual per day was predicted from a joint event-time and longitudinal GMI model. Mortality through Day 42 and overall response at the EOT included time-to-death and time-to-dropout, respectively, as the event-time outcome in each joint model. Dropout was defined if overall response was assessed prior at 84 days. Joint models are effective methods compared with classical linear mixed models to assess longitudinal GMI data. Two data sources of data are modeled simultaneously so that the underlying dependence between the longitudinal GMI and event-time is explicitly acknowledged (91-93). The joint model consisted of a linear model with individual-level intercept, slope and quadratic terms in the random effects model for the time course of GMI and Cox proportional hazard model for the event-time and took the form:

Equation 9

$$y_i(t) = \beta_0 + \beta_1 t + \beta_2 X + U_{0i} + U_{1i} t + U_{2i} t^2 + \varepsilon_i(t)$$

Equation 10

$$\lambda(t) = \lambda_0(t) \exp(\gamma(U_{0i} + U_{1i} t + U_{2i} t^2))$$

where $y_i(t)$ are longitudinal GMI at time t, X is the covariate for treatment (1=isavuconazole; 0=voriconazole) with regression parameter β_2, β_0 and β_1 are population-level (fixed) intercept and slope parameters, respectively, U are the corresponding random effects, ε accounts for measurement error in the time course of GMI, γ allows the association between GMI and event-time, and $\lambda(t)$ is the hazard rate

of event. We used joineR library in R language to fit joint models and “coxph” and “glm” functions in R language were used to fit the Cox and logistic regression models respectively..

For both assessments, we analyzed the total population primarily and then compared the two treatment groups. Prior to the analysis, the baseline co-morbidities were reviewed to evaluate for any imbalances between the isavuconazole and voriconazole populations.

Results

Overview of Patient Characteristics. The original study included 527 patients with 185 ITT patients (71%) having positive baseline serum GMI (48). Of these, 158 mITT patients (79 isavuconazole-treated and 79 voriconazole-treated) were available. Seventy-eight of the isavuconazole-treated patients with plasma concentrations were eligible for the PK-PD sub-analysis. The patient demographics and baseline characteristics are summarized in **Table 4**. The isavuconazole-treated patients included numerically more patients with hematological malignancies, allogeneic hematopoietic stem cell transplant, use of T-cell immunosuppressants, use of corticosteroids, and neutropenia at baseline. The median white blood cell (WBC) count at baseline was lower (0.3 versus 0.4 x 10^9 cells/liter; p=0.0152); however, this difference is not likely clinically relevant. Baseline median GMI in the isavuconazole group were significantly lower (0.8 versus 1.2; p=0.0011). Except for a significant difference in gender (p=0.0022), the remaining demographics were similar between the 2 treatment groups.

Table 4 Patient Demographics and Characteristics at Baseline

	Isavuconazole N=79	Voriconazole N=79	Total N=158	p-value (Chi-squared test)
Sex				
Male	36 (46%)	56 (71%)	92 (58%)	0.0022
Female	43 (54%)	23 (29%)	66 (42%)	
Race				
White	67 (85%)	56 (71%)	123 (78%)	
Asian	11 (14%)	23 (29%)	34 (22%)	
Other	1 (1%)	--	1 (1%)	
Age (years)				
Mean ± SD	52.4 ± 16.1	50.7 ± 15.2	51.5 ± 15.7	
Weight (kg)				
Mean ± SD	68.4 ± 14.6	69.9 ± 14.6	69.2 ± 14.6	
Underlying Disease				
Hematological Malignancy	77 (97%)	70 (89%)	147 (93%)	0.0563
Active Malignancy	60 (76%)	59 (75%)	119 (75%)	1.0
Allogeneic HSCT	27 (34%)	19 (24%)	46 (30%)	0.2203
Baseline Neutropenia	62 (78%)	55 (70%)	117 (74%)	0.2762
T-cell Immunosuppressants	40 (51%)	34 (43%)	74 (47%)	0.4254
Use of Corticosteroids	15 (19%)	11 (14%)	26 (16%)	0.5198
Baseline GMI				
Median (range)	0.8 (0.1 – 6.2)	1.2 (0.5 – 9.7)	1.0 (0.1 – 9.7)	0.0018
Duration of Therapy (days)				
Mean ± SD	50.2 ± 31.0	51.6 ± 31.6	50.9 ± 31.2	
Min-Max	5-85	2-88	2-88	

Median	53	53	53

Abbreviations: N: number; SD: standard deviation; HSCT: hematopoietic stem cell transplantation

The efficacy outcomes for the 2 treatment groups were comparable to the primary study analyses (48). However, the numerical differences in the outcomes were reflective of the higher number of immunosuppressed patients in the isavuconazole group **(Table 5)**.

Table 5 All-Cause Mortality through Day 42 and Overall Response at the End of Therapy

	Isavuconazole N=79	Voriconazole N=79	Total N=158	95% CI; p-value
All-Cause Mortality through Day 42	16 (20%)	12 (15%)	28 (17.7%)	-8.1, 20.3%; 0.5320
Successful Overall Response at EOT	26 (33%)	30 (38%)	56 (35.4%)	-21.2, 11.1%; 0.6178

Abbreviation: EOT: end of therapy

Change in GMI by Survival Status Through Day 42. The joint event-time longitudinal model predicted the Day 7 GMI very closely compared to measured values in the subset of subjects with available data, Pearson correlation coefficient 0.90, p=0.0001 (**Figure 6A-E**), increasing confidence about the associations between Day 7 GMI change and outcomes, even if Day 7 GMI was not measured in all patients. The average observed and predicted longitudinal trajectories for the outcomes are almost identical (**Figure 6A and B**). Residuals display no obvious systematic pattern (**Figure 6C** and **D)**, for the 42-day mortality and scatter plots were similar for the overall outcome). There is strong agreement between the predicted GMI and observed GMI at Day 7; the correlation coefficients were 0.89 and 0.91 ($p < 0.0001$) based on a log scale and original GMI scale, respectively, for the 42-day mortality (**Figure 6E**), and the values were similar for the overall response.

Figure 6 A-E Model statistics for joint event-time longitudinal model-predicted Day 7 GMI (A and B) Joint event-time longitudinal model predicted Day 7 GMI for mortality and overall response, respectively. (C, D, E) Model statistics demonstrating the acceptable predictions produced by the model for the predicted ay 7 GMI values.

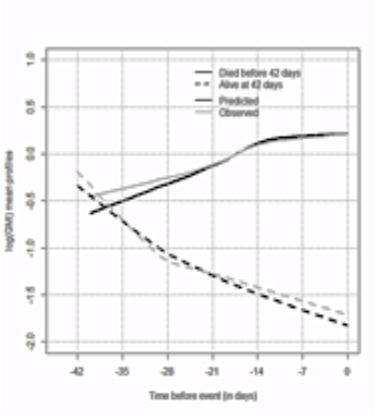

(A)

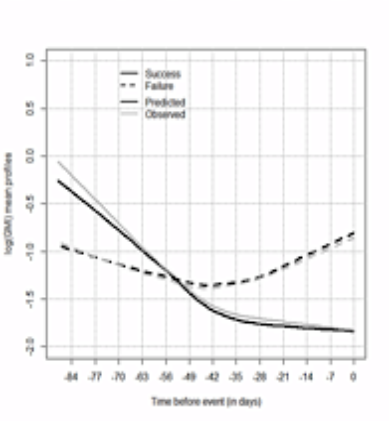

(B)

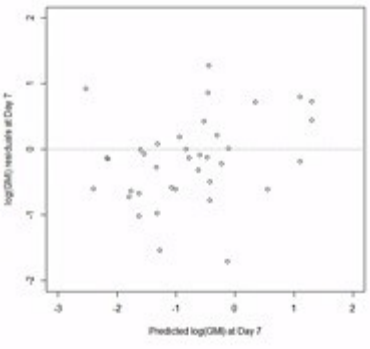

(C)

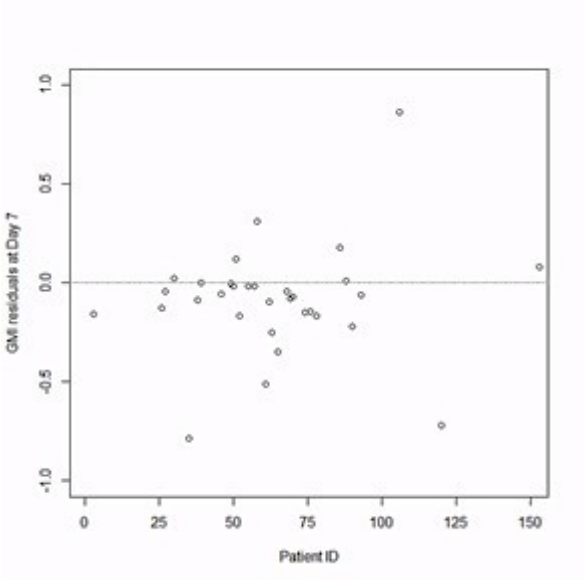

(D)

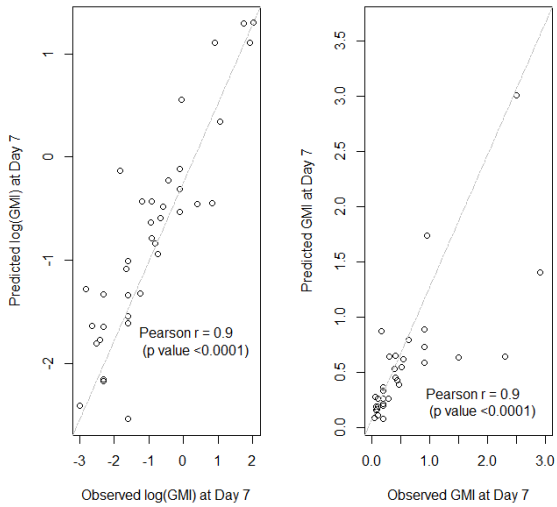

(E)

GMI steadily increased for the patients that died. The values for the patients that survived remained below 1.0, steadily declining during therapy (**Figure 7)**.

Figure 7 Predicted GMI mean profile from the joint model with treatment as a covariate in the longitudinal component for the overall population. Time=Day 0 is the time when a patient died (cases) or had last follow-up alive (controls). GMI values were predicted at each day before event (death/alive). Negative values correspond to days before event.

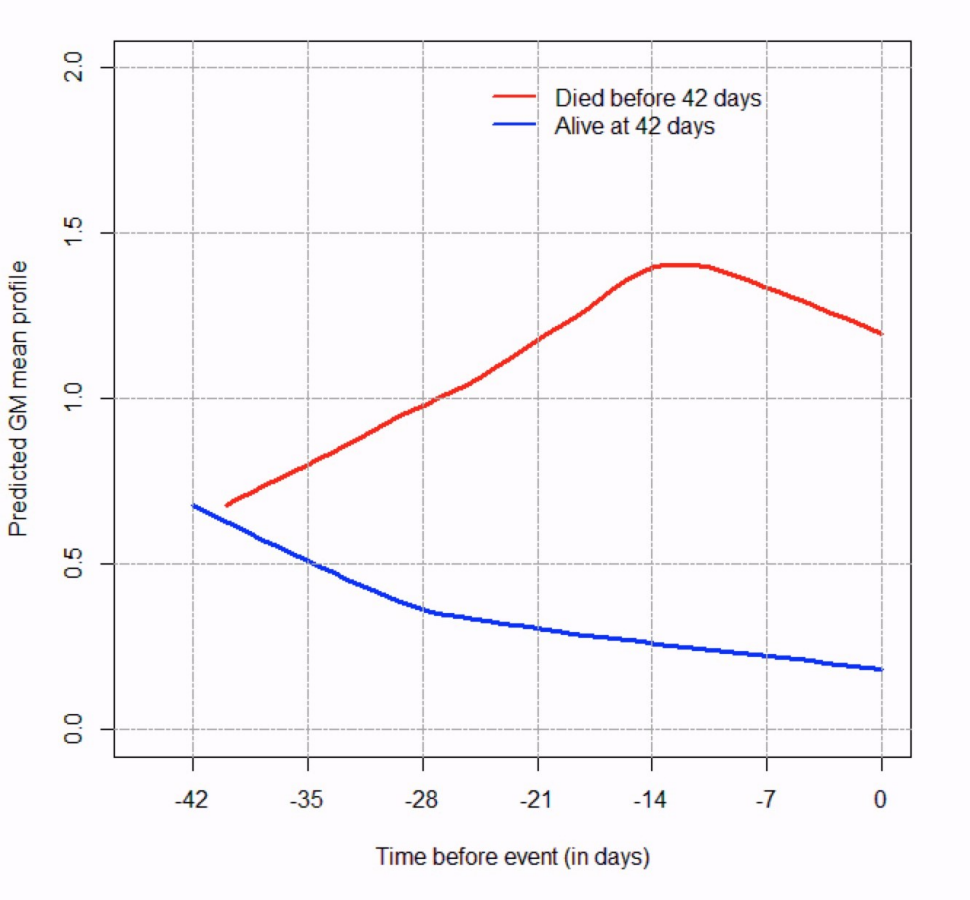

Changes in GMI by Day 7 (i.e. model-predicted Day 7 GMI minus baseline GMI) for the patients who died (**Figure 8A**) were more positive than for those that survived (**Figure 8B**). A 3- and 1.7-fold increase in the risk of death was found for each unit increase in GMI from baseline to Day 7 [Hazard Ratio (HR) 3.008; 95% confidence

interval (CI) 1.993, 4.541; p<0.0001] (test statistic 0.282 (p = 0.207)) and Day 14 [HR 1.69; 95% CI 1.368, 2.087; p<0.0001] (test statistic 0.327 (p = 0.119)), respectively.

Figure 8 Change in GMI at Day 7 from Baseline for patients who (A) died and (B) survived (Overall population). (A) Frequency of change in GMI value by Day 7 for patients that died. (B) Frequency of change in GMI value by Day 7 for patients that survived.

A.

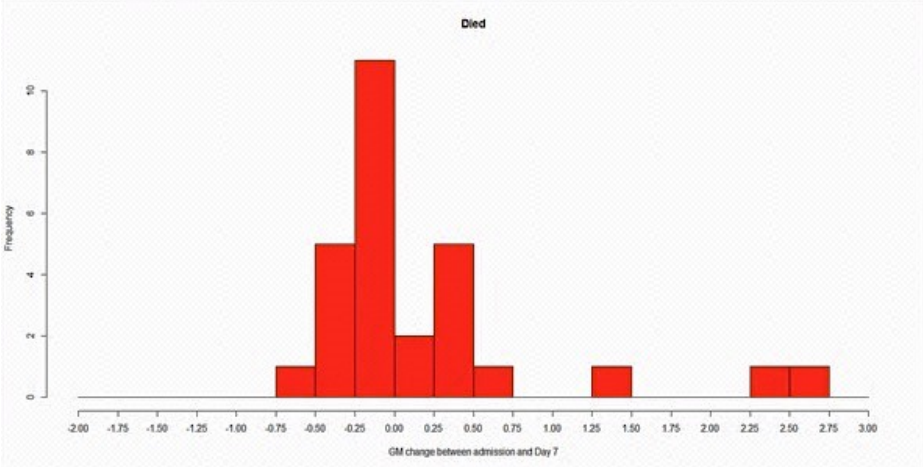

B.

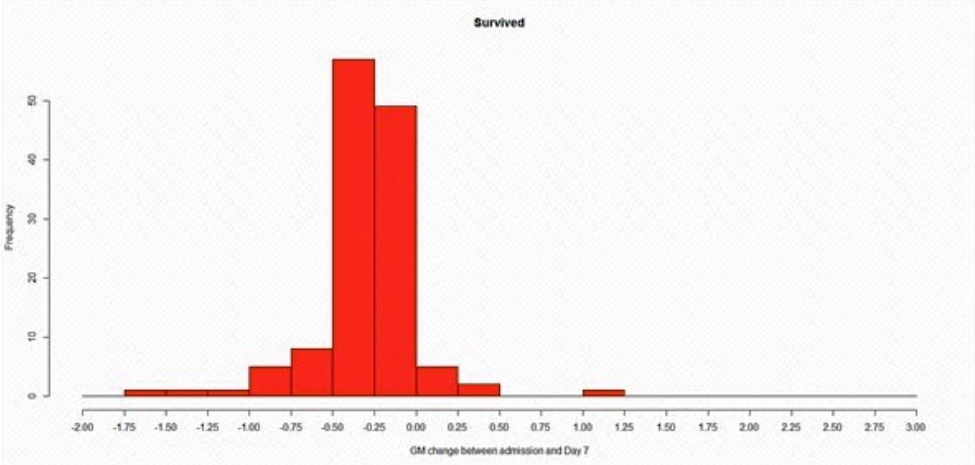

If GMI was treated categorically, an increase in GMI by Day 7 of more than 0.25 GMI units from baseline increased the overall risk of death nearly 10-fold higher than those patients with GMI changes ≤0.25 at Day 7 (test statistic 0.029 ($p = 0.878$)). The change in GMI of >0.25 from baseline to Day 14 predicted an overall 8-fold risk of death [HR 8.37; 95% CI 0.120, 3.748; $p<0.0001$] (test statistic 0.001 ($p = 0.996$)).

Because of differences in the underlying co-morbidities between the two treatment groups, we focused the analysis on the total population of patients rather than compare the two treatment groups. In patients that died, the GMI was higher among isavuconazole-treated patients (**Figure 9**). Neutropenia was assessed using a linear mixed-effects model for the longitudinal measures of GMI with an interaction term between neutropenia and drug arms. No prominent differences were found between drugs, neutropenic status, and GMI over time ($p=0.1127$).

Figure 9 Observed GMI mean profile for each treatment group in the longitudinal component. Time=Day 0 is the time when a patient died (cases) or had last follow-up alive (controls). Mean GMI values were computed at each day before event (death/alive). Negative values correspond to days before event. (Left) Patients treated with isavuconazonium sulfate, (Right) Patients treated with voriconazole.

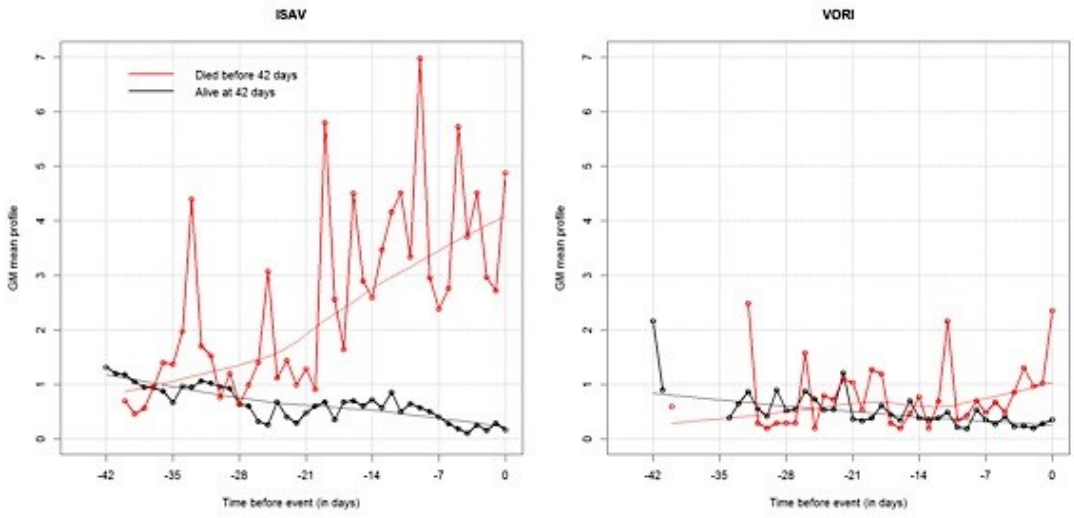

Change in GMI by Overall Response at the End of Therapy. The GMI at the EOT was also higher in patients that failed therapy compared to those with a successful overall response (**Figure 10**). For GMI increases of one unit from baseline to Day 7, the odds of successful overall response were reduced by half. Conversely, if the GMI decreased one unit by Day 7, the success rate more than doubled (odds ratio (OR)=2.154, 95% CI 1.173, 3.955). If the GMI decreased by more than 0.25 units, the successful overall response was increased by approximately 43% compared to that if GMI increased, although this change was not significant (p=0.0704). By Day 14, the success rate decreased by 35.5% for every unit increase in GMI (p=0.0318). If the GMI decreased by more than 0.25 units, the

success rate increased by approximately 21% compared to that if GMI increased, although this change was not significant (p=0.2360).

Figure 10 Predicted Mean GMI profile at the end of therapy for patients with a successful overall response (black line) and those that failed (dashed line). Time 0 represents the assessment day (end of therapy). (Overall population)

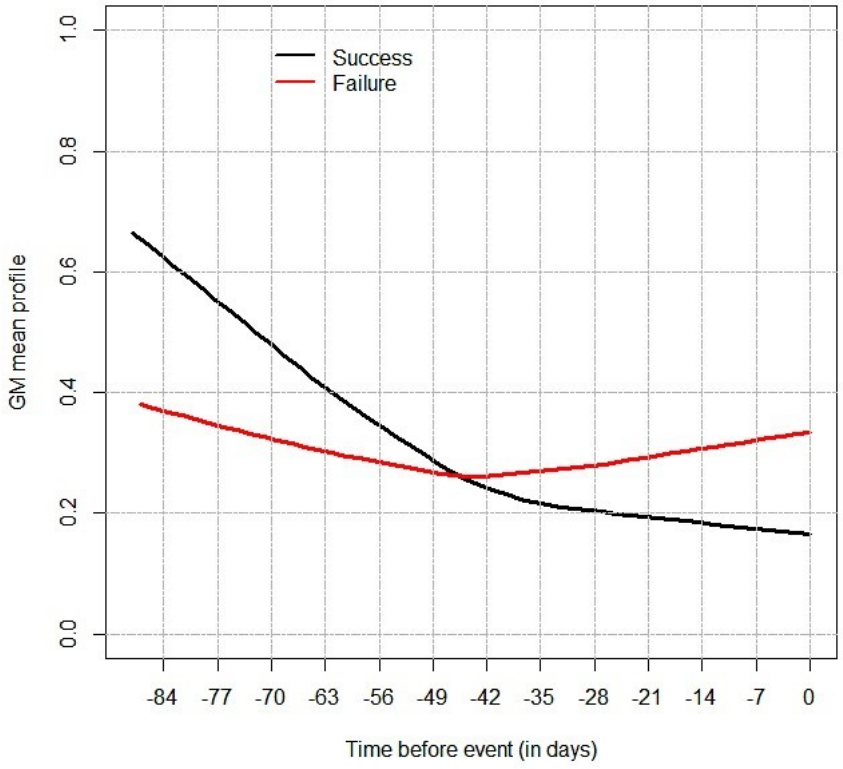

Pharmacokinetic-Pharmacodynamic Characteristics of Isavuconazole-Treated Patients. Seventy-eight isavuconazole-treated patients with positive baseline GMI had plasma concentrations and serial GMIs during therapy available for the PK-PD analysis. A 1-compartment model plus an absorptive compartment fitted the data well. Visual inspection of the observed versus predicted concentration values was acceptable. The

coefficient of determination (r^2) of predictions based on median Bayesian posterior parameter values for each subject was 0.829 and estimates of bias and imprecision were also acceptable (0.164 and 1.04, respectively).

The Bayesian posterior parameter estimates from the population PK model were calculated for each patient and included as fixed covariates in the data file. The fit of the linked PK-PD model to the data was good (see **Figure 11A and Figure 11B**). The coefficient of determination of the linear regression of observed-predicted values (r^2) after the Bayesian step was 0.859. Visual inspection of the observed-versus-predicted concentrations were acceptable and measures of bias and imprecision were reasonable (-0.155 and 0.328, respectively).

Figure 11 A and B. Regression plot of the observed (y-axis) versus model predicted (x-axis) plots from the linked PK-PD model for PK (A) and GMI (B). (A) Logistic regression of the observed versus predicted plasma concentrations. Coefficient of determination (r2) of 0.829. Measures of bias and imprecision of 0.164 and 1.04, respectively. (B) Logistic regression of the observed versus predicted GMI values: Coefficient of determination (r2) of 0.859. Measures of bias and imprecision of -0.155 and 0.328, respectively. Dotted lines represent the line of unity and open circles represent the individual values.

A.

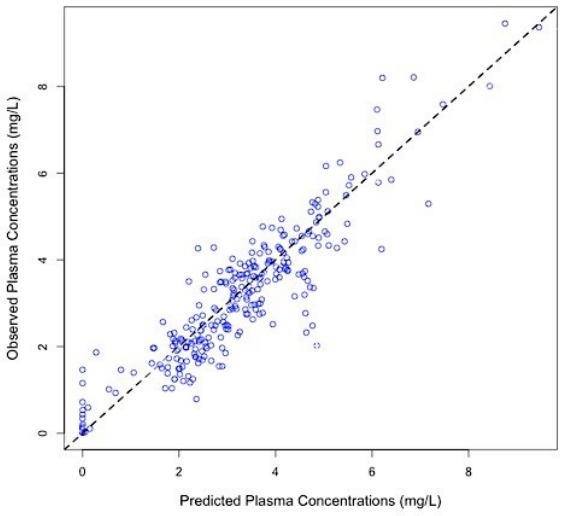

B.

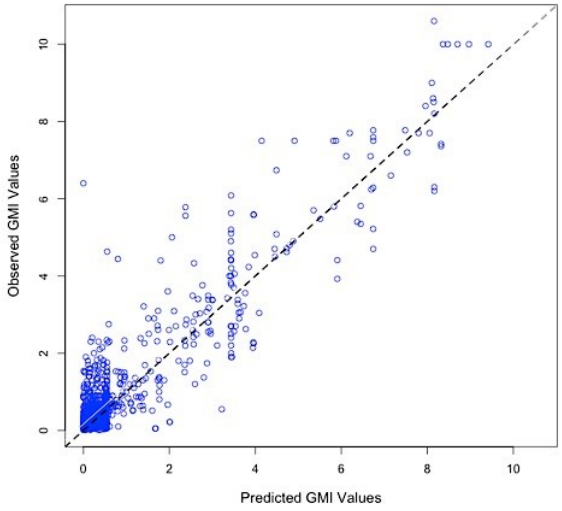

The parameter estimates from the final model for PK and PD are summarized in the **Table 6**.

Table 6 Mean and standard deviations (SD) values for each parameter estimated from the linked population PK-PD model

Parameter (units)	Mean	SD
Ka (h^{-1})	4.85	3.77
Cl/F (L/h)	2.08	0.93
V/F (L)	274.74	233.35
Kpmax (GMI/h)	0.01	0.03
Hs	14.80	5.35
EC_{50} (mg/L)	0.90	1.46
Ksmax (GMI/h)	0.01	0.04
IC (GMI)	1.27	1.55
Popmax (GMI)	5.24	2.34

SD**,** standard deviation; Ka, the first-order rate constant describing the movement of drug from the gut to the central compartment; Cl, clearance from the central compartment; F, bioavailability; V, volume of the central compartment; Kpmax, the maximum rate of GM production, Hs, the slope function for suppression; Ksmax, the maximum rate of GM suppression, EC_{50}, the amount of drug where there is half maximal suppression; IC, initial condition of GMI prior to drug exposure; Popmax, the theoretical maximum density of GMI.

The relationship of the exposure to the predicted GMI at the EOT is shown in **Figure 12**. An AUC:EC_{50} of 108.6 or more resulted in a GMI <0.5. No relationship between change in GMI by Day 7 or GMI at the EOT and average exposure (AUC_{ave}) was demonstrated, consistent with previous analyses (94).

Figure 12 Inhibitory sigmoid Emax curve demonstrating the PK-PD relationship of isavuconazole AUC:EC_{50} and GMI values at the end of treatment (terminal GMI). Logistic regression resulted in an r2 of 0.237. Solid line represents the sigmoid curve fit of the model to the data, black squares represent the observed GMI values for each patient, and GMI negative value is included as a dotted line.

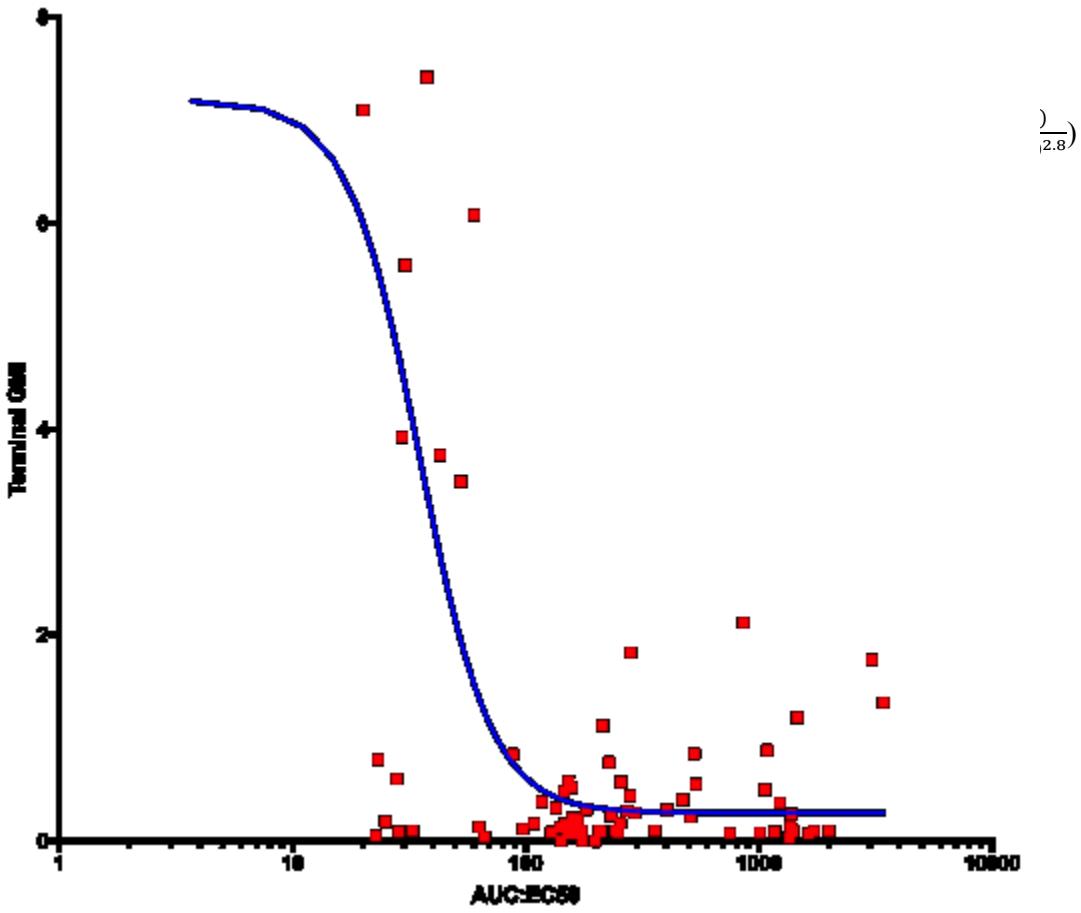

Discussion

We demonstrated that early changes in GMI (within 1 week) are significantly linked to clinical response and mortality. An increase in GMI after 1 week of therapy >0.25 GMI units is associated with a ~ 10-fold increased risk of death compared to patients who had no change from baseline, decreased GMI, or had an increase of <0.25 units. Based on

the Platelia GM assay performance, 0.25 units is within the range of inter-assay variability. However, our results suggest that this threshold of response by Day 7 is predictive of clinical response and mortality. Moreover, for any 1-unit increase in GMI from baseline to Day 7, the risk of mortality increases 3-fold. These results can now be used in a prospective study examining GM for directing antifungal therapy. If by the end of week 1 of treatment the GMI is increasing, and is >0.25 above the baseline value, treatment could be modified.

All-cause mortality in SECURE was 19.4% (48). In this subset, the rate was similar (17.7%); however, the number of deaths was just over a quarter of the number in the original study (28 versus 100 patients). Even with smaller numbers, the p values describing the significance of GMI change by Day 7 in predicting outcome are quite low, suggesting that attributable mortality associated with IA as per increasing GMI is relatively high.

This analysis is consistent with previous studies in which serial GMI measurements were correlated with patient outcomes. A meta-analysis of > 20 studies showed that a negative GMI within 1 week of outcome assessment is highly correlated with survival and successful outcome (alive or death without findings of aspergillosis at autopsy) (20). Most reports have consistently reported that increasing GMI during therapy correlate with unsatisfactory clinical responses or mortality (18, 19, 21, 38-40, 95). In contrast to another analysis of a clinical trial where a correlation was found for overall response but not for 12-week survival (39), we report a change in GMI by the end of week 1 was significantly higher for patients that died through Day 42 and in patients who had a failure in overall response at the EOT. In our study, a GMI change of >0.25 at 2-weeks

was significantly associated with mortality but not overall response. In each analysis, the association of GMI changes by Day 14 was not as strong as Day 7. As per Chai et al, status of the underlying disease and co-morbidities are increasingly powerful determinants of the final outcome with the passage of time (39).

Together with clinical care of patients with IA, these findings will be helpful for designing and assessing clinical trials of new anti-*Aspergillus* agents in GM positive patients. An increasing GMI of >0.25 after the first week of therapy could be validated, as an early marker of ultimate clinical failure and trigger a change in therapy, the addition of another agent, or an increase in dosage. A GMI <0.5 of >2 weeks duration was highly correlated with successful response and this has been proposed as a potential clinical trial endpoint (18). We did not find a specific GMI cut-off value that linked with outcome at the end of week 1. Rather, our analyses suggested that early stabilization of GMI was highly correlated with an increased likelihood of successful outcome and survival, suggesting that an individual patient may not require absolute negativity of their GMI early in therapy to achieve ultimate therapeutic success.

For the subset of patients with isavuconazole concentrations, we estimated the AUC:EC_{50} that results in a negative GMI at the EOT. We were unable to define a relationship between traditional measures of drug exposures (e.g. C_{min} and AUC) and either clinical response or survival (96). Our inability to identify a threshold of exposure (e.g. AUC_{ave}) linked with response (change in GMI) could be because the regimen used in the trial provided exposures above those where thresholds are detectable (i.e. drug exposures had already elicited maximal antifungal responses).

We used a newly described PD index of AUC:EC_{50} for our analysis because the MIC is rarely available for patients with IA. The EC_{50} is the estimated in vivo drug concentration that is required for half maximal antifungal killing. The EC_{50} requires some skills in PK-PD modeling and is estimated directly from the data rather than in the laboratory. It is an *in vivo* MIC where the patient declares what drug concentrations (s)he requires to adequately treat their individual disease. The AUC:EC_{50} provides an alternative way of evaluating the exposure-response relationships in the absence of a MIC for the invading pathogen, provided a biomarker, such as GMI, exists to determine the response of the organism to the drug concentrations.

Beyond drug, factors such as impaired host function, persistent neutropenia, dosage and duration of corticosteroids, immunosuppressive therapies, GVHD, and concomitant infections (e.g. CMV viremia) could drive poor outcomes. These factors cannot be accounted for in model equations. Thus, the results should be interpreted carefully.

Of the 185 patients with positive baseline GMI that were enrolled in the clinical trial, only 158 had serial GMI values and were included in this analysis. A review of the non-included patients was conducted to evaluate the potential for selection bias. The only reason for the exclusion of these patients was due to the missing serial GMI values after baseline, which were required for the analysis. All of the non-included patients had proven or probable IA. The largest proportion (65%) of the patients not included discontinued prior to the protocol requirement for serial GMI (D14). The median treatment duration of the patients not included was 7.5 days (range 1-84 days). Fifty percent of these cases died on or before day 42 compared to 18% for the population of patients included in the analysis. Often in research, missing data are imputed to reduce

the impact of selection bias. However, in the case of missing biomarker data such as GMI, it is inappropriate to impute.

In conclusion, our analyses suggest that early trends in GMI are highly predictive of the ultimate therapeutic outcome. Increases in GMI by the end of the first week after therapy could trigger a change in treatment. Further validation is required to determine if the results hold. Such information may improve the likelihood of improved clinical responses and survival for a disease for which therapeutic outcomes remain persistently suboptimal.

Chapter 5 Isavuconazole Population Pharmacokinetic Analysis Using Non-Parametric Estimation in Patients with Invasive Fungal Disease: Results from the VITAL Study

Abstract

Background. Isavuconazonium sulfate, a water-soluble prodrug of the triazole antifungal agent, isavuconazole, is available for the treatment of invasive aspergillosis (IA) and invasive mucormycosis (Astellas Pharma Inc, Cresemba® [isavuconazonium sulfate] 2015, http://www.astellas.us/docs/cresemba.pdf).

Methods. A population pharmacokinetic (PPK) model was constructed using non-parametric estimation to compare the pharmacokinetic (PK) behavior of isavuconazole in patients treated in the phase 3 VITAL open-label clinical trial, which evaluated the efficacy and safety of the drug for treatment of renally-impaired IA patients and in patients with invasive fungal disease (IFD) caused by emerging moulds, yeasts, and dimorphic fungi. Covariates examined were body mass index (BMI), weight, race, impact of estimated glomerular filtration rate (eGFR) on clearance (CL), and impact of weight on volume. PK parameters were compared based on IFD type and other patient characteristics. Simulations were performed to describe MIC covered by the clinical dosing regimen.

Results. Concentrations (n = 458) from 136 patients were used to construct a 2-compartment model (first-order absorption and central compartment). Weight-related covariates affected clearance, but eGFR did not. PK parameters and intersubject

variability of Cl were similar across different IFD groups and populations. Target attainment analyses demonstrated that the clinical dosing regimen would be sufficient for total drug area under the concentration-time curve (AUC):MIC targets ranging from 50.5 for *Aspergillus* spp. (up to CLSI MICs of 0.5 mg/L) to 270 to 5,053 for *Candida albicans* (up to MICs of 0.125 and 0.004 mg/L, respectively) and 312 for non-*albicans Candida* spp. (up to MICs of 0.125 mg/L). The estimations for *Candida* spp. were exploratory considering that no patients with *Candida* infections were in the current analyses. (The VITAL trial is registered at clinicaltrials.gov under NCT00634049.)

Conclusion. We constructed a PPK model with a goal to evaluate the exposures across different patient populations. We did not find significant differences between the populations of IFDs and different populations. It is important to continue to investigate the PK characteristics and exposure in critically ill patients to ensure exposures are adequate.

Introduction

Isavuconazonium sulfate is the water-soluble prodrug of the novel, broad-spectrum, triazole antifungal agent isavuconazole and is available in cyclodextrin-free intravenous (i.v.) and oral (p.o.) formulations (78). The US Food and Drug Administration and European Medicines Agency recently approved isavuconazole for the treatment of invasive aspergillosis (IA) and invasive mucormycosis (IM). The approval in the European Union for mucormycosis is for patients for whom amphotericin B is inappropriate. Many of the pharmacokinetic (PK) analyses reported to date are limited to healthy volunteers and patients treated for IA. There is a paucity of data regarding the population pharmacokinetics (PPK) in patients with a variety of invasive fungal infections and underlying diseases.

In vitro data for isavuconazole have demonstrated broad spectrum activity against a variety of fungi, including *Aspergillus* spp., *Candida* spp., Mucorales, *Cryptococcus* spp., and dimorphic and other rare fungi (50). *In vivo* models have also been conducted, demonstrating concentration-dependent antifungal activity for the treatment of invasive pulmonary aspergillosis, disseminated aspergillosis, disseminated candidiasis, mucormycosis, and cryptococcal meningitis (15, 51, 52, 54, 97). The VITAL clinical trial evaluated the efficacy and safety of isavuconazole for treatment of a variety of invasive fungal diseases (IFD), including the treatment of IA in patients with renal impairment and treatment of patients with diseases caused by emerging moulds, yeasts, and dimorphic fungi. Isavuconazole demonstrated successful outcomes for patients with IA and IM, with all-cause mortality rates through day 42 of 12.5% and 37.8%, respectively, for these patients. Successful outcomes have also been reported for patients with IA and renal

impairment, and for patients with infections caused by *Cryptococcus* spp., dimorphic fungi (such as *Coccidioides* spp., and *Paracoccidioides* spp.), *Fusarium* spp., and *Scedosporium* spp. (49, 55-59, 98).

A previous PPK analysis was conducted using isavuconazole concentration-time data collected from nine phase 1 pharmacokinetic (PK) studies of healthy subjects and the phase 3 SECURE trial of patients with IA (47). These analyses demonstrated that a 3-compartment model fit the data well (absorption, central, and peripheral compartments). The PK profiles were similar between healthy subjects and patients with IA. In addition, isavuconazole demonstrated linear PK over the range of dosages (40–400 mg) that were examined.

An understanding of the PK of novel compounds in various patient populations is a first critical step for optimal clinical use. The phase 3 VITAL trial provides the opportunity to compare PK characteristics of a population of patients infected with a variety of fungal pathogens. This is especially important for critically ill or severely immunosuppressed patients and in circumstances where organ function is compromised. In the current analysis, we constructed a PPK model for patients enrolled in the phase 3 VITAL trial, with the goal of comparing PK across the different patient populations to further understand the optimal use of isavuconazole.

Materials and Methods

***Study design*.** The VITAL trial (ClinicalTrials.gov identifier: NCT00634049) evaluated the efficacy and safety of isavuconazole for the treatment of proven or probable IA in patients with renal impairment and for treatment of patients with proven or

probable IFD caused by Mucorales and other emerging moulds, yeasts, and dimorphic fungi. Patients were eligible whether they required primary therapy or were refractory or intolerant to their previous systemic antifungal therapy. Patients received a loading regimen of either i.v. or p.o. isavuconazonium sulfate at a dose of 372 mg (equivalent to 200 mg isavuconazole) every 8 h for the first 48 h, followed by i.v. or p.o. isavuconazonium sulfate 372 mg once daily for up to a maximum of 180 days. The institutional review board at each center approved the study protocol, and all research subjects provided written informed consent.

Plasma PK sampling. Blood samples were collected from each patient on treatment days 7, 14, 42, and at the end of therapy. Collection was targeted at the time point 24 h after the start of the infusion or the p.o. dose the previous day (i.e., trough concentration). Full 24-h profiles were obtained from a subset of 33 patients. After collection, samples were processed immediately and stored at –80°C until shipment to the central research laboratory.

Bioanalytical analysis. Isavuconazole (BAL4815) and inactive cleavage product (BAL8728) concentrations in plasma samples were measured using a validated liquid chromatography-tandem mass spectrometry (LC-MS/MS) method at PPD, LLC (Pharmaceutical Product Development, LLC, Middleton, WI, USA). A plasma sample volume of 50 µL was combined with the internal standard (d_4-isavuconazole/pyridooxazinone) and subjected to protein precipitation using acetonitrile. Following centrifugation for 10 min at 5°C, 75 µL of the supernatant was isolated for dilution with water:formic acid:ammonium hydroxide (1000:10:0.5, vol/vol/vol)/acetonitrile (850:150, vol/vol) and then submitted for analysis.

Chromatographic separation was achieved using a Synergi Polar-RP column (20 mm by 2.0 mm by 4 µm, Phenomenex, Torrance, CA, USA) with a gradient mobile phase consisting of water, acetonitrile, methanol, and formic acid. An API3000 mass spectrometer (AB Sciex, Framingham, MA, USA) in positive ion mode was used to monitor the analytes. Multiple-reaction monitoring transitions were *m/z* 438.1→224.1 for isavuconazole, 165.0→121.2 for inactive cleavage product, 442.1→224.1 for d_4-isavuconazole, and 151.1→123.2 for pyridooxazinone. The validated curve range was 5 to 1,250 ng/mL for both isavuconazole and inactive cleavage product, and any samples measuring above the upper limit were diluted 5-fold, 10-fold, or 20-fold prior to analysis. The lower limit of quantification (LOQ) was 5 ng/mL. Inter-assay precision (coefficient of variation [%]) of the BAL4815 quality control samples (12.5, 25, 75, 250 and 1,000 ng/mL) was 6.1%, 4.6%, 3.1%, 2.5%, and 2.6%, respectively, while the inter-assay accuracy (relative error, [%]) were 2.4%, 3.6%, 3.1%, 2.3%, and 0.2%, respectively. Interassay precision of the BAL8728 quality control samples (12.5, 25, 75, 250 and 1,000 ng/mL) was 7.0%, 7.1%, 5.9%, 8.5%, and 6.5%, respectively, while the interassay accuracy was -1.9%, -0.4%, -1.0%, 2.1%, and 2.8%, respectively. All study samples were analyzed within the established long-term stability of the drug (isavuconazole) (955 days at –70°C). All PPK analyses were conducted on the isavuconazole concentrations due to the lack of antifungal activity of the cleavage product.

PPK Modeling. A PPK model was developed using nonparametric estimation in Pmetrics software (v1.3.2, University of Southern California, Los Angeles, CA, USA) (77). The model-fitting process included evaluations of both 2- and 3-compartment models, including absorptive compartments with and without a lag-time. Data were

weighted by the inverse of the estimated assay variance. Acceptance of the final model was evaluated by visual inspection of the observed versus predicted concentration values before and after the Bayesian step, the coefficient of determination (r^2) from the linear regression of the observed versus predicted values, and estimates for bias (mean weighted error) and imprecision (adjusted mean weighted squared error).

The impacts of body mass index (BMI), weight, and race (Asian versus other) on clearance, and of weight on volume were initially assessed as covariates by visual inspection of the graphical representation of each covariate versus clearance and volume to evaluate for inclusion in the final model. The covariates were chosen based on results of previous PPK studies with isavuconazole (99). In addition, this study permitted the enrollment of patients with renal impairment, in contrast to the phase 3 SECURE trial. Therefore, the impact of estimated glomerular filtration rate (eGFR) on clearance was also evaluated. The eGFR was calculated using serum creatinine level and the "modification of diet in renal disease" formula.

The average daily area under the concentration-time curve (AUC_{avg}) for each patient was calculated using the Bayesian posterior parameter estimates from the final model using the trapezoidal rule in Pmetrics. AUC_{avg} was calculated by determining the total AUC over the entire dosing period and dividing it by the number of days of therapy for each patient. The patients were subclassified according to the type of IFD diagnosed at baseline and baseline underlying disease. The PK parameters of the patient subsets were evaluated separately and compared with the overall data set and with those from the previously reported PPK model with isavuconazole (99). Statistical comparisons were performed in MYSTAT 12 (version 12.02; Systat Software, Inc.; http://www.systat.com).

Simulations of 5,000 patients were performed in Pmetrics to assess the probability of target attainment (PTA) for the approved clinical dosing regimen to achieve the various total drug AUC:MIC pharmacodynamic (PD) targets estimated from preclinical models for different organisms (i.e., *A. fumigatus*, *C. albicans*, *C. glabrata,* and *C. tropicalis*) (52, 100, 101). The choice to use total drug AUC:MIC targets was considered acceptable since protein binding is similar between humans and the animal models used to estimate the targets.

Results

Study population. In total, 458 isavuconazole concentrations from 136 patients were included in the model. **Table 7** summarizes the key patient demographics and clinical characteristics. The majority of the patients were white. The mean (± standard deviation [SD]) weight and BMI were 70.2 ± 19.5 kg and 24.4 ± 5.9 kg/m^2, respectively. Fifty-three patients (39%) had an eGRF < 60 mL/min/1.73 m^2 at baseline, and the mean eGFR for the total population was 80.2 mL/min/1.73 m^2. A total of 65 patients (48%) had one or more of the following: hematologic malignancy, active malignancy, or baseline neutropenia. Forty-one percent (*n* = 56) of the overall population had hematologic malignancies, and 30% (*n* = 41) had active malignancy at enrollment. One-fourth (*n* = 34) of patients were neutropenic (absolute neutrophil count [ANC] values of <500/mm^3) at baseline. Twenty-four of 65 patients with hematologic malignancies had all three baseline characteristics combined, 13 patients were described as having active hematologic malignancies at baseline and five had both hematologic malignancies and baseline neutropenia. Fourteen were reported as having only hematologic malignancies, four had only active malignancies, and five had only neutropenia. Seventy-one patients

did not have any of the three characteristics reported at baseline. Further, 17% had received an allogeneic hematopoietic stem cell transplant, and the use of T-cell immunosuppressants and corticosteroids was reported in 41% and 24% of the overall population, respectively. In addition to IM (n = 34) and IA (n = 20), the analysis included patients with IFD caused by other fungal pathogens as summarized in **Table 7**. After IM, the next most commonly enrolled IFDs were caused by dimorphic fungi, such as *Coccidioides* spp., *Paracoccidioides* spp., and *Histoplasma* spp.

Table 7 VITAL patient demographics and clinical characteristics

	No. of patients					
Patient population (*n*)	White	Asian	Black	Other	Body weight (kg) [a]	BMI (kg/m^2) [a]
Overall (136)	100	23	9	4	70.2 ± 19.5	24.4 ± 5.9
Patients with infection						
IA (20)	18	2	0	0	68.0 ± 20.7	23.2 ± 4.7
IM (34)	23	8	3	0	73.4 ± 18.6	25.3 ± 5.5
Other filamentous fungi and moulds (23)	17	4	2	0	72.8 ± 25.0	25.1 ± 7.1
Dimorphic (29)	20	4	2	3	64.2 ± 16.1	23.0 ± 5.8
Non-*Candida* yeasts (10)	5	3	1	1	61.9 ± 11.7	22.2 ± 3.3
Mixed infection (13)	11	1	1	0	75.0 ± 18.7	26.1 ± 7.5
No pathogen identified (7)	6	1	0	0	79.2 ± 20.4	27.7 ± 5.6

[a] Data are mean ± SD.

A 2-compartment model which included a first-order absorptive compartment fit the data well. **Figure 13** shows a schematic of the structural model. Compartment 1 represents the absorptive compartment (i.e., gut) and compartment 2 represents the central compartment.

Figure 13 Illustration of the structural model. The boxes represent the modeled compartments (1=theoretical absorptive compartment and 2=central compartment). The arrow connecting compartment 1 and 2 shows the flow of drug from the gut to the central compartment. The arrow from the central compartment represents elimination of drug from the central compartment at a rate associated with CL over V. Abbreviations: CL, clearance; F, oral bioavailability; Ka, first-order absorption rate constant; Tlag, lag-time; V, volume in the central compartment.

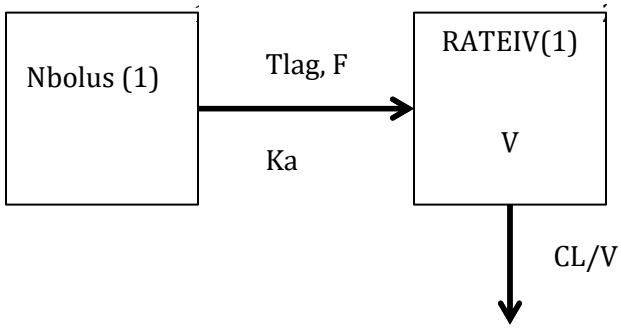

The fit of the PPK model was acceptable based on visual inspection of the observed versus predicted plots and the coefficient of determination (r^2) of 0.89 for the observed versus the posterior predicted values after the Bayesian step (**Figure 14**). The estimates of bias and imprecision were also acceptable (–0.0539 and 2.77, respectively). Evaluation of a 3-compartment model did not result in a better fit of the model to the data.

Figure 14 Observed versus posterior predicted concentrations (mg/L) from the final model after the Bayesian step. Statistics: r2= 0.89, slope = 1.05 [95%CI 1.01 to 1.08], intercept = -0.0484 [95%CI −0.179 to 0.0825]. The dotted line is line of unity where observed concentrations equal predicted concentrations.

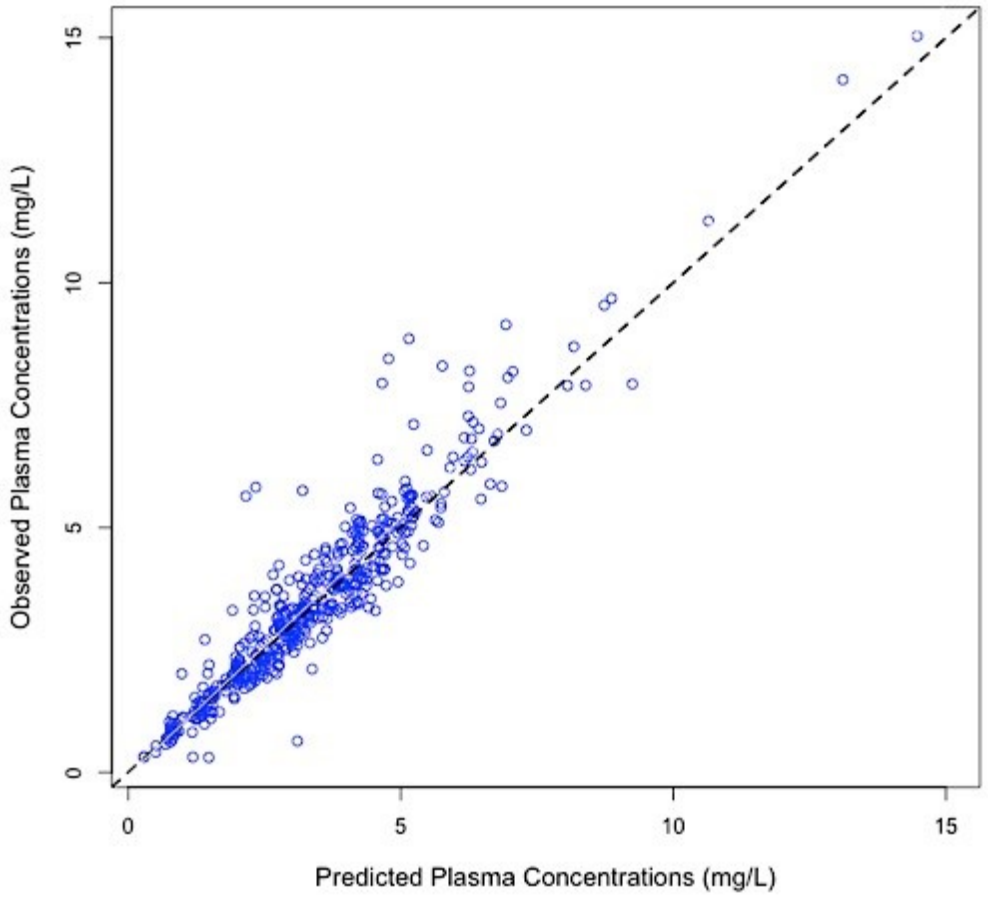

There was not a statistically significant impact of eGRF and Asian ethnicity on clearance (**Figure 15a** and **Figure 16**). However, for BMI and weight, the 95% confidence interval (CI) of the slope did not include zero, suggesting statistical significance **(Figure 15b** and **Figure 15c**). Weight was found to have a significant impact

on the volume of the central compartment (r^2 and slope were 0.06 and 2.36 [95% CI, 0.69 to 4.02], respectively) (**Figure 15d**).

Figure 15 Linear regression plots charting the impact of covariates on clearance and volume. (A) eGFR on clearance (r^2 and slope for each were 0.02 and 0 [95% CI 0 to 0.01], respectively) did not suggest a correlation. (B) BMI on clearance (r^2 and slope for each were 0.06 and 0.07 [95% CI 0.02 to 0.11], respectively) suggested a significant relationship. (C) Weight on clearance (r^2 and slope for each were 0.06 and 0.02 [95% CI 0.01 to 0.03], respectively) found a significant relationship. (D) Weight on volume in the central compartment (r^2 and slope for each were 0.06 and 2.36 [95% CI 0.69 to 4.02], respectively) suggested a significant correlation.

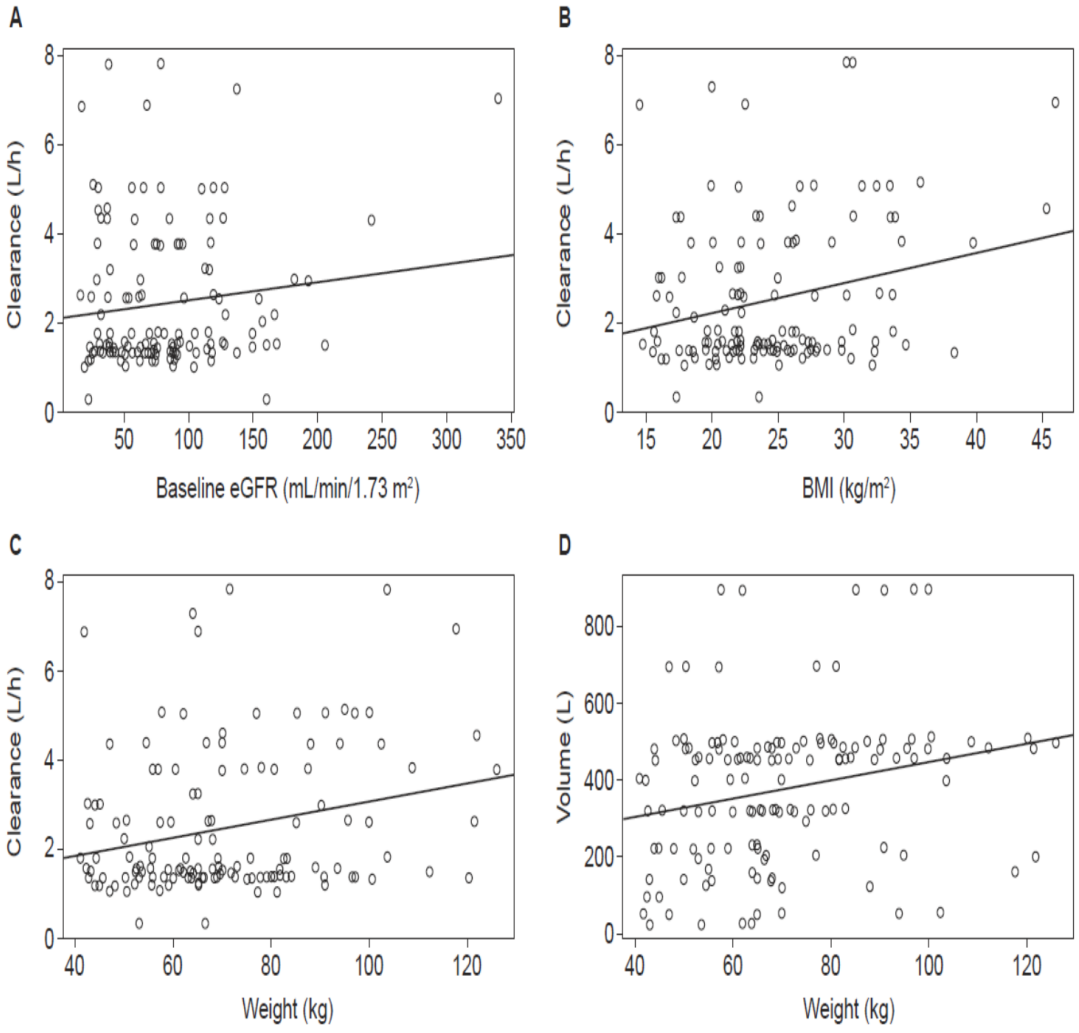

Figure 16 Impact of Asian race on clearance. Box plots for the clearance values for Asian patients (*n*=23) (median = 1.59 L/h) versus other patients (i.e., non-Asian; includes white, black, or African-American, and "other"; *n*=113) (median = 1.84 L/h) did not show a statistically significant difference (*P* = 0.06, Mann-Whitney U test).

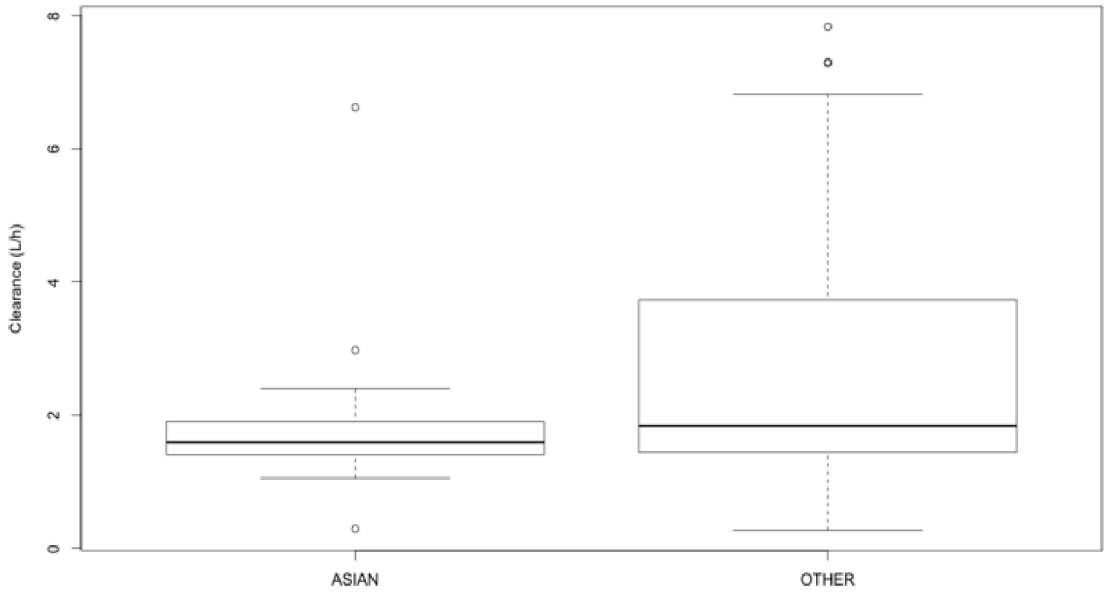

These covariates were then incorporated into the structural model to determine if their inclusion helped to better describe interpatient variability. Only one size-related covariate (weight) was included, since other measures, such as BMI, are less practical measures in clinical settings. Inclusion of the covariates did not improve fitting, as assessed by minimal changes in –2 log likelihood (decrease of 3 points) and Akaike's information criterion (increase of 5 points), as well as by visual comparisons of the observed versus predicted concentration-time plots for each patient. Therefore, the base model was used for further evaluation of model performance.

The mean (± SD) parameter estimates for the overall population and classified according to IFD type are shown in **Table 8**. The mean clearance for the entire population was 2.5 ± 1.6 L/h and the mean AUC_{avg} was 87.1 ± 41.0 mg·h/L. The mean values for clearance and AUC_{avg} ranged from 2.0 to 3.2 L/h and 70.4 to 94.0 mg·h/L, respectively, for the individual IFD types. The intersubject variability of clearance was 63% overall. AUC_{avg} and clearance values across the different types of IFD were similar (P = 0.420 and 0.248, Kruskal-Wallis nonparametric test). The mean estimate for bioavailability was 96.6% for the overall population (median 98.2%).

Table 8 Isavuconazole PPK parameters in VITAL study, based on infection

Patient population (*n*)	CL (L/h) (mean ± SD)	V (L) (mean ± SD)	AUC_{avg} (mg·h/L) (mean ± SD)	%CV of CL	F (%)
Overall (136)	2.5 (± 1.6)	361.2 (± 166.3)	87.1 (± 41.0)	63	96.6
Patients with infection					
IA (with renal impairment) (20)	2.3 (± 1.5)	412.2 (± 222.4)	92.0 (± 44.0)	64	97.4
IM (34)	3.0 (± 2.0)	364.1 (± 186.0)	87.7 (± 56.9)	68	95.0
Other filamentous fungi and moulds (23)	2.2 (± 0.9)	344.2 (± 99.7)	80.6 (± 29.2)	41	96.9
Dimorphic fungal infection (29)	2.0 (± 1.3)	343.0 (± 159.6)	94.0 (± 36.7)	62	97.5
Non-*Candida* yeasts (10)	2.5 (± 1.4)	318.2 (± 160.8)	92.0 (± 29.5)	55	94.9
Mixed infection (13)	3.2 (± 2.0)	389.8 (± 162.7)	70.4 (± 24.0)	62	97.7
Patients with no pathogen identified (7)	2.3 (± 1.6)	340.4 (± 107.5)	87.8 (± 29.1)	68.7	98.2

CL, clearance; V, volume in the central compartment; %CV, percent covariance on the intersubject variability; F, bioavailability.

A further review of the PK characteristics was also explored across the different underlying diseases (**Table 9**). Clearance values were comparable for patients with hematologic malignancies, active malignancies, or baseline neutropenia and patients without these conditions (P = 0.530, Kruskal-Wallis one-way analysis of variance). The mean clearance and AUC_{avg} values for patients with hematologic malignancies were 2.8 L/h and 85.1 mg·h/L, respectively. Patients with a combination of hematologic malignancy, baseline neutropenia, and active malignancy also had similar values (2.8 L/h and 85.1 mg·h/L for clearance and AUC_{avg}, respectively). Bioavailability did not vary significantly across the different underlying disease groups. Intersubject variability of clearance was consistent across the underlying disease groups and similar to the overall population values, with values ranging from 59% to 62%.

Table 9 Isavuconazole PPK parameters in the VITAL, based on underlying disease[a]

Underlying disease (*n*)[b]	CL (L/h) (mean ± SD)	V (L) (mean ± SD)	AUC_{avg} (mg·h/L) (mean ± SD)	%CV of CL	F (%)
Overall (136)	2.5 (± 1.6)	361.2 (± 166.3)	87.1 (± 41.0)	63	96.6
Hematologic malignancy (56)	2.6 (± 1.6)	378.7 (± 171.0)	85.1 (± 50.2)	60	96.2
Active (at baseline) malignancy (41)	2.6 (± 1.6)	382.2 (± 165.3)	84.4 (± 54.0)	59	95.9
Baseline neutropenia (34)	2.7 (± 1.8)	406.3 (± 168.0)	82.8 (± 57.9)	59	96.0
Combined hematologic malignancy, active (at baseline) malignancy, baseline neutropenia (24)	2.8 (± 1.8)	391.7 (± 187.2)	85.1 (± 68.0)	62	94.7
None[c] (71)	2.8 (± 1.8)	391.8 (± 187.2)	85.1 (± 68.0)	62	94.7

[a] CL, clearance; V, volume in the central compartment; %CV, percent covariance on the inter-subject variability; F, bioavailability.

[b] Patients in each category are not mutually exclusive.

[c] Patients without hematologic malignancy, active (at baseline) malignancy, or baseline neutropenia.

The total drug AUC:MIC ratio is the PK-PD index that appears to best link isavuconazole exposure with efficacy in preclinical models (100, 101) and PD targets have been defined for both *Aspergillus* spp. and *Candida* spp. in a range of preclinical models (52, 100, 101). Steady-state AUCs (at day 21) for 5,000 simulated subjects were assessed over a range of MICs to determine the ability of the clinical dosing regimen to achieve the various PD targets as a function of the known MIC distribution. For *Aspergillus* spp., the PD target estimated by Seyedmousavi and colleagues (100) for *A. fumigatus* was a total drug AUC:MIC value of 50.5. For *Candida* spp., Lepak and colleagues (101) established targets in neutropenic mice for *C. albicans* (total drug AUC:MIC = 5,053) and non-*albicans Candida* (total drug AUC:MIC = 312). **Figure 17** shows the MIC coverage for each PD target for the isavuconazonium sulfate clinical dosing regimen. Each graph illustrates the proportion of 5,000 simulated subjects achieving each of the PD targets at each MIC value after administration of the clinical dosing regimen of isavuconazonium sulfate. Depending on the species, the clinical dosing regimen would be predicted to adequately cover Clinical and Laboratory Standards Institute MIC values of 0.5 mg/L or lower for *A. fumigatus* and 0.004 and 0.125 mg/L or lower for *C. albicans* and non-*albicans Candida* spp., respectively. The same analysis was conducted using PD targets from an additional PK-PD model that was reported for isavuconazole and *C. albicans* (52). In this model, PD target values of 270 and 670 were estimated depending on the extent of neutropenia (temporary or persistent, respectively). If these total drug AUC:MIC targets are used for the PTA analysis, the results would demonstrate that the clinical dosing regimen will achieve the target for the

majority of *C. albicans* MIC distribution (up to MICs of 0.125 to 0.06 mg/L, respectively), which has a MIC_{90} of 0.06 mg/L.

Figure 17 PTA (left *y*-axis) for PD targets estimated in PK-PD animal models for the common fungal pathogens. (A) *A. fumigatus*, (B) non-*albicans Candida*, and (C) *C. albicans* The blue line shows the frequency (%) of the 5000 simulated subjects that would achieve the PD target at each MIC value after administration of the clinically recommended dosage of isavuconazonium sulfate (372 mg every 8 hours for days 1 and 2, followed by 372 mg once daily thereafter). Isavuconazole CLSI MIC frequency distributions (right *y*-axis) are provided for (A) *A. fumigatus* (*n* = 855), (B) *C. glabrata* (*n* = 254) and *C. tropicalis* (*n* = 130), and (C) *C. albicans* (*n* = 844); represented by the red bars.

A

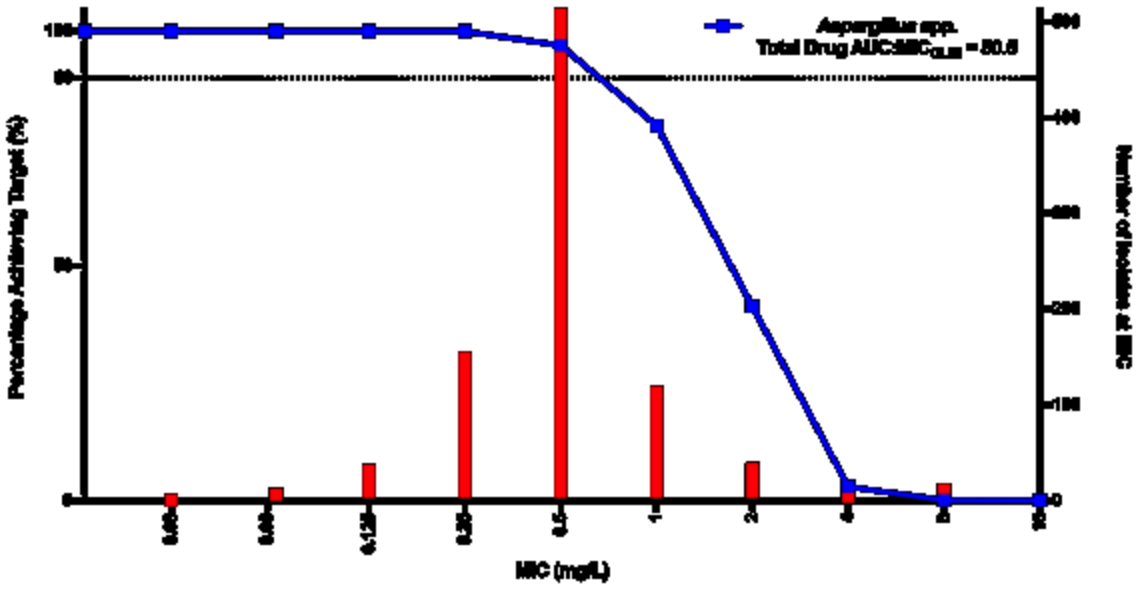

B

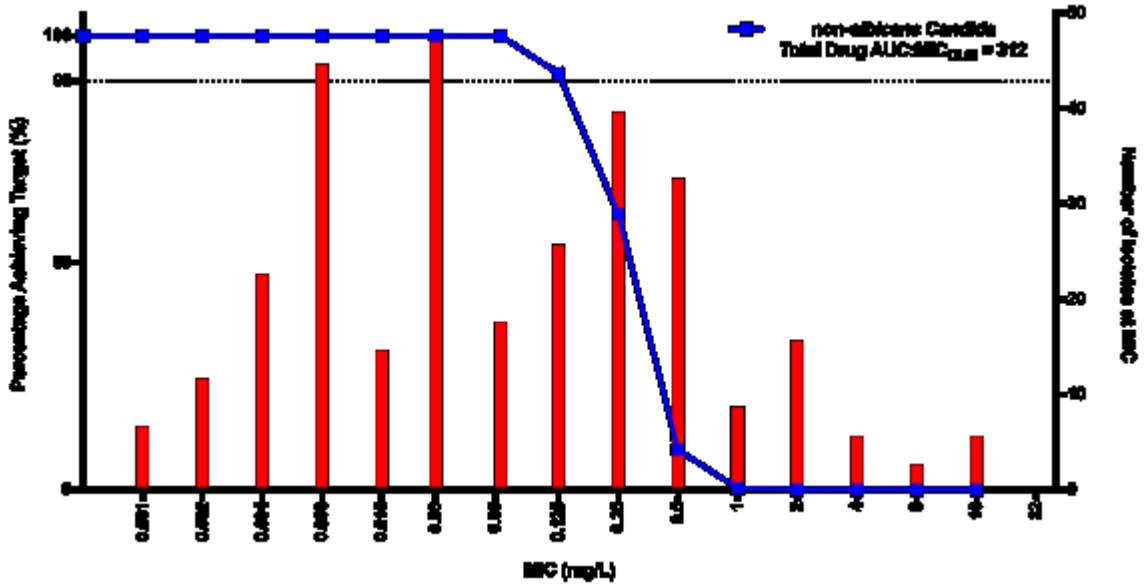

C

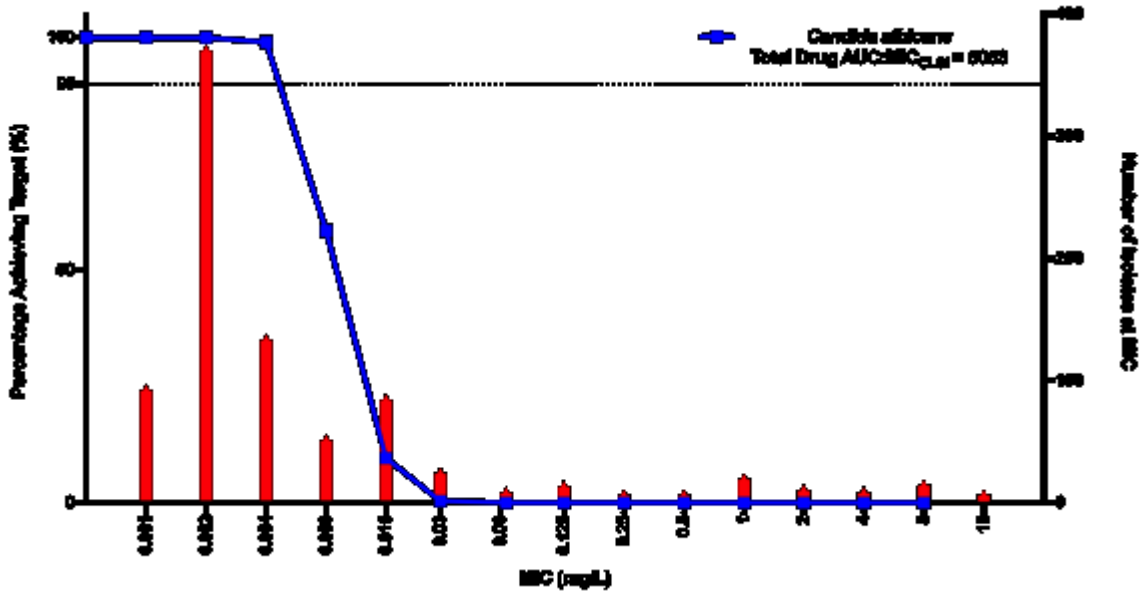

Discussion

Nonparametric estimation was used to establish a PPK model for isavuconazole by using Pmetrics and plasma drug concentrations collected from phase 3 clinical trial patients being treated for a variety of IFDs. A 2-compartment model including an absorptive compartment with first-order absorption fit the data well. Evaluation of the

impact of covariates on clearance revealed a statistically significant relationship with BMI and weight but no relationship between either eGFR or Asian race and clearance. Weight also had a significant relationship with volume of the central compartment. However, inclusion of the covariates in the structural model did not improve the fit of the model to the data. This is likely due to a weak relationship compared with the relatively large unexplained PK variability. The overall population parameters did not differ greatly from the individual IFD types or across the underlying diseases evaluated, even for severely immunocompromised patients.

We further assessed the adequacy of currently approved regimens by conducting PTA analyses using PD targets defined from experimental models for specific fungal pathogens. The results were consistent with previous data reported for *Aspergillus* spp. (99). For *Candida* spp., this represents the first report of a PTA analysis conducted using the PD targets for *Candida* spp. Importantly, however, this study did not include patients with invasive candidiasis. The majority of such cases occur in the context of critical illness, where the PK may be reasonably different and have an impact upon both the PD and PTA. Further analyses must be performed to characterize any differences in PK for patients with invasive candidiasis and then determine if these differences have any impact on the exposure coverage of the MIC distribution for these organisms. The isavuconazole MIC_{50} and MIC_{90} for *C. albicans* were 0.002 and 0.06 mg/L, respectively, for a collection of 844 isolates (102-114). For the non-*albicans Candida* spp. tested in the PK-PD model of disseminated candidiasis, the isavuconazole MIC_{50} and MIC_{90} were 0.03 and 1 mg/L for *C. tropicalis* (n = 130) and 0.06 and 1 mg/L for *C. glabrata* (n = 254) (102-114). If no differences in the PK of isavuconazole exist for patients with candidemia or invasive

candidiasis and the patients described herein, the current analysis suggests that the clinical dosing regimen will achieve the PD target reported by Lepak and colleagues (101) for the majority of the non-*albicans Candida* spp. but not for *C. albicans*. However, a second model, which evaluated the PD target for *C. albicans*, was also explored and gave difference results (52). These total drug AUC:MIC targets demonstrated that the clinical dosing regimen would achieve the target for the majority of the *C. albicans* MIC distribution (up to MICs of 0.125 and 0.06 mg/L). For other important fungi, such as organisms of the Mucorales order, *Cryptococcus* spp., and dimorphic fungi, validated *in vivo* PK-PD models have not been fully established. This demonstrates a clear knowledge gap for optimizing therapy for life-threatening infections with these organisms.

A previous PPK model was conducted for isavuconazole by using parametric estimation in NONMEN 7.2 software (47), using plasma concentration data from nine trials involving healthy subjects and one large phase 3 clinical trial of patients with IA or infections with other filamentous fungi (SECURE trial). Desai et al. (47) employed a Weibull absorption function and did not estimate the lag time and bioavailability. In our analysis, a 2-compartment model with an absorptive compartment was better than a 3-compartment model with an absorptive compartment as previously described by Desai. This is likely due to sparse sampling for the large majority of patients. Regardless of the differences between the two structural models, the mean clearance values estimated from both models are similar (2.5 L/h versus 2.4 L/h). Important patient characteristics that potentially have an impact on drug exposure were also explored. We did not identify differences in the heterogeneous population based on IFD type and underlying diseases. The intersubject variability of clearance was consistent among the populations, even for

the severely immunocompromised (i.e., patients with hematologic malignancy, active malignancy, and neutropenia combined at baseline).

We did not find a statistically significant relationship between race and clearance, in contrast to a previous report by Desai et al. that race (Asian) is associated with reduced clearance (47). The relationship between race and clearance in the current data may not have been seen because of the differences in sample size. The current analysis included 23 Asian patients, whereas the study of Desai et al. included 53 Asian patients. Desai et al. suggested that the influence of race-dependent CYPs on clearance is likely to be minimal because isavuconazole is not a substrate of CYP2D6 or CYP2C19 isoenzymes (47). However, additional pharmacogenetic studies are required to further elucidate the potential impact of race on clearance and drug exposure. Desai et al. did not report a relationship for weight and clearance but did find a relationship between BMI and volume. Both race and weight impacts on clearance and weight impacts on volume were included in the final model. While we identified significant covariates, inclusion of the covariates in the structural model did not significantly change the model fit to the data. The reasons for this could be that the size of the Asian population and range of weights in the data set were not large enough to significantly affect the model or that the relationships of these covariates to clearance and volume are not strong.

We report the AUC_{avg} for the population by calculating the total AUC for the dosing duration and dividing it by the number of days of therapy. It is important to note that the average treatment duration of therapy for the population in the PK data set was only 14 days, compared to the average duration for the study, which was 135 days. Therefore, the values for AUC_{avg} reported here are slightly lower than they would be if we were

reporting steady-state AUC. The population mean estimate of AUC_{avg} was 87.1 mg·h/L, and the mean steady-state AUC for the 5,000 simulated patients was 94.4 mg·h/L. This was comparable to the mean estimates obtained for each of the individual IFD types and to that obtained for the patients from the SECURE trial (47).

Isavuconazole clearance and AUC were not different across the various IFD and underlying diseases from the VITAL trial and were similar to the reported clearance and AUC values from patients with IA in the SECURE analyses (47). The values for intersubject variability of clearance across the populations, even for the small group of patients with severe immunosuppression, and between the VITAL and SECURE studies were similar, further illustrating the predictability of the PK of isavuconazole in most patients. For comparison, the reported intersubject variability of AUC for posaconazole ranges from 62 to 80% and that for voriconazole ranges from 120-168%, depending on the formulation administered and patient population studied (115, 116).

Most of the patients in this analysis were receiving numerous concomitant medications. A comprehensive review of the concomitant medications and the potential impact on the plasma concentrations was not performed. This could be a limitation in the analysis and the ability to detect differences may be influenced by this missing information. However, in principle, the study design excluded the use of medications known to significantly change the plasma concentrations of isavuconazole; and therefore, is not felt to have influenced the study results greatly.

PTA analysis offers an estimate of the coverage of MIC values provided by the clinical dosing regimen for common fungal pathogens. The results suggest that for the

most common pathogens for which PD targets have been estimated, the clinical dosing regimen provides adequate coverage of the majority of the wild-type distribution of *A. fumigatus*, *A. flavus,* and *A. terreus* strains, and the results support previous PTA analyses (99) for these organisms. For *C. albicans* and non-*albicans Candida* spp., the results suggest reasonable coverage of the isavuconazole MIC distribution from a large collection of *in vitro* susceptibility studies. However, further analyses are necessary to characterize the PK characteristics for patients infected with invasive candidiasis and candidemia. This is especially important given recently completed phase 3 clinical trial of the treatment of candidemia did not meet the primary endpoint of overall response at the end of the intravenous isavuconazole therapy compared to caspofungin (117). If there are PK differences in critically ill patients treated for candidemia and invasive candidiasis, this may affect the outcome of the clinical breakpoint selection, and potentially the recommended dosing regimen for treatment of invasive candidiasis.

Chapter 6 The Impact of Mucositis on Absorption and Systemic Drug Exposure of Isavuconazole

Abstract

Background. Isavuconazonium sulfate is the water-soluble prodrug of isavuconazole. Population analyses have demonstrated relatively predictable pharmacokinetic (PK) behavior in diverse patient populations. We evaluated the impact of mucositis on the oral isavuconazole exposure using population PK modeling.

Methods. We evaluated patients treated in two phase 3 trials of isavuconazole, SECURE for treatment of invasive aspergillosis (IA) and other filamentous fungi and VITAL for patients with mucormycosis, invasive fungal disease (IFD) caused by other rare fungi, or IA and renal impairment. Mucositis was reported by site investigators and its impact on oral bioavailability was assessed. Use of the oral formulation was at the discretion of the investigator. Patients with plasma samples collected during the use of isavuconazonium sulfate were included in the construction of population PK model.

Results. Of 250 patients included, 56 patients had mucositis at therapy onset or as an adverse event during oral isavuconazole therapy. Oral bioavailability was comparable of 98.3% and 99.8%, respectively. The average drug exposures (AUC_{ave}) calculated from either the mean or median parameter estimates were not different between patients with and without mucositis. Mortality and overall clinical response was similar between patients receiving oral therapy with and without mucositis.

Conclusion. Isavuconazole exposures and clinical outcomes in this subset of patients with mucositis who were able to take oral isavuconazonium sulfate were comparable to those without mucositis, despite the difference in oral bioavailability. Therefore, mucositis may not preclude use of the oral formulation of isavuconazonium sulfate.

Introduction

Invasive mould diseases (IMDs) are life-threatening conditions that require timely and intensive treatment. Patients with hematological disorders or who have undergone hematopoietic stem cell transplantation (HSCT) are a leading risk group for IMDs. Anti-neoplastic chemotherapy for acute myeloid leukemia (AML) or acute lymphocytic leukemia (ALL) and conditioning regimens for HSCT often cause mucosal disruption of the gastrointestinal (GI) tract (i.e. mucositis) that may compromise oral bioavailability (118). An evaluation of the impact of mucositis on the oral absorption of antifungal agents is required to ensure optimal antifungal therapy (119).

Isavuconazonium sulfate, the water-soluble prodrug of the triazole antifungal agent isavuconazole, is approved by the US FDA for the treatment of invasive aspergillosis (IA) and invasive mucormycosis (IM) and by the EMA for the treatment of IA, and for IM in patients for whom amphotericin B is inappropriate (43, 120). The clinical formulations include both intravenous and oral capsules. The pharmacokinetics have been well characterized from sub-studies embedded in clinical trials (44-47). The pivotal clinical trials included more than 400 patients with >60% with hematological malignancies or other conditions that required intensive chemotherapy and the potential for mucositis (48, 49).

Here, we examine the impact of mucositis on the bioavailability and drug exposure following the administration of oral isavuconazonium sulfate. We fitted a population pharmacokinetic model to the plasma concentrations from patients receiving oral isavuconazole in patients with and without mucositis and used this model to evaluate

bioavailability and the ultimate drug exposure. We consider the potential impact for dosing and therapeutic drug monitoring of isavuconazole in the setting of mucositis.

Methods

Study design. Patients treated with isavuconazonium sulfate from two Phase 3 clinical trials, SECURE and VITAL, were eligible for inclusion if plasma concentrations were available. The SECURE trial (ClinicalTrials.gov identifier: NCT00412893) evaluated the efficacy and safety of isavuconazole compared with voriconazole for the primary treatment of invasive mould disease caused by *Aspergillus* spp. and other filamentous fungi (48). The VITAL trial (ClinicalTrials.gov identifier: NCT00634049) evaluated the efficacy and safety of isavuconazole for the treatment of IA in patients with renal impairment and in patients with IFD caused by Mucorales and other emerging moulds, yeasts, and dimorphic fungi (49). Eligibility criteria for both studies are detailed elsewhere (48, 49). Patients received a loading regimen of isavuconazonium sulfate at a dose of 372 mg (equivalent to isavuconazole 200 mg) every 8 h for the first 48 h. In the SECURE trial, the loading dose was required to be administered intravenously (i.v.), while in the VITAL trial treatment could commence using either the i.v. or oral formulation. The maintenance regimen for both studies was i.v. or oral isavuconazonium sulfate 372 mg once daily for up to 84 or 180 days, respectively. Patients received i.v. or oral drug at the discretion of site investigators.

Identification of Patients with Mucositis. The medical history (MH) and adverse event (AE) records from the case report forms were reviewed for MedDRA preferred terms suggestive of "mucositis" or "stomatitis" (e.g. mucosal inflammation, radiation mucositis, stomatitis, gastrointestinal inflammation). From there, the patients were further

reviewed to determine the degree of likelihood that the MH and AE reported represented significant disease, such as recent radiation therapy or intensive chemotherapy. Patients with mucositis were only included if administration of the oral formulation occurred during the episode of mucositis AND plasma PK concentrations coincided with the oral administration and episode of mucositis. Patients without mucositis with plasma PK measurements during oral administration were classified as non-mucositis patients.

Plasma PK sampling. Blood samples were collected on treatment days 7, 14, 42, and end of therapy (EOT) in both trials. Collection was targeted for 24 hours after the start of the infusion or the oral dose on the previous day (i.e., trough concentration). Full 24-hour profiles were obtained from a subset of 43 patients (including 6 patients with mucositis). After collection, samples were processed immediately and stored at –80°C until shipment to the central research laboratory. Isavuconazole concentrations were measured at the completion of the study using a validated LC-MS/MS method as previously described (44).

Population Pharmacokinetic (PPK) Modeling. Raw plasma concentration data from the 2 groups during oral administration that was collected after Day 7 were compared to determine if any trends in the data were observed. A PPK model was developed using non-parametric estimation using Pmetrics (v1.4.1, University of Southern California, Los Angeles, CA, USA) (77). The model-fitting process included evaluation of both 2- and 3-compartment models including absorptive compartments and a lag-time. The presence of mucositis (yes=1, no=0) was used as a covariate on oral bioavailability (F) as a secondary equation, which took the following form:

Equation 11

$$F = F1 \cdot (1 - MUC) + F12 \cdot MUC$$

where, F1 refers to the oral bioavailability in patients without mucositis (MUC=0) and F12 refers to the oral bioavailability in patients with mucositis (MUC=1).

Data were weighted by the inverse of the estimated assay variance. The final model was assessed by a visual inspection of the observed-versus-predicted concentration values before and after the Bayesian step, the coefficient of determination (r^2) from the linear regression of the observed-versus-predicted values, as well as estimates for bias (mean weighted error) and precision (adjusted mean weighted squared error).

The average AUC (AUC_{ave}) for each patient was calculated using the Bayesian posterior parameter estimates from the final model using the trapezoidal rule in Pmetrics. AUC_{ave} was calculated by determining the total AUC over the entire dosing period and dividing by the number of days of therapy for each patient. Statistical comparisons were performed in MYSTAT 12 version 12.02 (https://systatsoftware.com) and GraphPad Prism version 6.0h (http://www.graphpad.com).

Exposure-Response Analysis. The AUC_{ave} for patients with and without mucositis were compared by patient outcomes defined as All-Cause Mortality through Day 42 or Overall Response to explore if any impact on exposure was associated with differences in response. Statistical comparisons were performed in MYSTAT 12 (version 12.02, http://www.systat.com).

Results

Study Population. A total of 250 patients were included in the analysis of which 56 had mucositis. **Figure 18** shows the flow of patient inclusion in the study.

Figure 18 Flowchart illustrating flow of isavuconazole-treated patients into the mucositis and non-mucositis populations

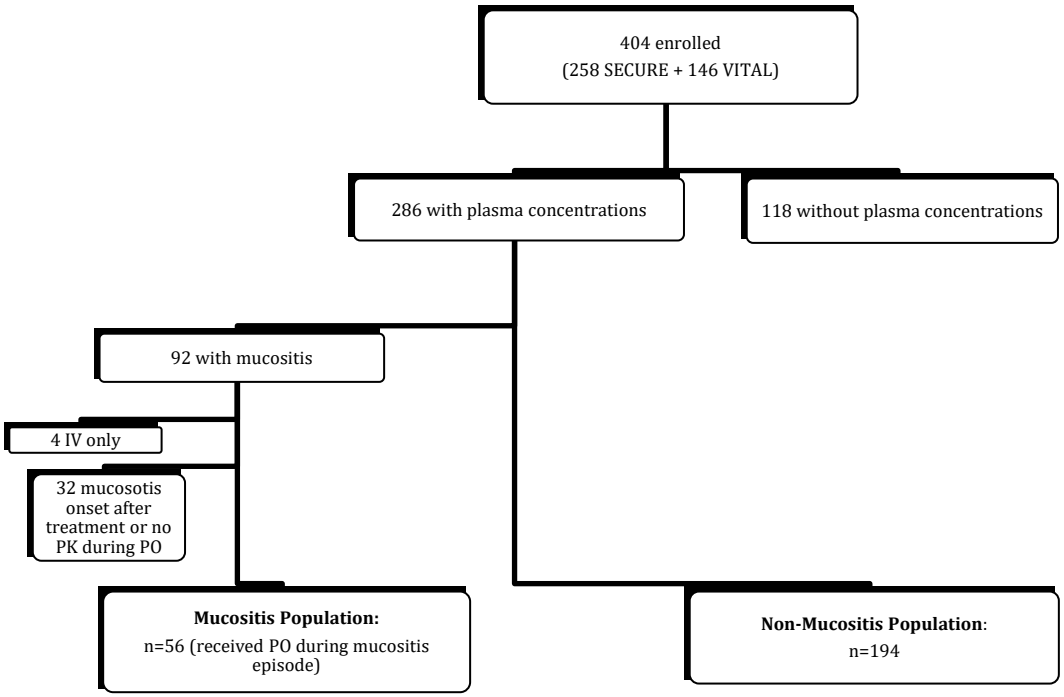

The majority of the mucositis patients had a hematologic malignancy (89.3%) that was active at the time of enrollment and were neutropenic at the start of antifungal treatment (78.2%) (**Table 10**). Only 6 patients did not have a hematological malignancy [aplastic anemia (n=3), uterine leiomyosarcoma (n=1), X-linked adrenomyeloneuropathy (n=1), squamous cell carcinoma of the tongue (n=1)]. A quarter (26.8%) of the patients with mucositis had received a HSCT. Sixteen percent of mucositis patients had baseline

renal impairment (eGFR-MDRD < 60 mL/min/1.73m^2) compared with 27.6% of those without mucositis. The majority of the overall population were males (62%), Caucasian (78.8%), and the average age (± SD) and weight (± SD) were 50.3 ± 16.1 years and 70.0 ± 18.3 kg, respectively.

Table 10 Demographics, Background Disease and Duration of Therapy

	Mucositis N=56	Non-Mucositis N=194	Total N=250
Age (years)			
Median (min-max)	50 (18-79)	52 (19-92)	52 (18-92)
Sex			
Male	32 (57%)	123 (63%)	155 (62%)
Race			
White	48 (86%)	149 (77%)	197 (79%)
Asian	7 (13%)	31 (16%)	38 (15%)
Black	1 (2%)	9 (5%)	10 (4%)
Other	0	5 (3%)	5 (2%)
Weight (kg)			
Mean ± SD	71.7 ± 18.1	69.5 ± 18.4	70.0 ± 18.3
Underlying Disease			
Hematological Malignancy	50 (89.3%)	101 (52.1%)	151 (60.4%)
Active Malignancy	40 (71.4%)	76 (39.2%)	116 (46.4%)
Allogeneic HSCT	15 (26.8%)	33 (17.0%)	48 (19.2%)
Baseline Neutropenia	43 (78.2%)	64 (41.8%)	107 (51.4%)
T-cell Immunosuppressants	23 (41.8%)	82 (51.9%)	105 (49.3%)
Use of Corticosteroids	8 (14.3%)	47 (24.2%)	55 (22.0%)

Duration of Therapy (days)			
Median (range)			
Total duration	75.5 (8-735)	83 (1-882)	82 (1-882)
IV formulation	9 (2-45)	7 (0.5-77)	7.5 (0.5-77)
Oral formulation	58 (1-690)	79.8 (0.5-882)	73 (0.5-882)

Type of Fungal Infection in Patients with Mucositis. Thirty-two patients had proven or probable IA and 7 patients had possible IA (with appropriate host factors, clinical features but no mycological evidence of disease). Eight patients had proven or probable infection caused by various mould and rare yeasts including Mucorales (n=1), *Fusarium* spp. (n=3), *Culvularia lunata* (n=1), *Alternaria* spp. (n=1), *Acremonium* spp. (n=1), and *Trichosporon* spp. (n=1). Five patients did not have enough evidence for probable or proven IFD after review of the Data Review Committees.

PPK Model. Comparisons of the raw plasma concentrations for the patients with mucositis and patients without mucositis during oral administration beyond Day 7 revealed a statistical difference between the 2 groups **(**p-value = 0.0011**)** (**Figure 19**), although the concentrations largely overlapped. A 2-compartment model including an absorptive compartment fit the data well.

Figure 19 Comparison of plasma concentrations drawn during oral administration after day 7 of therapy between the mucositis and non-mucositis patients. Comparison of the plasma concentrations between patients without mucositis (non-mucositis) and patients with mucositis **(***p-value* = 0.0011; Mann-Whitney U test, non-parametric**)**

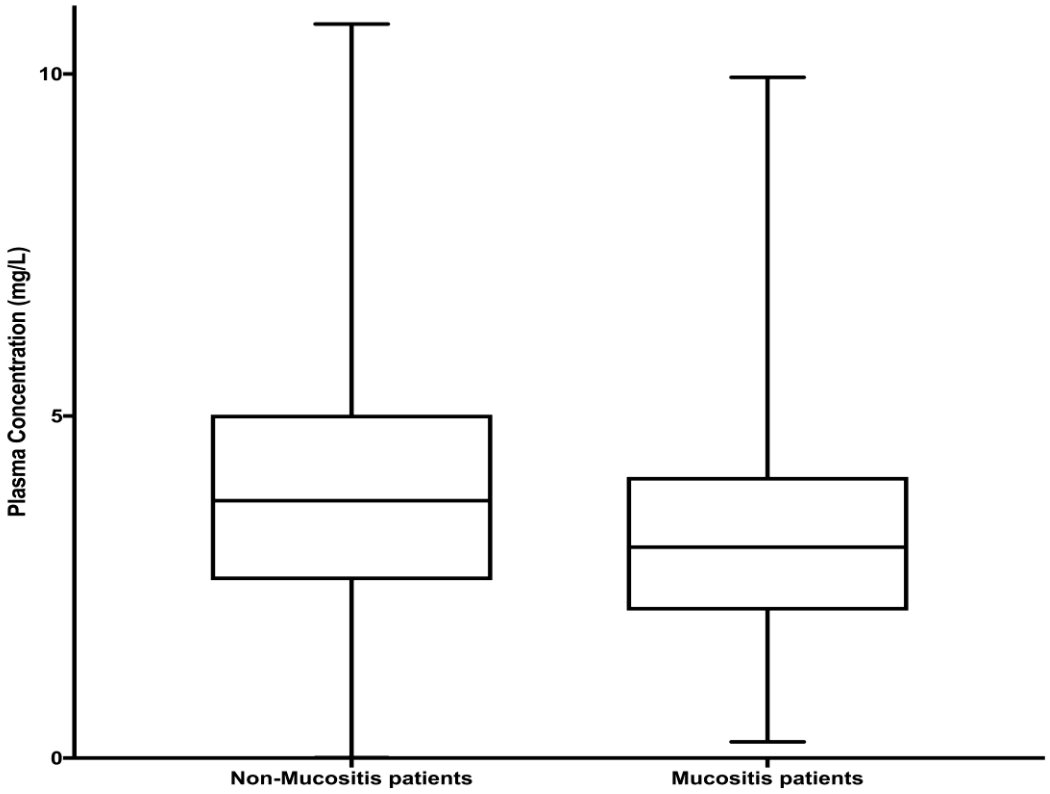

An illustration of the structural model is provided in **Figure 20** where the first compartment represents the gut (oral compartment) and the second representing the central compartment.

Figure 20 Illustration of the Structural Model. Compartment 1 represents the gut for oral administration (box on left); Compartment 2 represents the central compartment (box on right); Arrow between compartments 1 and 2 represents drug flow from the gut to the central compartment. The arrow from the central compartment represents elimination of drug at a ratio of CL/V. Abbreviations: CL, clearance; F, bioavailability; Ka, first-order absorption rate constant; Tlag, lag-time; V, volume in the central compartment; RATEIV(1) specifies infusions going directly into the central compartment.

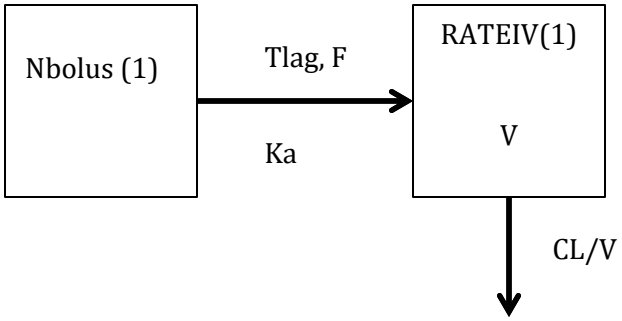

The fit of the model to the data was acceptable based on visual inspection of the observed-versus-median predicted plots and the coefficient of determination (r^2) of 0.813 after the Bayesian step (**Figure 21**). The estimates of bias and imprecision were also acceptable (0.11 and 0.938, respectively). The observed-versus-mean predicted plots showed similar statistics with a coefficient of determination (r^2) of 0.792 (slope = 0.976) after the Bayesian step.

Figure 21 Observed versus median posterior predicted concentrations (mg/L) from the final model after the Bayesian step. Statistics: r^2= 0.813, slope = 0.98 [95%CI, 0.956 to 1], intercept = -0.0181 [95%CI, −0.115 to 0.0792]. Dotted line is line of unity where observed concentrations equal predicted concentrations.

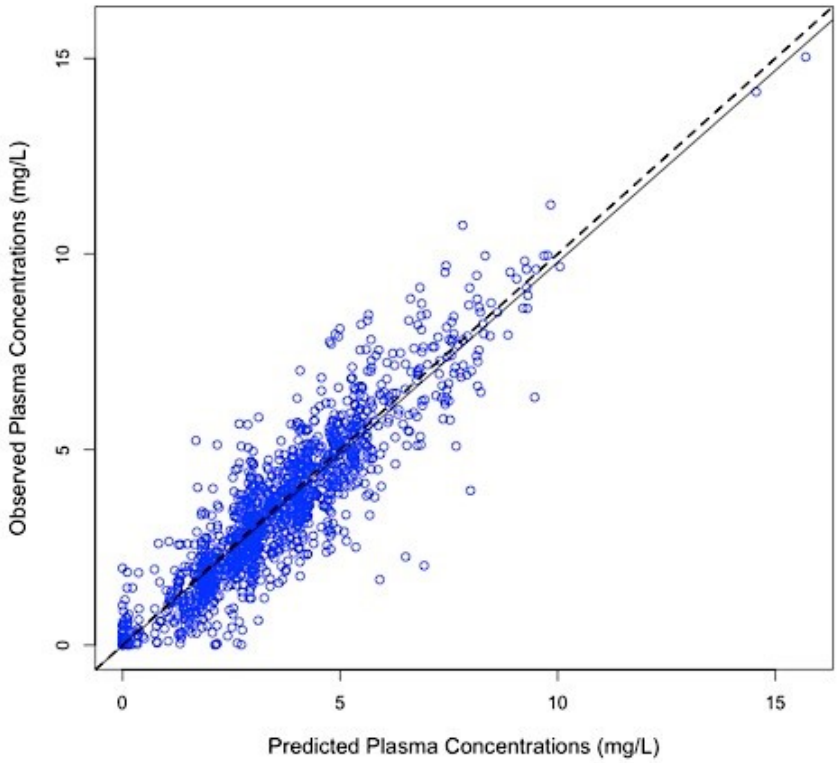

The median parameter estimates are included in **Table 11**.

Table 11 Median Parameter estimates from the PPK model

	Mucositis				Non-Mucositis			
	Mean ± SD	Median	Range	%CV	Mean ± SD	Median	Range	%CV
Ka (h^{-1})	7.0 ± 2.6	7.9	0.0-8.0	38%	6.5 ± 3.0	7.9	0.0-8.0	46%
Cl/F (L/h)	2.2 ± 1.0	1.9	0.5-4.1	44%	2.3 ± 1.1	1.9	0.1-5.9	47%
V/F (L)	331.4 ± 154.9	347.7	6.8-895.5	47%	354.1 ± 182.5	349.8	5.8-895.5	52%
Lag time (h)	1.2 ± 1.2	1.0	0.0-5.0	94%	1.3 ± 1.3	1.0	0.0-5.0	103%
F (%)	86.0 ± 18.5	98.3	50.3-99.7	21%	97.4 ± 6.9	99.8	70.2-99.9	7%
AUC_{ave} (mg·h/L)	105.3 ± 55.9	91.9	45.9-315.5	53%	114.1 ± 141.2	100.2	30.8-1944.3	124%

Abbreviations: SD, standard deviation; Ka, first-order absorption rate constant; CL, clearance; F, bioavailability; V, volume in the central compartment, AUC_{ave}, average area-under-the concentration curve.

***Comparison of Oral Bioavailability*.** The mean (range) oral bioavailability (F) estimates for mucositis and non-mucositis patients were 86.0% (50.3-99.7%) and 97.4% (70.2-99.9%), respectively. Comparison of the mean and median bioavailability estimates for the two populations demonstrated a significant difference between the 2 groups ($p < 0.0001$, Mann-Whitney U non-parametric Test) (**Figure 22**).

Figure 22 There is a significant difference in the median estimates for bioavailability between the 2 groups. Boxplot illustrating the comparison of oral bioavailability estimates for patients with mucositis and patients without mucositis (non-mucositis) ($p<0.0001$, Mann-Whitney U Test, non-parametric).

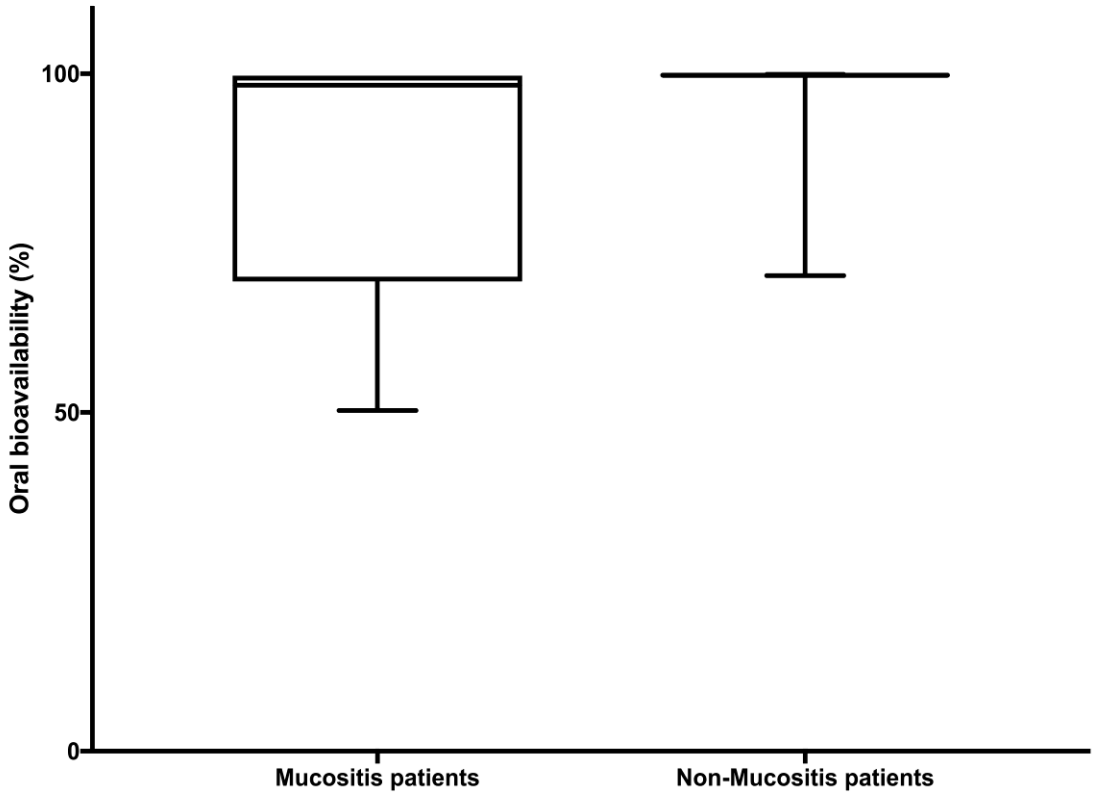

However, this 11.4% difference in bioavailability did not have a significant impact on the distribution of exposures (AUC_{ave}) between the two groups (p=0.706, Mann-Whitney U Test, non-parametric) (**Figure 23**).

Figure 23 No significant difference in average AUCs between mucositis and non-mucositis patients. Boxplot illustrating the comparison of AUC_{ave} estimates for patients with mucositis and patients without mucositis (non-mucositis) (*p*=0.706, Mann-Whitney U Test, non-parametric). AUCs calculated from the median parameter estimates after the Bayesian step

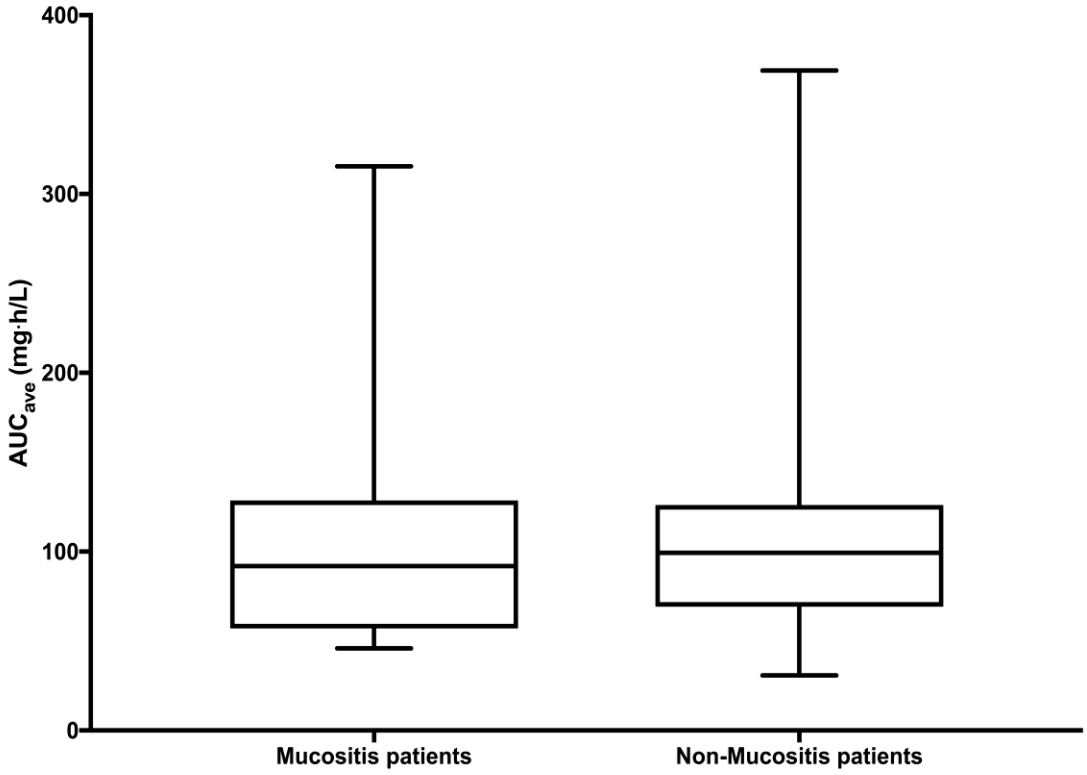

All-Cause Mortality through Day 42. All-cause mortality through treatment day 42 for the patients with and without mucositis was 7.1% (4/56) and 14.4% (28/194),

respectively. The oral bioavailability and AUC_{ave} were 83.6% and 91.3 mg·h/L, 92.7% and 164.9 mg·h/L, 99.7% and 56.5 mg·h/L, and 99.7% and 216.9 mg·h/L for the four patients with mucositis who died. The median bioavailability estimates for the non-mucositis patients that died were all above 90% except for one patient with an estimate of 70.2%. The mean AUC_{ave} was 100.5 mg·h/L and ranged from 34.9-369.1 mg·h/L.

Overall Response at the End of Therapy (EOT). Overall Response at the EOT was available for 232 mITT patients in the analysis. Fifty-eight percent [n=43; 95% CI 42.13, 72.99] and 42.9% [n=189, 95% CI 35.68, 50.42] of the patients with and without mucositis had a successful response, respectively. In the mucositis patients who failed at the EOT (n=25), the mean oral bioavailability was 84.9 ± 17.9%, (range 50.4-99.7%; median 90.3%) and the mean AUC_{ave} was 117.9 ± 69.4 mg·h/L, (range 45.9-315.5 mg·h/L; median 94.2 mg·h/L). Six of the patients (n=18; 33%) who failed at the EOT had oral bioavailability estimates < 80% (range 50.4-69.5%) with AUC_{ave} values ranging from 45.9-176.3 mg·h/L and 8 of the patients (n=25; 32%) with successful responses at the end of therapy had bioavailability estimates of <80% (range 50.3-75.5%) with AUC_{ave} ranging from 48.2-155.2 mg·h/L.

Discussion

Biological factors that have an impact on drug absorption include the pH along the GI tract, tissue perfusion, the presence of bile and mucus, the surface area per volume of the lumen, and the epithelial integrity. Mucositis manifests as erythema, inflammation, ulcerations, and hemorrhage of the mucosal surfaces of the GI tract and causes gastric motility dysfunction. This mucosal disruption can significantly affect drug absorption after the oral administration of medications. Using oral medications in the setting of

mucositis requires an understanding of the determinants of drug absorption.

Table 12 summarizes the determinants of oral bioavailability for triazole antifungal agents. Isavuconazole and fluconazole have similar characteristics that include the absence of clinically relevant effect on absorption from food, changes in pH, or increases in GI motility (43, 121, 122). Posaconazole and itraconazole oral solutions should be administered with high-fat meals, carbonated soda, or nutritional supplements (119, 123-128). Plasma concentrations are decreased when gastric acidity is reduced (119, 123-128). Absorption of posaconazole oral solution may be improved when daily doses are fractionated compared with less frequent dosing (129). The newer posaconazole tablets are not affected by changes in gastric pH and absorption is not improved by the consumption of high-fat meals (126, 130). Voriconazole plasma concentrations are reduced when taken with food; however, absorption is not clinically significantly affected by changes in pH or by drugs such as omeprazole (131). H2-blockers were not found to cause clinically significant changes in voriconazole absorption kinetics (132). Voriconazole exhibits decreased oral bioavailability in patients with cystic fibrosis (CF) compared to patients without CF after lung transplant (133). Thus, factors that affect the absorption of triazoles such as mucositis differ markedly.

Table 12 Comparison of factors impacting oral absorption of triazole antifungal drugs

	Isavuconazonium sulfate	Voriconazole	Posaconazole (124)		Itraconazole (125)		Fluconazole (122)
Formulation	capsule	tablets	solution	tablets	solution	capsule	tablet
Water Solubility	Y (prodrug)	N	N		N		Y
Bioavailability (%)							
Healthy Subjects	98 (121)	96 (134)	8-48 (fasted)	54 (fasted)	55		90
Patients	97 (44)	64 (135)					
GI motility agents	none	No data found	Decreases	none	No data found		No data found
pH Effect	none	none	Decreases in reduced acidity	none	Decreased in reduced acidity		none
Food Effect	none	Decreases concentrations	Increases concentrations (especially high	Cmax and AUC increases 16% and 51%	Increases concentrations		none

			fat, nutritional supplement or acidic carbonated beverage)	with high fat foods			
Other		F significantly lower in CF lung tx (23%) pts versus non-CF lung tx (63%) (133); 2 factors significant association with F in lung tx pts: CF, post-operative time (increased with increasing time) (133)	Divided doses increases absorption				
Substrate of Pgp	no	no	yes	yes	yes	yes	no

Abbreviations: Y: yes; N: no; GI: gastrointestinal; F: bioavailability; CF: cystic fibrosis; Pgp: P-glycoprotein

Drugs that require food to increase bioavailability or experience decreased bioavailability with increased gastric emptying (increased gastric motility) suggest that passive diffusion is slow and likely occurs primarily from the stomach. In these circumstances, absorption is improved by longer transit times in the stomach and upper small intestine. Aside from the prodrug formulation of isavuconazole, the other azoles are limited by the insufficient dissolution in stomach prior to delivery in the duodenum, where absorption is maximal. A meal that is high in fat increases luminal volume and bile and pancreatic secretions, and delays gastric emptying. The absorption for drugs such as posaconazole may be optimized by the use a more fractionated regimen (123, 136, 137). However, studies have suggested that this may be due to the high-fat meal increasing the solubility versus delayed gastric emptying (123). Another study failed to associate factors such as P-glycoprotein on the absorption of posaconazole (138). In contrast, the absorption for isavuconazole and fluconazole (and to a lesser extent voriconazole) is not significantly influenced by these factors, suggesting passive diffusion occurs more quickly and the majority of the absorption occurs in the upper small intestine.

In this analysis, the presence of mucositis did not have a significant overall impact on the clinical outcomes in the patients treated with isavuconazonium sulfate from the SECURE and VITAL trials despite the statistical differences in oral bioavailability between the groups with and without mucositis. In addition, the drug exposure between the groups was not significantly different. The results held whether mean or median parameter estimates were used for the comparisons.

The current study has several limitations. First, details on the presence or severity of mucositis were not available for the majority of patients with the condition.

Quantification of severity may have allowed for a deeper understanding of the impact for the degree of mucosal disruption and the impact on oral bioavailability. Second, patients were allowed to switch back and forth from oral to intravenous medication during the treatment period. However, only patients with mucositis coinciding with oral administration were selected for analysis. Third, the administration of i.v. or oral formulations was at the discretion of the site investigators making it difficult to assess the impact of the severity of mucositis on oral bioavailability. Patients with more severe grades of mucositis patients may have remained on i.v. therapy longer, while patients with less severe mucositis may have been switched to oral therapy. In addition, identification of mucositis patients for this study relied on the reporting of the events by the treating investigator, which could be underrepresenting the incidence in the study. We did not utilize a validated mucositis score or a biomarker, such as citrulline to capture severity as has done in other studies (139). Finally, we assumed compliance was 100%, which may be overly optimistic.

These analyses are important as many patients who will be treated with isavuconazonium sulfate are at risk or could have mucositis at the onset of therapy caused by the harsh treatments used to treat their underlying co-morbidities. Patients with slightly lower bioavailability had outcomes similar to those with higher bioavailability. Therefore, use of the oral formulation of isavuconazonium sulfate during episodes of mucositis may be acceptable; however, treating physicians may consider extending isavuconazole intravenous therapy during episodes of mucositis or monitoring levels to ensure they are within the range reported from the clinical trial. However, additional studies in this population may be warranted.

Chapter 7 Exposure-Response Analysis of Micafungin in Neonatal Candidiasis: Pooled analysis of two clinical trials

Abstract

Background. Neonatal candidiasis causes significant morbidity and mortality in high-risk infants. A micafungin dosage regimen of 10 mg/kg established for the treatment of neonatal candidiasis is based on a laboratory animal model of neonatal hematogenous *Candida* meningoencephalitis and pharmacokinetic (PK)-pharmacodynamic (PD) bridging studies. However, little is known about the how these PK-PD data translate clinically.

Methods. Micafungin plasma concentrations from infants were used to construct a population PK model using Pmetrics software. Bayesian posterior estimates for infants with invasive candidiasis were used to evaluate the relationship between drug exposure and mycological response using logistic regression.

Results. Sixty-four infants aged 3 to 119 days old were included, of which 29 (45%) infants had IC. A 2-compartment PK model fit the data well. Allometric scaling was applied to clearance and volume normalized to the mean population weight (kg). The mean (SD) estimates for clearance and volume in the central compartment were 0.07 (0.05) L/h/1.8kg and 0.61 (0.53) L/1.8kg, respectively. No relationship between AUC_{ave} or AUC_{ave}:MIC ratio and mycological response was demonstrated ($p>0.05$). Although not statistically significant, mycological response was numerically higher when AUCs were at or above the PD target.

Conclusion. While an exposure-response relationship was not found, PK-PD experiments support higher exposures in infants with invasive candidiasis. More patients would clarify this relationship; however, low incidence deters the feasibility of these studies.

Introduction

Neonatal candidiasis results in significant morbidity and mortality in premature infants (60-62). The associated mortality with invasive candidiasis (IC) is three-times higher than that of uninfected infants of similar gestational age and birth weight (63). The involvement of the central nervous system (CNS) is especially detrimental for subsequent neurodevelopmental outcomes and mandates meticulous attention to the selection of safe and effective antifungal regimens (64-66).

There is a large safety and efficacy database that supports the role of micafungin for the treatment of IC in both adults and children (67, 140-142). Micafungin has broad-spectrum anti-*Candida* coverage and a favorable safety profile (68, 69). Micafungin demonstrates linear pharmacokinetics (PK), dose adjustment is not required in the setting of renal and/or hepatic impairment, and therapeutic drug monitoring is not required in any patient populations (143).

The pharmacodynamics (PD) of micafungin for the treatment of hematogenous *Candida* meningoencephalitis (HCME) has been explored in a well-characterized experimental model (70). PK-PD bridging studies suggest that a neonatal regimen of 10 mg/kg is required for effective treatment of *Candida* infections in the CNS (70, 72). These studies were used to justify the choice of this high dose regimen for treatment of infants with IC. Unfortunately, however, inherent difficulties in conducting neonatal trials and the general decrease in the incidence of neonatal candidiasis resulted in early termination of one of the studies after the enrollment of only 30 infants with the primary and safety results reported elsewhere (144).

Ideally, predictions from preclinical models should be tested clinically to prospectively validate the PK-PD relationships. Establishing preclinical-to-clinical linkages are increasingly viewed as fundamental for the establishment of effective antimicrobial therapies. In this study, we examined the clinical relevance of reaching the PD target established in preclinical models. We combined micafungin plasma concentrations from four neonatal clinical trials to construct a population PK (PPK) model and then explored whether increasing micafungin drug exposures resulted in improved clinical outcomes in infants with IC.

Methods

***Study Design*.** Micafungin plasma concentrations from four pediatric clinical trials were available for population PK modeling. Each study has been described in detail elsewhere (72, 144-147). Briefly, the dataset consists of two PK and safety studies with dosages ranging from 0.75 to 10 mg/kg and two efficacy, safety, and PK studies with dosages ranging from 2 to 10 mg/kg/day. The local Institutional Review Board/Ethics Committee at each site approved the studies and parental consent was obtained for each infant prior to initiation of study procedures within each study. Plasma sampling is described in the respective publications. The micafungin concentrations were analyzed using high performance liquid chromatography (HPLC), as detailed in the individual publications (72, 145, 146). Estimated gestational age was not available for all clinical trials so we were unable to incorporate this variable in the analysis or to use it to calculate other age descriptions such as post-conceptional age.

PPK modeling. A PPK model was constructed using the population PK program Pmetrics (v1.5.1, University of Southern California, Los Angeles, CA, USA) (77). The

observations were weighted by the inverse of the estimated assay variance. Initial parameter estimates were anchored on two prior population PK models. The first study included 47 infants < 4 months which used prior knowledge from adult population PK modeling and standardized estimates of clearance and volume in the central compartment to a 70-kg adult weight (71). The second study utilized 293 pediatric patients including the 64 infants in the present analysis (unpublished data). This population PK model normalized the clearance and volume to the mean weight of the 293 pediatric patients based on prior knowledge from previous pediatric population PK analysis (148). The structural model included allometric scaling terms for clearance and volume, which were also standardized to the mean body weight of the population (1.8 kg). The differential equations for the final structural model with allometric scaling are as follows:

Equation 12

$$\frac{dX(1)}{dt} = R(1) - \left[Kcp + \frac{CLstd \cdot \left(\frac{weight}{1.8}\right)^{0.75}}{Vstd \cdot \frac{weight}{1.8}} \right] \cdot X(1) + [Kpc \cdot X(2)]$$

Equation 13

$$\frac{dX(2)}{dt} = Kcp \cdot X(1) - Kpc \cdot X(2)$$

where CL_{std} and V_{std} represent the normalized clearance and volume values using the mean body weight of the population, R represents the infusion of micafungin into compartment 1, K_{cp} and K_{pc} represent the rate of drug transfer to and from the central (compartment 1) and peripheral (compartment 2) compartments, respectively.

The fit of the model to the data was evaluated by visual inspection of the observed-versus-predicted concentrations before and after the Bayesian step, and the coefficient of determination (r^2) from the linear regression of the observed-versus-predicted values. In addition, the estimates for bias (mean weighted error) and imprecision (adjusted mean weighted squared error) were assessed.

Bayesian posterior estimates from the best model were used to estimate area-under-the concentration-time curve (AUC) for each patient for the entire dosing interval in Pmetrics using trapezoidal rule. The average daily AUC was then determined by dividing the total AUC for the treatment course by the number of days of micafungin therapy. Using daily average AUC avoids the issue of having to define what time in the course of therapy that AUC is important for efficacy (e.g. AUC at the end of dosing or on a specific day during therapy).

Exposure-Response Analysis. A subset of 29 infants who received micafungin for the treatment of proven invasive candidiasis was used for the exposure-response analysis. Mycological response was used as an outcome measure. Successful mycological response was defined as eradication (documented by negative fungal cultures) through 1 week post the receipt of the last dose of micafungin. In most patients, after documentation of eradication during therapy, follow-up cultures were sparse or not performed due to lack of clinical need (i.e. a successful response). Therefore, an additional part of the definition of "successful response" was that no new antifungal therapy was required after completion of micafungin. Failure (persistence of infection) was defined as continued positive cultures or in the absence of repeat cultures, there was a requirement to switch to an alternative antifungal therapy for further treatment.

The relationship of AUC_{ave} and AUC_{ave}:MIC to mycological response (binary data) was analyzed using logistic regression in SAS® (version 9.3, SAS Institute Inc., Cary, NC, USA). The exposure parameters were added in an automated stepwise approach with α=0.3 for model inclusion and α=0.05 for model retention. Additional statistical comparisons were performed in MYSTAT 12 (version 12.02, http://www.systat.com).

Attainment of Pharmacodynamic Targets. Drug exposures from the 29 infants with IC were used to verify if the 10 mg/kg dosage ensured attainment of the PD target (AUC and AUC:MIC ratio) representing the near-maximal effect determined in the *in vivo* rabbit model of *Candida* meningoencephalitis (70, 71) and to assess if achieving this target improved survival and/or mycological response.

Results

Study Population for PPK. A summary of the demographics of patients enrolled included from the 4 studies is provided in **Table 13.** Four micafungin clinical trials with a combined total of 64 infants aged 3 to 119 days were available. There were slightly more males than females (n=35 males, 55%), the mean (SD) age was 35 days (27 days), and the mean (SD; range) weight was 1.8 kg (1.1 kg; 0.5-4.8 kg). The treatment duration ranged from 1 to 34 days, with a mean (SD) of 6.8 days (7.9 days).

Table 13 Description of Micafungin Pediatric Studies included in the PPK model

Study	n	Description	Age Range (days)	Weight Range (kg)	Sex (% males)	Dose (mg/kg)	Infusion Duration	Duration (days)
Heresi, 2006 (145)	22	Single-dose PK and tolerability study in premature Infants requiring systemic antifungal	3.6 – 61.9	0.6-2.0	60.9%	0.75, 1, and 3	30 minutes	1
Benjamin, 2010 (72)	13	Multiple-dose PK and safety study for empiric therapy	3.0 – 118.7	0.54-1.4	46.2%	7 and 10	1 hour	4-5
Queiroz-Telles, 2008 (147)/ Undre, 2012 (146)	17	Efficacy, safety, and PK study in the treatment of IC	3.6 – 94.6	0.9-3.3	64.7%	2; dose increase to 4 for therapeutic effect	1 hour	Up to 42
Benjamin, 2015 (144)	12	Efficacy, safety, and PK study in the treatment of IC	12.0 – 116.8	0.7-4.8	33.3%	10	2 hours	Up to 42

Abbreviations: PK: pharmacokinetics; IC: invasive candidiasis

Population PK model. A total of 287 micafungin concentrations were retrieved for the population PK analysis. A description of the 4 studies is included in **Table 13**. A two-compartment model with allometric scaling fit the data well. A visual inspection of the observed-versus-predicted concentrations after the Bayesian step was acceptable with a coefficient of determination (r^2) of 0.945 (**Figure 24**) using the median parameter values. Similar results were observed for the mean posterior predicted values (r^2 = 0.941 for the linear regression of the observed-versus-predicted values). Estimates of bias and imprecision were also acceptable (-0.126 and 0.902, respectively).

Figure 24 Observed versus posterior predicted concentrations (mg/L) from the final model after the Bayesian step (A) Linear and (B) Log Scale. *Upper (A)*: Linear scale (r^2= 0.945, slope = 0.995 [95%CI 0.967 to 1.02], intercept = 0.24 [95%CI −0.104 to 0.584]). *Lower (B)*: Log scale () (r^2= 0.947, slope = 0.946 [95%CI 0.92 to 0.972], intercept = 0.0496 [95%CI 0.0284 to 0.0709]). Dotted line is line of unity where observed concentrations equal predicted concentrations.

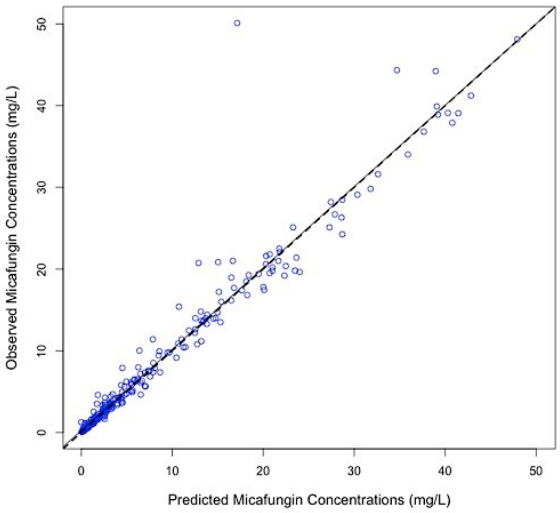

A.

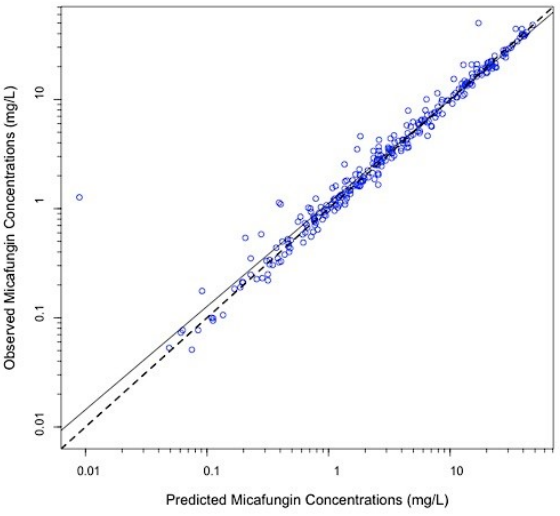

B.

The mean parameter estimates are included in **Table 14**. The mean (SD) clearance and volume in the central compartment were 0.07 (0.05) L/h/1.8 kg and 0.61 (0.53) L/1.8 kg, respectively.

Table 14 Mean, medians, standard deviations (SD), and coefficients of variation (%CV) for the parameter estimates

Parameter	Cl_{std} (L/h/1.8 kg)	V_{std} (L/1.8 kg)	Kcp (h^{-1})	Kpc (h^{-1})
Mean (range)	0.07 (0.002-0.299)	0.61 (0.192-2.780)	1.74 (0.035-5.966)	1.92 (0.090-5.970)
SD	0.05	0.53	1.57	1.29
Median	0.06	0.43	0.99	2.00
%CV	68.8	85.9	89.9	67.1

Abbreviations: Cl: clearance; std: standard; V: volume in the central compartment; L: liters: kg: kilogram; Kcp: represents rate of drug moving from the central to the peripheral compartments; Kpc: represents rate of drug moving from the peripheral to the central compartments

Exposure-Response Population and Analysis. Twenty-nine infants ranging in age from 4 to 117 days received micafungin for the treatment of proven invasive candidiasis or candidemia; 17 infants received a dose of 2 mg/kg in a trial comparing micafungin to liposomal amphotericin B (147) and 12 infants received a dose of 10 mg/kg in a trial comparing micafungin to conventional amphotericin B (144). The median (range) body weight of the 29 infants was 1.95 kg (0.68 to 4.85 kg). The median (range) treatment duration was 14 days (1-34 days). Minimum inhibitory concentration (MIC) values from the 2 mg/kg and 10 mg/kg studies were available for all but 2 infants with values ranging from 0.004-2 mg/L and 0.03-2 mg/L, respectively. All but 3 patients had candidemia. The other 3 patients had proven infections in the urinary tract (n=2) and disseminated disease (n=1; eye, CSF, blood). Seventy-six percent and 92% of infants receiving 2 and 10 mg/kg survived, respectively. Successful mycological response was achieved in 83% and 76%

of patients receiving 2 and 10 mg/kg, respectively. **Table 15** summarizes the exposure estimates (AUC_{ave} and AUC_{ave}:MIC) for the 2 and 10 mg/kg dosages from each study.

Table 15 Estimates of AUC_{ave} and AUC_{ave}:MIC for infants less than 4 months of age with IC treated with micafungin at doses of 2 mg/kg and 10 mg/kg

	AUCave (mg·h/L)	AUC_{ave}:MIC ratio
10 mg/kg	n=12	n=11
median	401	6475
range	198-815	115-18,675
%CV	43%	100%
% ≥ 166.5 mg·h/L or ≥ 1332*	100%	55%
2 mg/kg	n=17	N=16
median	62	2395
range	27-179	74-89,354
%CV	68%	133%
% ≥ 166.5 mg·h/L or ≥ 1332*	12%	56%

*$AUC_{0\text{-}144.5}$ or $AUC_{0\text{-}144.5}$:MIC ratio representing the PD target for the near-maximal effect in the HCME rabbit model.

The CNS PD target AUC for near-maximal effect that was demonstrated in the rabbit model of HCME was approximately 166.5 mg·h/L (70, 71). All infants treated at a dose of 10 mg/kg achieved the CNS PD target, while only two (12%) of the infants receiving 2 mg/kg achieved the CNS PD target (**Table 16**). Successful mycological response was achieved by 86% of patients who reached the PD target as compared to 73% of patients

who did not meet the PD target, but this difference was not statistically significant (p=0.396). Of those infants reaching the AUC:MIC ratio PD target for near-maximal effect of 1332, successful mycological response was achieved by 92% and 83% of those who reached and did not reach the target, respectively.

Table 16 MIC Values and Treatment Response by dose groups and by patients that did or did not achieved the CNS PD target

	10 mg/kg (n=12)	2 mg/kg (n=17)
MIC (mg/L) Range	0.03-2	0.004-2
MIC_{90}	2	1
Survival	11 (92%)	13 (76%)
Mycological Response	10 (83%)	13 (76%)
Treatment Response in Patients Reaching PD target		
	≥ 166.5 mg·h/L[*] (n=14)	≥ 1332[*#] (n=15)
Survival	12 (86%)	11 (73%)
Successful Mycological Response	12 (86%)	11 (73%)
Treatment Response in Patients Not Reaching PD target		
	< 166.5 mg·h/L[*] (n=15)	< 1332[*#] (n=12)
Survival	12 (80%)	11 (92%)
Successful Mycological Response	11 (73%)	10 (83%)

[*] $AUC_{0\text{-}144.5}$ or $AUC_{0\text{-}144.5}$:MIC ratio representing the PD target for the near-maximal effect in the HCME rabbit model.

[#] Only 27 infants had MIC values to be included in this analysis.

There was no clear relationship between mycological response (success or failure) and either AUC_{ave} and AUC_{ave}:MIC when examined using logistic regression ($p > 0.05$). **Figure 25a** and **Figure 25b** illustrates the similarity in the drug exposure measures for those patients with successful and failure of mycological response.

Figure 25. **Boxplot illustrating the relationship between mycological response and AUC_{ave} (A) and AUC_{ave}:MIC (b).** Boxplots illustrating the comparison of AUC (A) and AUC:MIC (B) estimates for infants based on the mycological response [success (left) or failure (right)].

A.

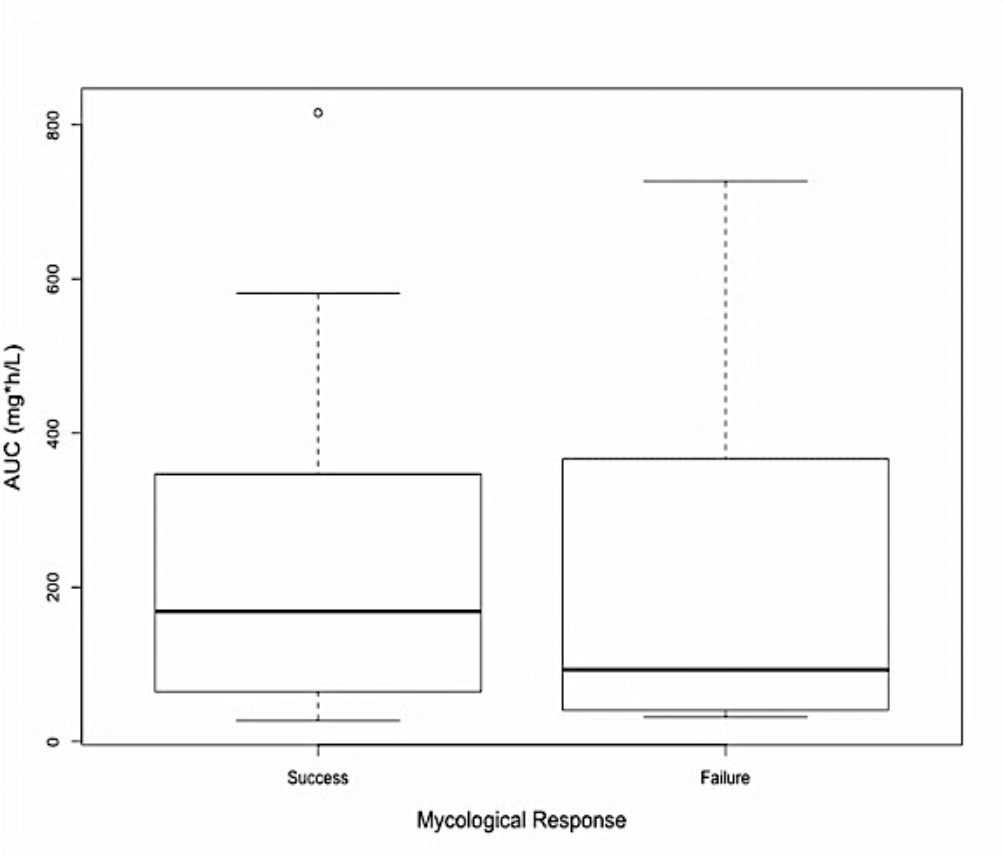

B.

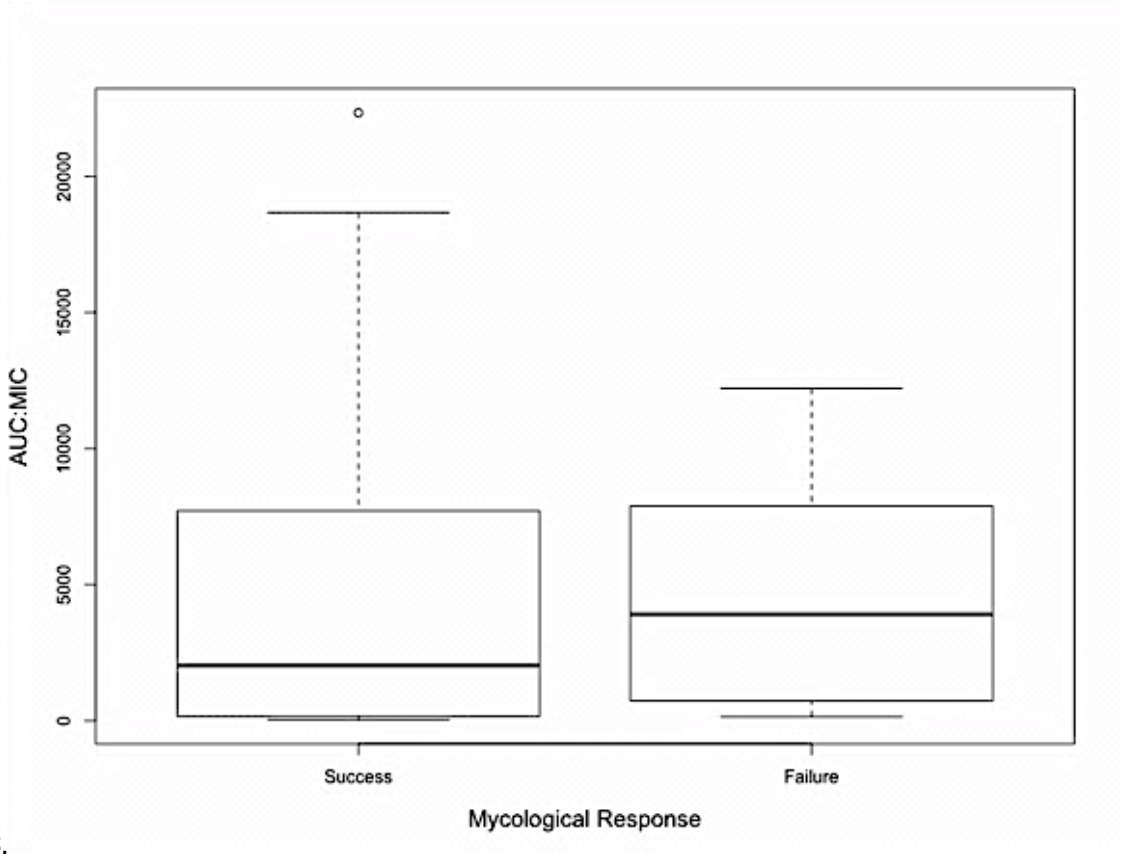

Discussion

In the current population PK analysis, robust estimates of drug exposures for individual patients were obtained. However, no statistically significant relationship between drug exposure and treatment outcomes was demonstrated. There are several potential reasons for this observation. First, the number of infants (n=29) was small, and therefore, the study lacked adequate power to detect a difference despite the numerically better response rate in the group with higher exposures [86% versus 73%, p=0.396]. Assuming the mycological responses rates of 86% and 73% from the two groups, the study would require a sample size of approximately 142 to yield at least 80% power (two-sided, 5% significance level). Second, there is extreme heterogeneity in the clinical

characteristics of neonates and young infants with many factors that are extraneous to the infection that potentially confound outcome measures (e.g. gestational age, birth weight, and other concomitant co-morbidities). Third, there is significant heterogeneity in the clinical presentation and prognosis of *Candida* infections in this population. Disease may range from simple colonization to dissemination and devastating involvement of the brain. It may be possible to stratify patients to more effectively account for the heterogeneity; however, there simply are not adequate laboratory and clinical tools to do this accurately.

Outcome measures used in these studies have a number of inherent limitations. Previous studies have demonstrated that infants that survive IC have poorer neurodevelopment outcomes compared to those without IC regardless of the presence of candidemia or confirmed CNS infection (66). The extent of correlation between short-term outcome measures and longer-term neurodevelopment outcomes is not known. The demonstration of negative fungal cultures is central to definitions of disease resolution. However, the lack of sensitivity of fungal cultures (<50%) (149) impairs the clinical utility of this metric. Clinical signs and symptoms are neither sensitive nor specific enough to assess therapeutic response (150). The strongest predictor of septicemia in one study was hypotension, present in less than 5% of the infants, which had only a 31% positive predictive value (151). All-cause mortality is obviously an important endpoint, but is invariably confounded by comorbidities that may swamp the signal coming from the drug-pathogen interaction. The use of biomarkers such as (1→3) β–D-glucan could aid in the objective assessment of the response to therapy (152, 153). These data and

others suggest that fungal biomarkers be included for assessment of therapeutic response in future clinical trials (154).

A further problem resides in substantial difficulties in conducting clinical trials in this patient population. Enrollment in the micafungin clinical trials was extremely slow. For example, the recently terminated study enrolled only 30 of the 225 planned patients in 2 and a half years (144). Reasons for such slow recruitment may be related to the decreased incidence of invasive candidiasis in this population (155). A recent study reported in 2014 that the annual US incidence of invasive candidiasis decreased from 3.6 episodes to 1.4 episodes per 1000 infants, from 24.2 to 11.6 episodes per 1000 infants with a birth weight of 750– 999 g, and from 82.7 to 23.8 episodes per 1000 infants with a birth weight < 750 g (155). The terminated study provides a recent example of the difficulty of conducting these studies (144). This study had 70 sites from 23 countries available to screen patients. Only half of the sites found appropriate infants to screen and only 22% of them were able to enroll at least one infant.

Clinical trials may not be the most efficient way to identify safe and effective regimens for relatively rare fungal infections. Preclinical-to-clinical bridging studies represent one of the few ways regimens can be de-risked for clinical study. Importantly, however, there is relatively little experience with this approach and certainly no consensus on the type of studies that are required. We have recently reflected and summarized some of the necessary factors in a PK-PD package for the development of new antifungal agents in adults (156). The same exercise now needs to be performed for infants. This topic was discussed in detail at a recent FDA workshop (http://www.fda.gov/Drugs/NewsEvents/ucm507958.htm). Some important factors

identified in the workshop include: (1) using preclinical models that are a faithful mimic of human neonatal disease. Such an approach enables pharmacodynamic idiosyncrasies in infants to be accounted for; (2) using neonatal strains and studying more than one strain; (3) cross validating findings from various models and understanding the reasons for the differences; (4) using positive controls that have a clinical indication and an effective regimen with enough information to enable an experimental-clinical PK-PD bridge. If we could build a collection of these "positive controls" for future drug development in infants, the performance of a new agent could be geared to compete with the positive control; (5) setting up experimental models that produce "on scale" readouts. Model behavior is governed by the chosen experimental conditions, such as strain, inoculum, background immunosuppression, delay in initiation of treatment, and treatment duration. The key thought is that clinically relevant exposures of a positive control induces a response in the middle of the drug exposure-response curve.

While stating all this, clinical data from neonates is still a critical piece of finding the safest optimal dose. For safety data we still need to evaluate dosing in neonates and models such as registries for clinicians to enter important information when rare conditions are treated with newer drugs and drug dosing may be another way to address these challenges.

In conclusion, a statistically significant drug exposure-response relationship for micafungin for neonatal candidiasis was not found. However, PK-PD studies suggest higher exposures are warranted in the setting of suspected or proven CNS infections. This is especially true for neonates and young infants where the risk of CNS infection is high. Without larger numbers of patients and better, more reliable outcome measures, linkage

of the PK-PD experiments to the clinic remains uncertain. Therefore, carefully designed experimental programs coupled with PK-PD bridging studies provide the best way to develop new drugs for neonates and infants.

Chapter 8 Population Pharmacokinetic of VL-2397, A Novel Systemic Antifungal Agent with Activity Against Triazole-Resistant Aspergillus spp.

Abstract

Background. VL-2397 is a novel, natural product isolated from *Acremonium persicinum* that has potent *in vitro* and *in vivo* fungicidal activity against *Aspergillus* species. The pharmacokinetics from single ascending dose (SAD) and multiple ascending dose (MAD) cohorts in a Phase 1 study were combined to construct a population pharmacokinetic (PPK) model for VL-2397.

Methods. Healthy subjects 18 to 55 years of age received single doses of VL-2397 at 3, 10, 30, 100, 300, 600, and 1200 mg, multiple doses of 300, 600, and 1200 mg for 7 days, or 300 mg three-times per day for 7 days followed by 600 mg once daily for the next 21 days. Plasma samples for analysis were collected throughout the dosing interval. PPK model development was performed using Pmetrics (v1.5.1, U of Southern CA).

Results. A total of 1908 plasma concentrations from 66 subjects were included. The drug concentrations over time increased in a less than dose proportional manner for all doses above 30 mg. This was further confirmed by plotting dose-normalized concentrations over time that did not overlap. A non-linear saturable binding model with 3 compartments fit the data well. Estimates of clearance increased with dose with mean values ranging from 0.4 L/h at 3 mg and 8.5 L/h at 1200 mg. Mean estimated volume in the central compartment ranged from 4.8 L to 6.9 L. In the first 24 hours, once daily

dosing results in a rapid decrease in plasma concentrations by hour 16 to approximately 1 mg/L, regardless of dose, with a slow clearance of the molecule over time. Administration of 300 mg every 8 hours achieved concentrations above 1 mg/L over an entire 24-hour period. There was a significant relationship of body surface area to clearance.

Conclusion. The data suggests that VL-2397 has non-linear saturable binding kinetics. Protein binding is the likely primary source of the non-linearity. The PPK model can be used to optimize dosing by bridging the kinetics to efficacious pharmacodynamic targets.

Introduction

Invasive aspergillosis (IA) is a rapidly life-threatening fungal disease that most commonly affects patients with significant immunodeficiency (157). There has been a progressive expansion of anti-*Aspergillus* agents in recent years. Nevertheless, suboptimal therapeutic outcomes have resulted from antifungal drug resistance, a limited spectrum of antifungal activity, drug toxicity, drug-drug interactions, and pharmacokinetic variability (158, 159). Hence, there is an urgent need to develop new antifungal agents with novel mechanisms of action (MOA).

VL-2397 is a natural product isolated from *Acremonium persicinum,* strain MF-34733 that exhibits potent *in vitro* and *in vivo* fungicidal activity against medically important *Aspergillus* species (73, 74). VL-2397 is a hexapeptide with a molecular weight of 915.4 Da (74). The complex structure resembles ferrichrome, which is a siderophore that chelates iron via the siderophore transporter, Sit1 (**Figure 26**).

Figure 26 Chemical Structure of VL-2397. Abbreviations: C=carbon; O=oxygen; H=hydrogen; N=nitrogen; Al=aluminum

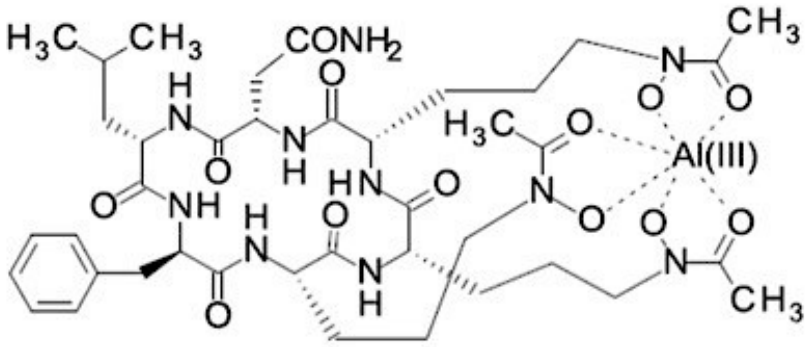

The intracellular target that is ultimately responsible for antifungal activity is not known (74, 75). Mammalian cells do not utilize the Sit1 siderophore transporter, which is one potential explanation for differential activity in fungi and animals (160). Thus, VL-2397 represents an exciting future alternative to overcome some current limitations of modern antifungal therapy.

VL-2397 demonstrates rapid (within the first 2-4 hours) and potent *in vitro* fungicidal activity (MIC_{90} values ≤ 2 mg/L) against *Aspergillus fumigatus* (including triazole-resistant *A. fumigatus*), *A. terreus*, *A. flavus*, *A. nidulans, Candida glabrata, C. kefyr, Cryptococcus neoformans,* and *Trichosporon asahii*. The agent demonstrates limited *in vitro* activity (MIC_{90} values ≤ 8 mg/L) against *Fusarium solani* and does not appear to be active (MIC_{90} values > 16 mg/L) against *A. niger*, *Candida* spp. (with the exception of *C. glabrata* and *C. keyfr*), Mucorales, *Scedosporium apiospermum* and *Fonsecaea pedrosoi*. Live cell imaging suggests that VL-2397 causes arrest of hyphal elongation (75). VL-2397 causes dose-dependent prolongation of survival and reduction in fungal burden in the lung of immunocompromised mice with invasive pulmonary aspergillosis (76).

A first in human Phase I clinical trial with VL-2397 (VL2397-101) has been completed. Herein, we describe the population PK from this study, which was a randomized, dose-ranging, double-blind, placebo-controlled study to assess safety, tolerability and pharmacokinetics (PK) of intravenous (i.v.) infusion of VL-2397 to normal healthy subjects. These data and population PK models provide one of the critical steps in defining safe and effective regimens for patients with IA.

Methods

Study Design. An i.v. formulation of VL-2397 was used. The regimens are summarized in **Table 17**. Healthy adults in single ascending dose (SAD) Cohorts 1-7 received a single dose of VL-2397 ranging from 3 mg to 1200 mg. Subjects in multiple ascending dose (MAD) Cohorts 8-10 received multiple dosages of 300, 600, and 1200 mg once-daily for 7 days, while Cohort 11 received 300 mg every 8 hours (q8h) for 7 days followed by 600 mg every 24 hours (q24h) for the next 21 days. Infusion times varied with each regimen and ranged from 6 to 240 minutes.

Table 17 Description of Dosage Regimens in SAD and MAD Cohorts with VL-2397

Cohort	VL-2397 Dose (mg)	Volume (mg/mL)	Infusion Duration (min)	Number of Dosing Days (days)
1	3	0.12	6	1
2	10		20	
3	30		60	
4	100	1.2	20	
5	300		60	
6	600		120	
7	1200		240	
8	300		60	7
9	600		120	
10	1200		240	
11	300 q8h D1-7, 600 q24h D8-28		60 and 120, respectively	28

Pharmacokinetic Sampling. Plasma samples from the subjects in the single-dose Cohorts 1-7 occurred pre-dose (within 60 minutes prior to the start of the infusion),

midway through the infusion, at the end of the infusion, 15 and 30 minutes, and 1, 2, 3, 4, 6, 8, 12, 24, 36 to 48 hours relative to the start of the infusion. Additional follow-up samples were drawn on Days 5 and 11.

Plasma samples from the subjects in the MAD Cohorts 8-10 occurred pre-dose (within 60 minutes prior to the start of the infusion), midway through the infusion, at the end of the infusion, 15 and 30 minutes, and 1, 2, 3, 4, 6, 8, 12, and 24 hours (prior to day 2 dosing) relative to the start of the infusion on Day 1. During the 7-day dosing period, plasma samples were collected within 60 minutes prior to dosing on Days 3, 4, 5, and 6. On Day 7, samples were collected pre-dose (within 60 minutes prior to the start of the infusion), midway through the infusion, at the end of the infusion, 15 and 30 minutes, and 1, 2, 3, 4, 6, 8, 12, 24, 36, and 48 hours relative to the end of the infusion. Follow-up plasma samples were also collected on Days 11 and 17.

Plasma sampling for the MAD Cohort 11 occurred on Day 1 pre-dose (within 60 minutes prior to the start of infusion), midway into the infusion, at the end of the infusion, and 3, 7, 8, 11, 15, 16, and 19 hours relative to the end of the first infusion. The 7- and 8-hour time points were immediately before and after the administration of the second dose on Day 1. The 15-and 16-hour time points were immediately before and after the administration of the third dose on Day 1. Additional samples were drawn prior to the first infusion on Days 2 through 6. A 24-hour PK profile (pre-dose just prior to the start of the infusion, at the end of the infusion, and 3, 7, 8, 11, 15, 16, and 19 hours relative to the end of the first infusion on Day 7) was also collected. After day 7, single samples were drawn prior to the infusion on days 8 to 10, 15, and 22. A 48-hour profile (pre-dose just prior to the start of infusion, midway into the infusion, at the end of the

infusion, and at 15 and 30 minutes, and 1, 2, 3, 4, 6, 8, 12, 24, 36, and 48 hours relative to the end of the Day 28 infusion) was also collected. Additional plasma samples were drawn on Days 32 and 38.

Bioanalytical Analysis. VL-2397 plasma concentrations were determined using high performance liquid chromatography-tandem mass spectrometry (HPLC—MS/MS). The analysis was performed by MicroConstants (San Diego, CA, USA). VL-2397 was detected in human plasma samples with VL-2397-I.S. (internal standard) and sodium heparin (anticoagulant) precipitated using acetonitrile. Samples were vortexed and centrifuged. The supernatant was transferred to a clean tube and evaporated under nitrogen. The residue was reconstituted and an aliquot was analyzed by reverse-phase HPLC using Restek Allure Biphenyl column. The mobile phase was nebulized using heated nitrogen in a Z-spray source/interface set to electrospray positive ionization mode. The ionized compounds were detected using MS/MS. The dynamic range of the assay was 0.002 to 1 mg/L. The lower limit of quantification (LOQ) was 0.002 mg/L. The interday precision was below the acceptance criteria (≤15%) and ranged from 4.93 to 7.24%. The interday accuracy was below the acceptance criteria (≤+15%), ranged from -1.83 to 0.50%. The intraday precision failed the acceptance criteria of ≤15% (2.63 to 36.5%). The intraday accuracy passed (≤+20%) at a range of -12.0 to 14.0%.

***Population PK (PPK) Modeling*.** The plasma concentrations for each cohort were plotted versus time to evaluate the concentration-time profiles for each regimen (**Figure 27**). To assess for the presence of non-linearity the plasma concentrations for each patient were normalized by the daily dose.

Figure 27 VL-2397 Plasma concentration versus time over the first 24 hours after dosing for all cohorts on a linear (upper) and semi-logarithmic (lower) scale. Mean values (±SD) for each time point at each dosage level are represented by the symbols and bars above and below each symbol. Mg doses are represented in the graph, MD=multiple dose.

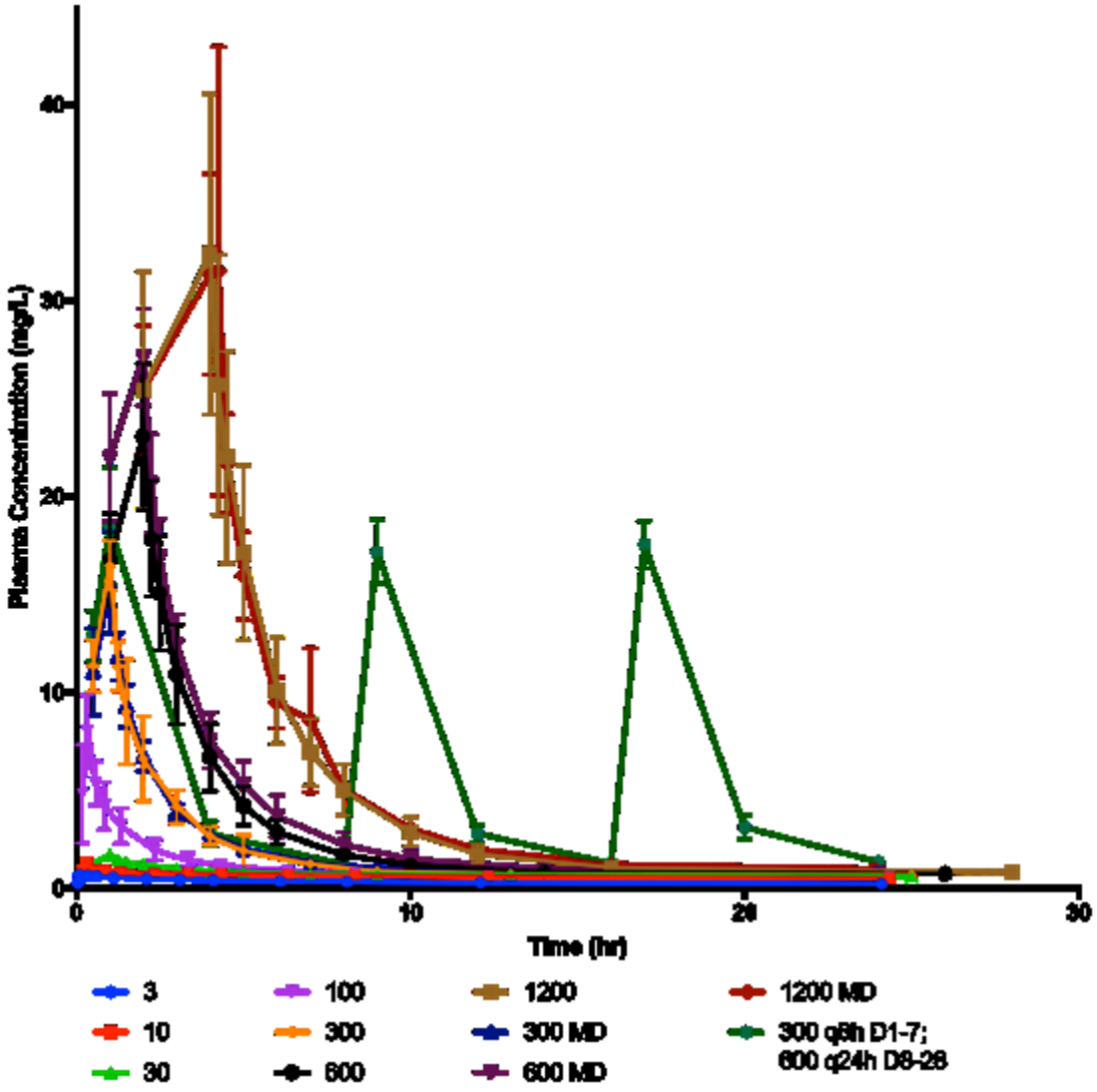

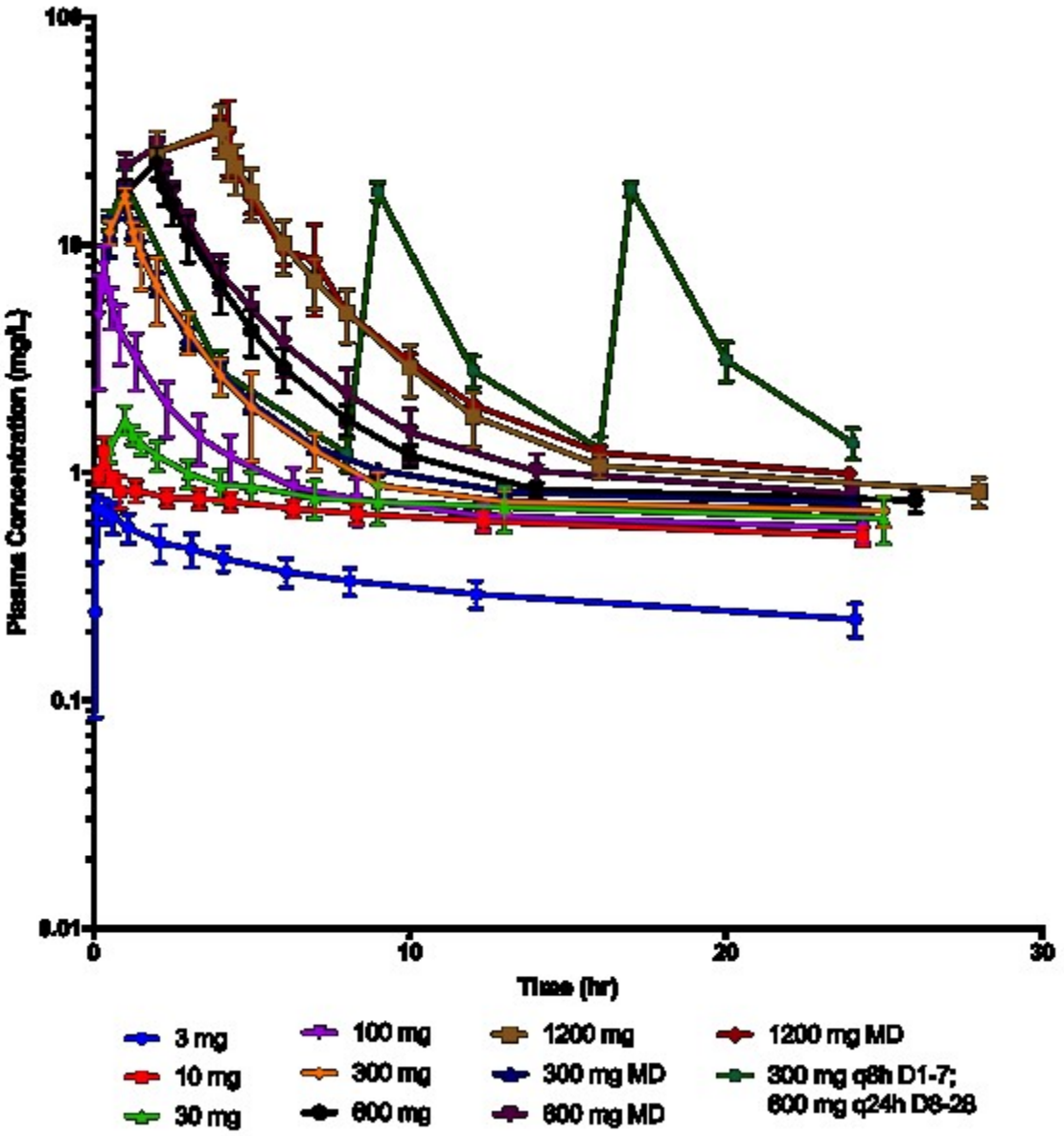

The PPK model was developed using nonparametric estimation with Pmetrics (v1.5.1, University of Southern California, Los Angeles, CA, USA) (77). Inspection of the plasma concentration over time curves suggested multiple phases of distribution and elimination. Therefore, 2, 3, and 4 compartment models were fitted to the data. These multi-compartment linear PK models could not account for the observed non-linear PK.

A saturable binding compartment was used to account for the observed non-linearity. This compartment accounted for phenomena that may be responsible for the observed non-linear PK such as the binding of drug to proteins, drug transporters, or to the endothelium. In standard PK models drug in the central compartment is fully mixed and is a combination of bound and free drug. In the model fitted to the VL-2397 data, total drug was separated into two distinct compartments. The central compartment represents free unbound drug, while a binding compartment represents bound drug. Measured drug concentrations are the sum of the bound and free compartments divided by the volume of the central compartment, i.e. (X(1)+X(3))/V.

The PK was further complicated by the presence of a prolonged terminal elimination phase suggesting an elimination process that was not accounted for by clearance from the central compartment. Therefore, a degradation component was added to the binding compartment that represents irreversible loss of drug from that compartment. The mathematical formula of the saturable binding model is shown:

Equation 14

$$XP(1) = RATEIV(1) - Kcp \cdot X(1) + Kpc \cdot X(2) - \left(\frac{Cl}{V}\right) \cdot X(1) - \left(\frac{Kon}{10^6}\right) \cdot \left((Rtot * 10^4) - X(3)\right) \cdot X(1) + \left(\frac{Koff}{10^6}\right) \cdot X(3) - Kcf \cdot X(1) + Kfc \cdot X(4)$$

Equation 15

$$XP(2) = Kcp \cdot X(1) - Kpc \cdot X(2)$$

Equation 16

$$XP(3) = \left(\frac{Kon}{10^6}\right) \cdot \left((Rtot * 10^4) - X(3)\right) \cdot X(1) - \left(\frac{Koff}{10^6}\right) \cdot X(3) - Kdeg$$

Equation 17

$$XP(4) = Kcf \cdot X(1) - Kfc \cdot X(4)$$

where K_{cp}, K_{pc}, K_{cf}, and K_{fc} represent first-order intercompartmental rate constants (c, central; p, peripheral 2; f, peripheral 3 compartments) with units h^{-1}. K_{on} and K_{off} are the constants for the rates of association and dissociation, respectively, with units of h^{-1}. Because both K_{on}, K_{off}, and Rtot values are extreme numbers relative to the other rate constants; therefore, to minimize the stiffness in the model each constant and Rtot were divided by 10^6 and multiplied by 10^4, respectively, to assist program estimation (161). R_{tot} represents the maximum binding and units are moles. Kdeg is a constant in the binding compartment (3), which regulates the slow turnover of the binding site and irreversible loss of drug from that compartment.

The PK data were weighted by the inverse of the estimated assay variance. Model acceptance was evaluated by visual inspection of the observed-versus-predicted concentration values before and after the Bayesian step, the coefficient of determination (r^2) from the linear regression of the observed-versus-predicted values, and estimates for bias (mean weighted error) and imprecision (adjusted mean weighted squared error).

The Day 1 (24-hour) area under the concentration-time curve ($AUC_{0\text{-}24}$) and Day 7 (24-hour) $AUC_{144\text{-}168}$ for each subject was calculated using the Bayesian posterior parameter estimates from the final model using the trapezoidal rule embedded within

Pmetrics.

Covariate Assessment and Model Building. Parameter estimates, clearance and volume, were evaluated against age, sex, weight, body mass index (BMI), body surface area (BSA), and race to determine if one or more should be considered for inclusion in the structural model. Each continuous covariate (age, weight, BMI, and BSA) was evaluated by plotting the variable to the individual parameter. If the confidence interval around the slope excluded zero, the covariate was considered to be significant.

Results

Study Population. Sixty-six healthy subjects from the 11 cohorts contributed data for analysis. The median (range) age, weight, and height were 43 years (range 21-55 years), 74.2 kg (range 56.5-109.3 kg), and 168.2 cm (146.8-195.1 cm), respectively. The majority of patients were Caucasian (53/66; 80%). All subjects completed the dosing schedules as planned except for 2 subjects from MAD Cohort 10 (1200 mg) who were discontinued early due to adverse events after 1 and 2 doses, respectively.

Assessment of plasma concentrations versus time. A total of 1908 plasma concentrations were included. The drug concentrations over time did not increase proportionally with dose. **Figure 27** shows plots of the first 24 hours for Cohorts 1-11 in the first 24 hours on both a linear and semi-logarithmic scale. Within the first 16 hours, the concentrations for the once-daily doses were at or below 1 mg/L and remained at this level through the rest of the dosing interval. This suggested a rapid and saturable distribution phase. **Figure 28** shows the plasma concentrations-versus-time for each

patient after normalizing each by the daily dose. There was minimal overlap of these plots suggesting non-linearity, especially above dosages of 30 mg per day.

Figure 28 Dose-normalized plasma concentrations-versus-time by cohort (A, B, and C). (upper, A) Dose-normalized concentrations over the first 24 hours; Cohorts 1-11. (middle, B) Dose-normalized concentrations over time for the single-dose Cohorts 1-7. (lower, C) Dose-normalized concentrations over time for the multiple-dose Cohorts (8-11). Mean values (±SD) for each time point at each dosage level are represented by the symbols and bars above and below each symbol. (mg doses are represented in the graph; MD=multiple dose).

A.

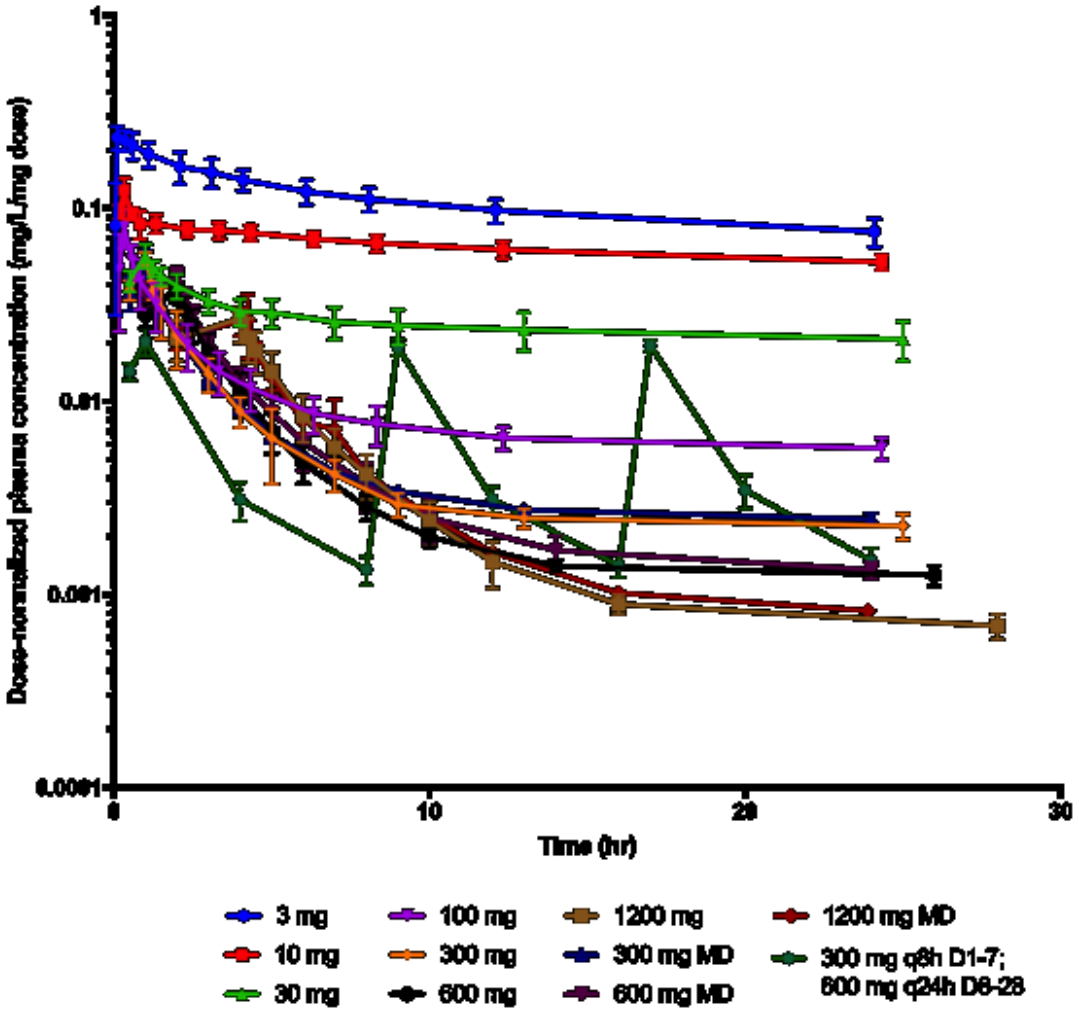

B.

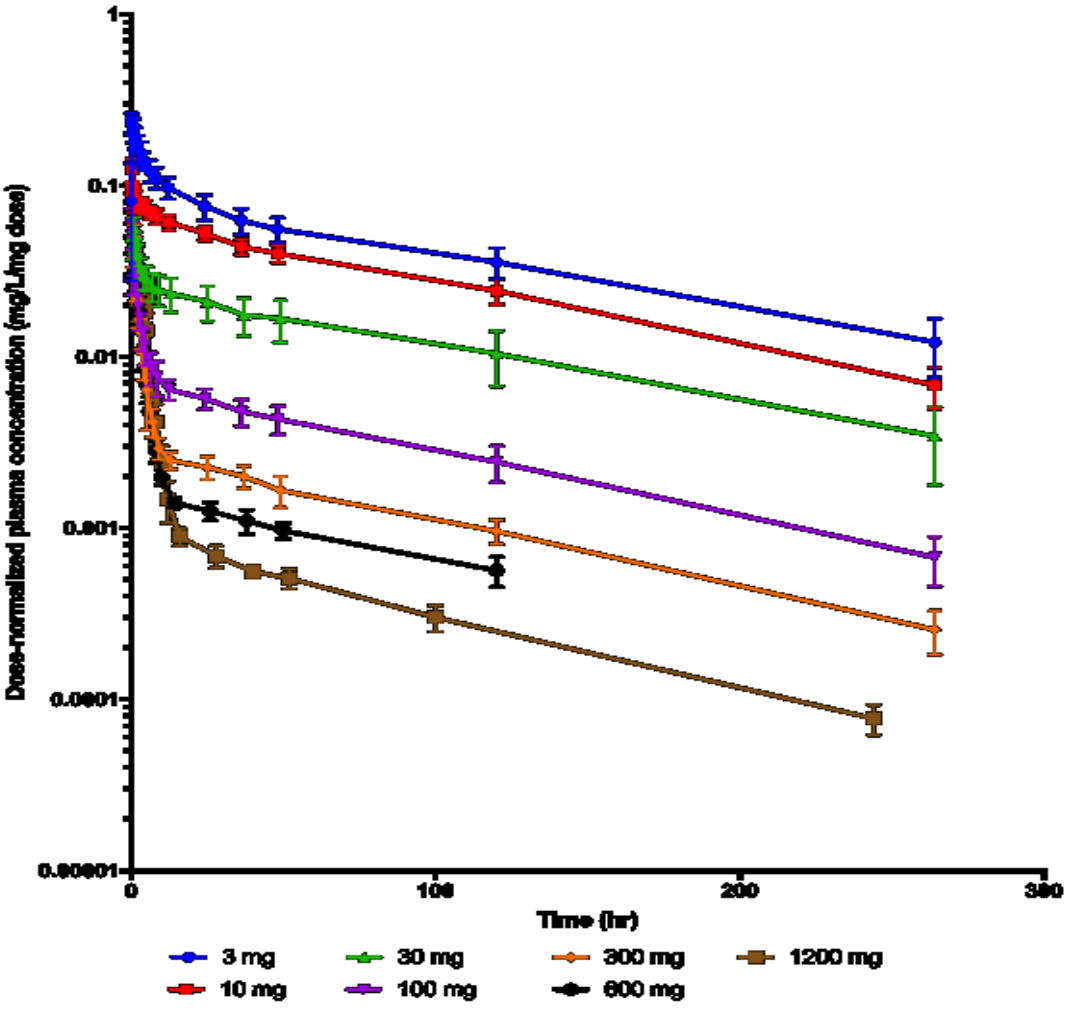
Dose-normalized plasma concentration (mg/L/mg dose)
1
0.1
0.01
0.001
0.0001
0.00001
0
100
200
300
Time (hr)
3 mg
10 mg
30 mg
100 mg
300 mg
600 mg
1200 mg

C.

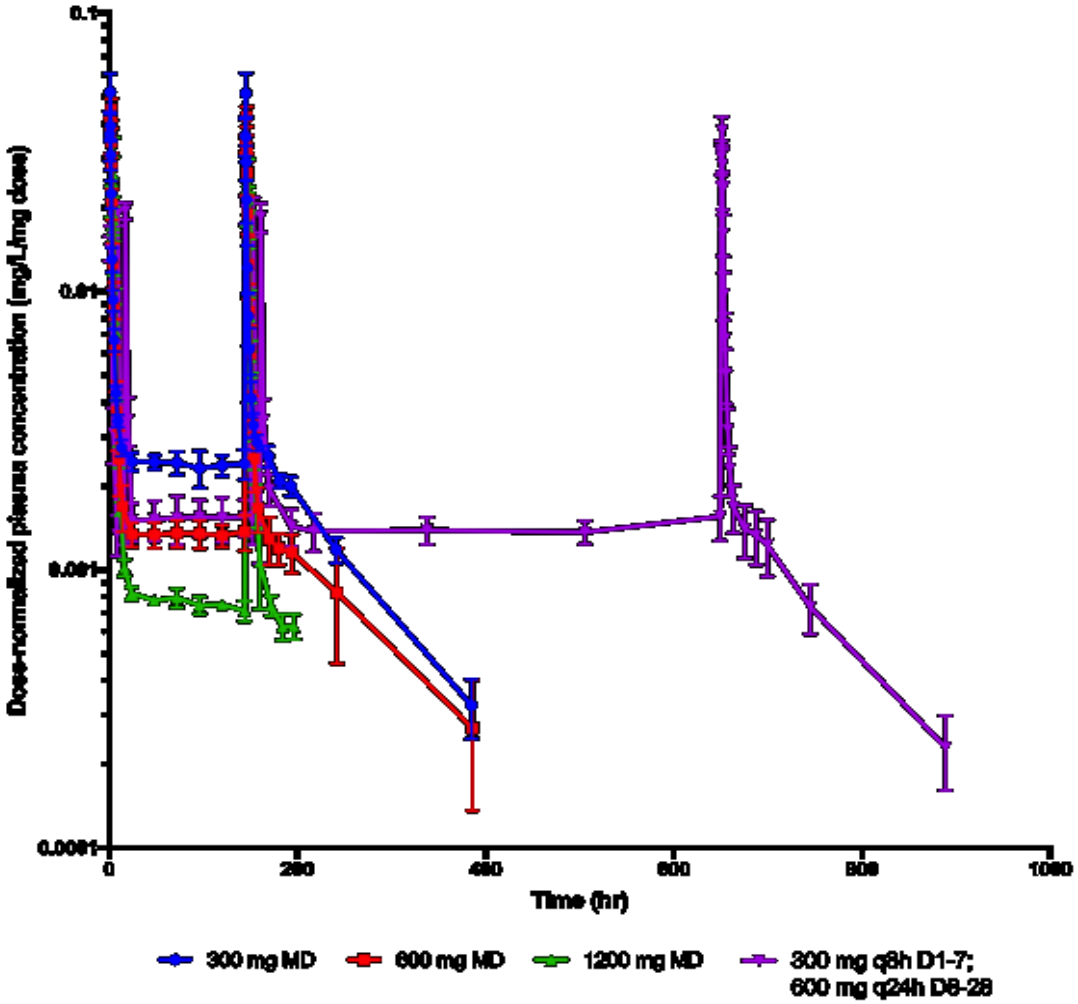
Dose-normalized plasma concentration (mg/L/mg dose)
0.1
0.01
0.001
0.0001
0
200
400
600
800
1000
Time (hr)
300 mg MD
600 mg MD
1200 mg MD
300 mg q8h D1-7;
600 mg q24h D8-28

Population Pharmacokinetic Modeling. A non-linear saturable binding model with 3 compartments fit the data well. The structural model is illustrated in Figure 29**.**

Figure 29 Illustration of Structural PPK Non-Linear Saturable Binding Model. Structural illustration of the population PK model. Boxes represent the plasma compartments (1=central, 2 and 3 are peripheral). The circle represents the binding compartment. Arrows demonstrate the flow of drug through the compartments and elimination. Abbreviations: Cl: clearance; V: volume in the central compartment; Kcp, Kcp, Kpc, Kcd, and Kdc: rate constants for drug moving from the different compartments (c, central; p, peripheral; f, third compartment): Kon and Koff: rate constants of association and dissociation; Rtot: maximum binding; Kdeg: rate constant regulating clearance from the binding compartment.

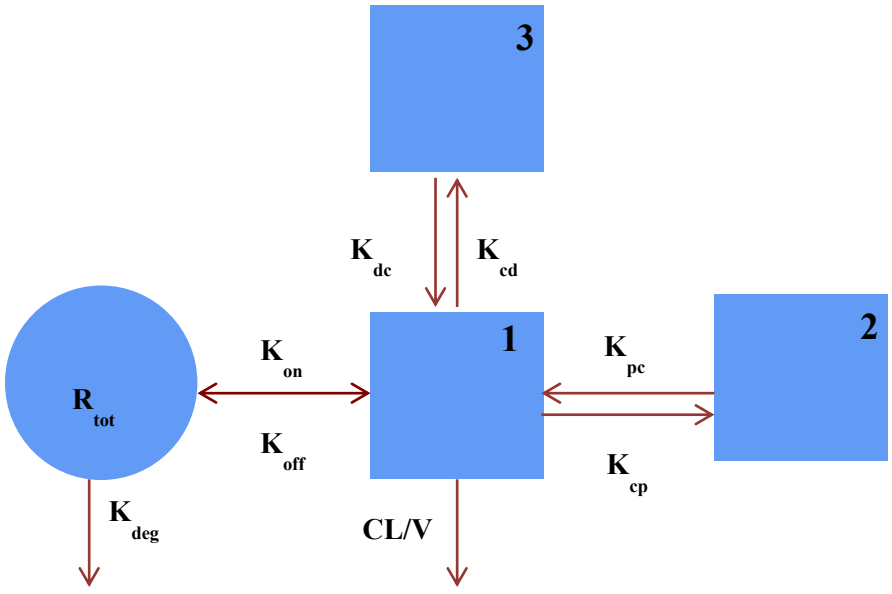

Visual inspection of the observed-versus-posterior predicted concentrations after the Bayesian step was acceptable. The coefficient of determination (r^2) was 0.987 (slope = 1.01 [95% confidence interval 1 to 1.01]) for the linear regression of the observed versus predicted mean concentrations (Figure 30). Measures of bias and imprecision were also acceptable (-0.124 and 1.04, respectively).

Figure 30 Observed-versus-predicted concentrations (mg/L) from the best model after the Bayesian step (A. population predicted; B. posterior predicted). *Upper* (A): Logistic regression of the observed versus median population predicted plasma concentration values. *Lower* (B): Logistic regression of the observed versus median individual posterior predicted plasma concentration values. Dotted line is the line of unity where the observed versus predicted values are equal.

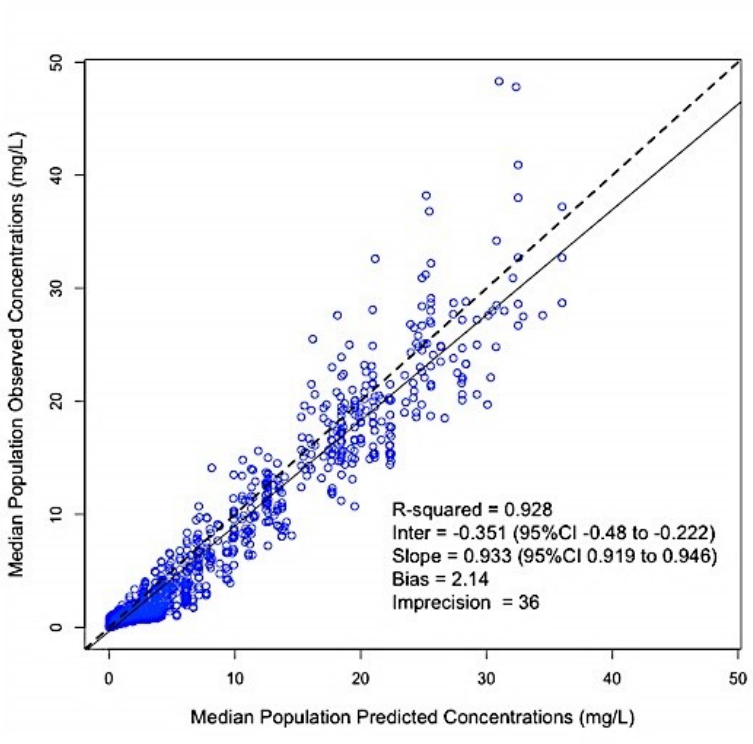

A

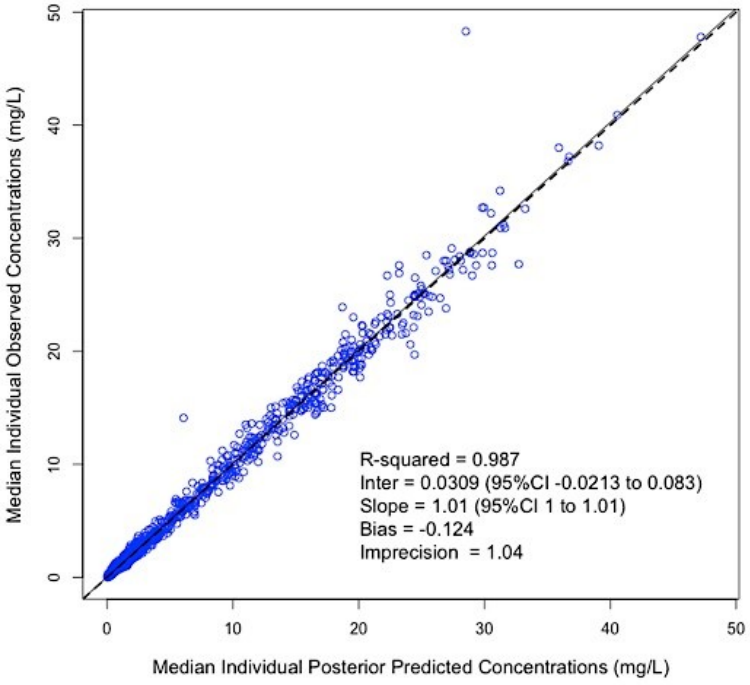

B

Individual plots for each subjects' observed and predicted concentrations over time showed good predictions by the model (Figure 31).

Figure 31 Overlay of Observed and Predicted Plasma Concentration Values for individual Subjects. Lines represent predicted concentrations and '+' are the observed values at each time point for the subject.

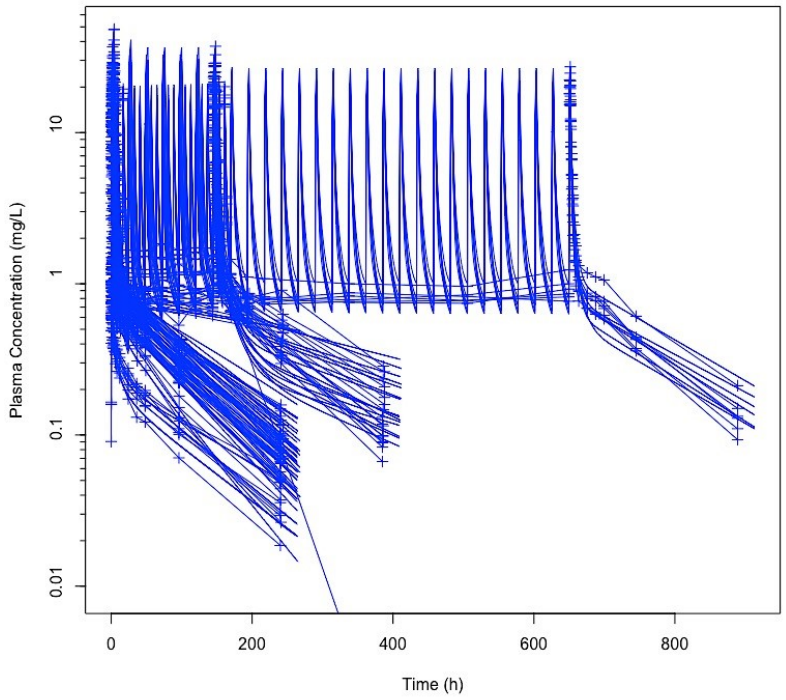

The estimated model parameters are included in **Table 18.**

Table 18 Median posterior parameter estimates for the best model

	Mean	Population SD	Median	Range
Cl/F (L/h)	5.56	3.57	6.80	0.25-9.95
V (L)	6.68	2.58	6.10	3.50-14.80
Kcp (h^{-1})	2.31	1.75	2.45	0.025-4.98
Kpc (h^{-1})	2.86	1.83	2.68	0.04-5.97
Kon (h^{-1})	0.57 x 10^{-6}	0.44 x 10^{-6}	0.35 x 10^{-6}	0.008 x 10^{-6}-1.49 x 10^{-6}
Koff (h^{-1})	21.01 x 10^{-6}	20.25 x 10^{-6}	10.33 x 10^{-6}	0.35 x 10^{-6}-49.75 x 10^{-6}
Rtot (mol)	1.79 x 10^{4}	1.25 x 10^{4}	1.46 x 10^{4}	0.52 x 10^{4}-3.98 x 10^{4}
Kcf (h^{-1})	0.50	0.35	0.45	0.06-1.42
Kfc (h^{-1})	0.69	0.90	0.22	0.02-2.99
Kdeg (h^{-1})	0.010	0.010	0.010	0.0003-0.050

Abbreviations: Cl: clearance; F: bioavailability; V: volume in the central compartment; Kcp, Kcp, Kpc, Kcf, and Kfc: rate constants for drug moving from the different compartments (c, central; p, peripheral; f, third compartment): Kon and Koff: rate constants of association and dissociation; Rtot: maximum binding; Kdeg: rate constant regulating clearance from the binding compartment.

The area under the plasma concentration-time curve (AUC) for each dose cohort is summarized in **Table 19**. As illustrated by the dose-normalized plots, AUC did not increase in a proportional manner.

Table 19 AUC values estimated from the PPK for each Dose Cohort

	Cohort (dose)	AUC_{inf} (mg·h/L)	
Single-Dose	1 (3 mg)	27.1 (4.2)	
	2 (10 mg)	70.1 (7.6)	
	3 (30 mg)	80.8 (24.9)	
	4 (100 mg)	83.6 (28.8)	
	5 (300 mg)	104.3 (12.8)	
	6 (600 mg)	150.6 (17.7)	
	7 (1200 mg)	236.0 (46.7)	
	Cohort	$AUC_{0\text{-}24}$ (mg·h/L) (Day 1)	$AUC_{144\text{-}168}$* (mg·h/L)
Multiple-dose	8 (300 mg)	319.9 (26.5)	133.1 (6.3)
	9 (600 mg)	711.2 (104.5)	206.1 (24.9)
	10 (1200 mg)	1352.1 (801.6)	302.6 (17.7)
	11 (300 mg q8h D1-7; 600 mg q24h D8-28)	856.51 (120.0)	1237.2 (127.0)

*$AUC_{144\text{-}168}$ is only applicable to the multiple dose Cohorts (8, 9, 10, and 11)

Assessment of covariates. **Figure 32** and **Figure 33** illustrate the relationship of age, weight, BMI, and BSA on clearance and volume, respectively. The only covariate relationship found to be significant was BSA on clearance based on linear regression. Clearance decreases with increasing BSA (95% confidence interval for the slope was -10.19 to -1.61) (**Figure 32**). There was no relationship between sex and race on clearance or volume ($p > 0.5$). Of note, the low clearance values in the graph are real values from the lowest dose cohort (3 mg).

Figure 32 Linear regression analysis to describe the relationship of clearance and age (upper left), weight (upper right), BMI (lower left), BSA (lower right). *Cl vs age (Upper left)*: Slope -0.03 [95% CI -0.12 to 0.07], r^2=0.005; p value =0.59. *Cl vs weight (Upper right)*: Slope -0.07 [95% CI -0.14 to 0.0002], r^2=0.06; p value =0.05. *Cl vs BMI (Lower left)*: Slope 0.08 [95% CI -0.28 to 0.43], r^2=0.003; p value =0.66. *Cl vs BSA (Lower right)*: Slope -5.9 [95% CI -10.2 to -1.6], r^2=0.12; p value =0.008.

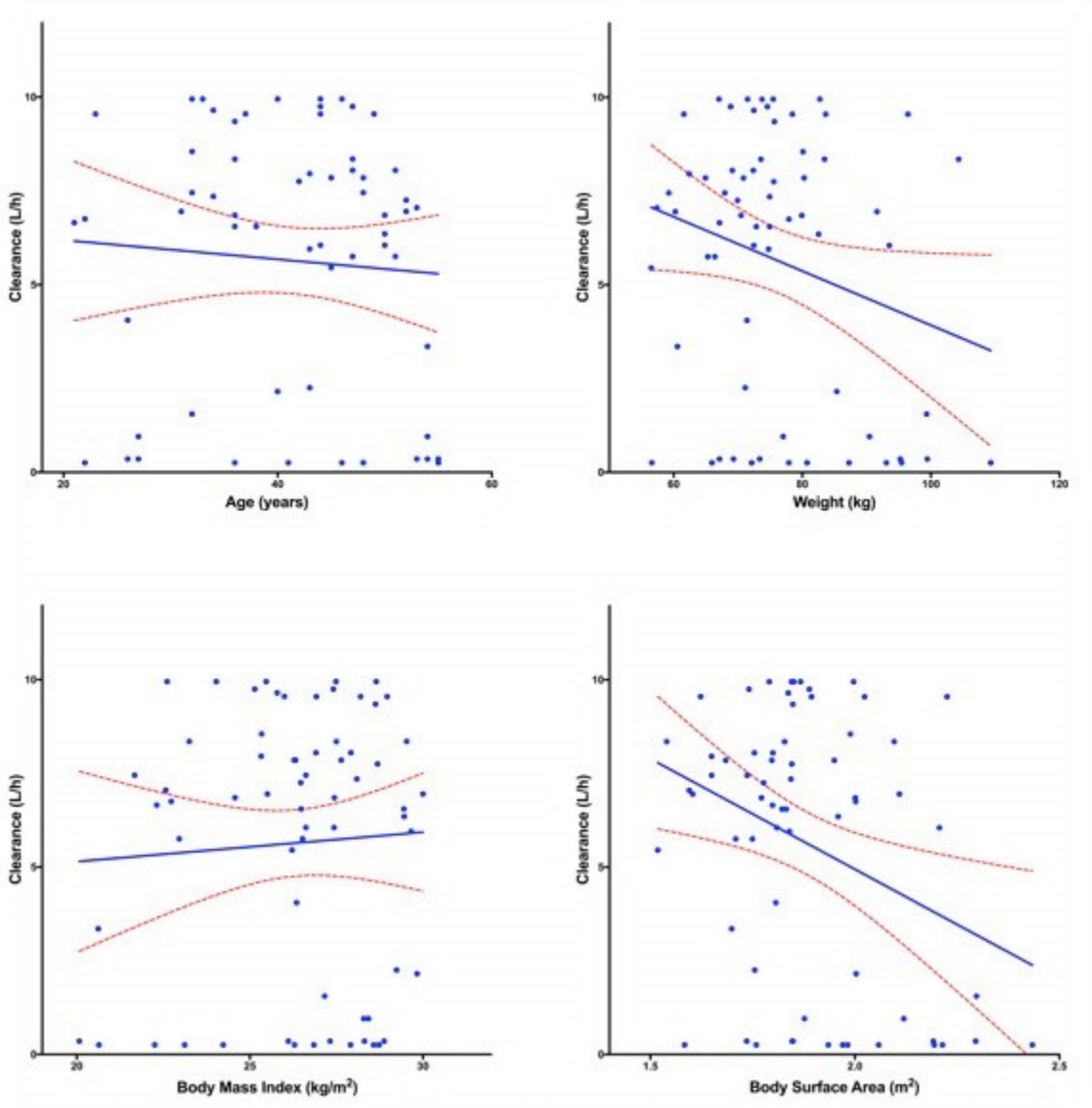

Figure 33 Linear regression analysis to describe the relationship of volume and age (upper left), weight (upper right), BMI (lower left), BSA (lower right). *V vs age* (Upper left): Slope -0.02 [95% CI -0.09 to 0.05], r^2=0.006; p value =0.53. *V vs weight* (Upper right): Slope 0.05 [95% CI -0.006 to 0.1], r^2=0.05; p value =0.08. *V vs BMI* (Lower left): Slope 0.008 [95% CI -0.25 to 0.27], r^2=0.000; p value =0.95. *V vs BSA* (Lower right): Slope 2.1 [95% CI -1.15 to 5.42], r^2=0.03; p value =0.20.

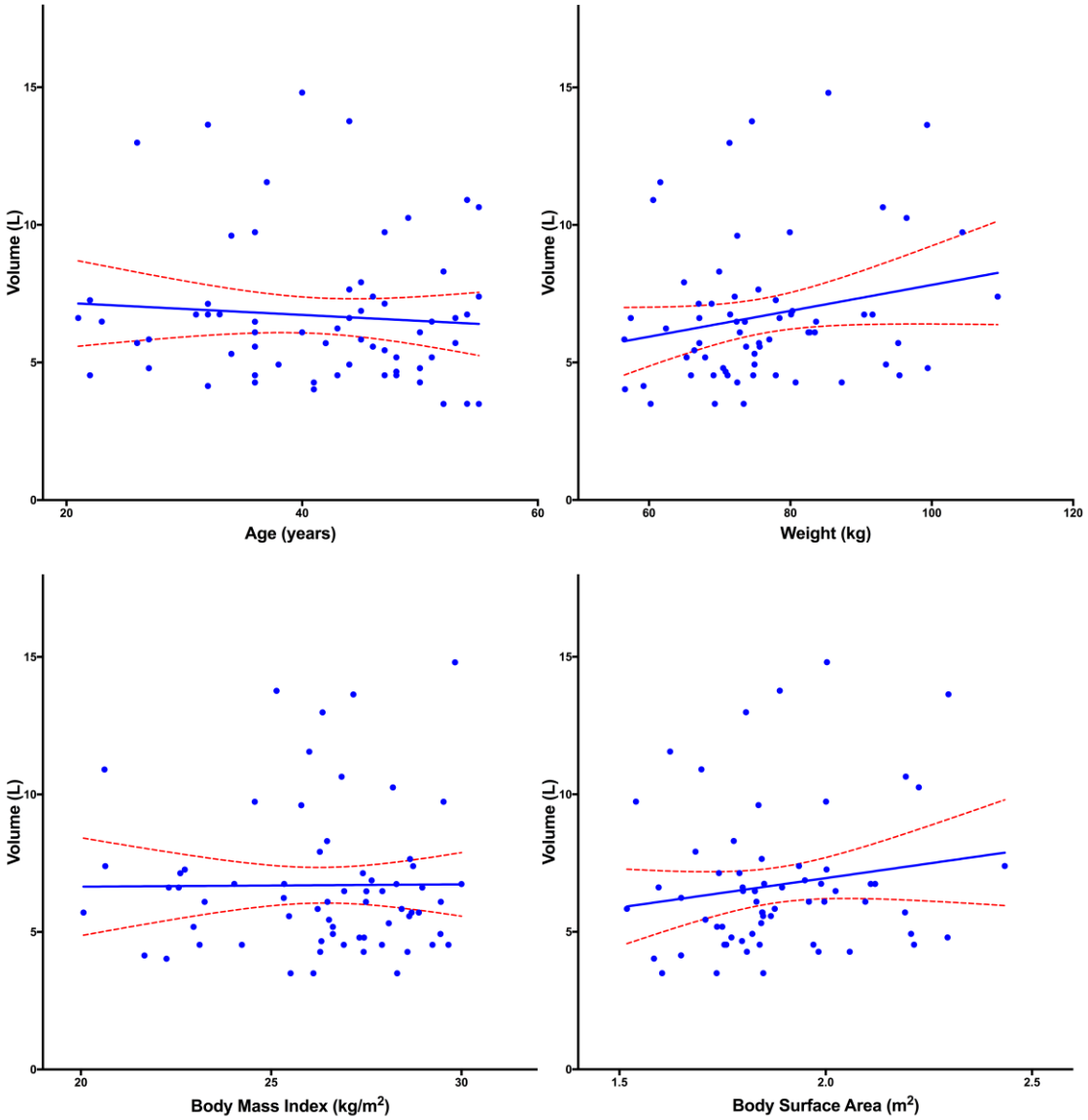

Discussion

VL-2397 is a systemic antifungal agent that is being developed for the treatment of invasive aspergillosis and is one of few agents in development with a novel MOA that have the potential to overcome some of the deficiencies of currently licensed agents. Non-compartmental analysis of the pharmacokinetic data in this study revealed that VL-2397 exhibited non-linear pharmacokinetics and neither demonstrated dose proportionality nor dose linearity.

Early *in vitro* studies using equilibrium dialysis suggested non-linear protein binding might be responsible for the non-linearity pharmacokinetics of VL-2397 kinetics (unpublished data). This knowledge and evaluation of the raw data led to development of a saturable binding compartment and to split the total drug concentration into a free and bound compartments. The saturable binding model used was derived from modifications to standard Michaelis-Menten terms and target mediated drug disposition models (163). While this model did result in a significant improvement in the goodness of fit, it did not adequately describe the terminal phase where there was considerable over-prediction of the observed concentrations. To account for this deficiency degradation component was added to the binding compartment to represent proteolytic loss of drug. The addition of this loss component improved the goodness of fit and resulted in acceptable predictions. The binding compartment at this stage is hypothetical, but based on evidence of saturable *in vitro* protein binding in plasma, and may need to be further confirmed by *in vitro* binding assays.

In the future, it will be important to better understand the mechanism of the non-linearity. This will be especially important for utilizing the PPK model for further dose

selection in Phase 2 and 3 clinical studies. An in-depth understanding of protein binding in the preclinical models of invasive fungal infections will also be important to ensure bridging studies are appropriately designed and interpreted.

In this study, no significant relationship was found between age, weight, and BMI and clearance or volume. Increases in BSA were associated with decreases in clearance.

In conclusion, in this Phase 1 study in healthy volunteers, VL-2397 demonstrated non-linear saturable binding kinetics. Protein binding is likely the primary source of the non-linearity. A saturable binding model best described the data. BSA was the only covariate with a significant relationship to clearance. The PPK model can be used to optimize dosing by bridging the kinetics to efficacious pharmacodynamic targets.

Chapter 9 Discussion and Conclusions

The purpose of this thesis is to utilize different PK-PD techniques to explore exposure-response relationships of several antifungal agents. The work starts with mathematically linking the time course of isavuconazole drug exposure with the time course of response to antifungal therapy measured as changes in biomarker concentrations (Chapter 3). In this effort, the recent results of phase 3 clinical trials for the same antifungal agent were available to enable validation of the *in vivo* results. The availability of the clinical trials results afforded the opportunity to demonstrate usefulness of the *in vivo* rabbit model and the endpoints utilized for isavuconazole and has implications for clinical interpretive breakpoints for *Aspergillus* spp. Uniquely, it provides validation for a path of investigation for future antifungal agents in development. Expanding on this work, the GM data from the same isavuconazole clinical trial was used to look for early changes in GM that could be used to predict patient outcomes and guide therapeutic decisions early in the treatment course (Chapter 4). Chapters 5 and 6 focus on the characterization of pharmacokinetic data of isavuconazole, evaluating those characteristics in different patient settings, infection types, and conditions (e.g. mucositis), and evaluating any potential impact on efficacy. The focus then switches to the PK-PD evaluation of the echinocandin antifungal, micafungin, in the treatment of neonatal candidiasis (Chapter 7). A population PK model was constructed and efficacy data from 2 efficacy trials were combined to provide a linkage from the experimental data to the clinic. Chapter 8 provides the first attempt to construct a population PK model for a novel investigational antifungal agent, VL-2397, from the initial phase 1 healthy volunteer clinical studies.

In Chapters 3 and 4, the PD of isavuconazole, was explored using GM as a prognostic tool both from an *in vivo* model and clinical trial. The biomarker, GM, is important experimental and monitoring tool in the management of patients with invasive aspergillosis. As discussed in Chapter 1, critical steps to establish the clinical utility of this biomarker continue to be made. However, more work is needed in patients to better define ways of using GMI early in the treatment course to facilitate therapeutic decisions that can be beneficial for an individual patient. As evidence accumulates, it is likely that GM will be incorporated into clinical outcome criteria and can therefore be used to assess the response to antifungal therapy for future clinical trials. An analysis of serial serum GMI in patients with invasive aspergillosis from a phase 3 clinical trial demonstrated that increases in GMI in the first week of therapy significantly increase the likelihood of death and unsuccessful response. These analyses can be utilized to further validate and eventually establish early intervention measures for use during therapy.

Various intrinsic and extrinsic factors impact the pharmacokinetics of antifungal agents. These factors can be explored using population PK-PD techniques to determine if exposures and ultimately efficacy are impacted. For antibiotics that rely on thresholds of drug concentrations and time above MICs, evaluation of any possible sub-populations or conditions that threaten the ability to reach or maintain these thresholds is important to ensure adequate therapy. In Chapters 5 and 6, the impact of factors such as disease state (type of infection), underlying disease (e.g. hematological malignancy), and other medical conditions (e.g. mucocitis) on the PK-PD of isavuconazole are evaluated. In these efforts, there were several findings and hypotheses generated. Across the various IFD and underlying diseases, isavuconazole clearance and AUC did not differ

significantly. PTA analysis allowed for an estimate of the MIC coverage provided by the isavuconazole clinical dosing regimen for common fungal pathogens, such as *A. fumigatus*, *A. flavus,* and *A. terreus* strains, and the results support previous PTA analyses (99) for these organisms. For *C. albicans* and non-*albicans Candida* spp., the coverage of the isavuconazole MIC distribution from a large collection of *in vitro* susceptibility studies was reasonable. However, the PK characteristics for patients infected with invasive candidiasis and candidemia have not been evaluated by the time of this report. Given that the recently completed phase 3 clinical trial of the treatment of candidemia did not meet the primary endpoint of overall response at the end of the intravenous isavuconazole therapy compared to caspofungin (117), characterization of the PK in IC patients directly is critical. If different, it could affect the clinical breakpoint selection and potentially the recommended dosing regimen for treatment of IC.

In Chapter 6, patients with slightly lower bioavailability had outcomes similar to those with higher bioavailability. Therefore, use of the oral formulation of isavuconazonium sulfate during episodes of mucositis may be acceptable; however, treating physicians may consider extending isavuconazole intravenous therapy during episodes of mucositis or monitoring levels to ensure they are within the range reported from the clinical trial. However, additional studies in this population may be warranted.

In Chapter 7, an effort was made to evaluate linkage between *in vivo* PK-PD experimental findings to the clinic for an area of significant unmet medical need. Neonatal candidiasis represents a significant morbidity and mortality burden in affected infants (150). Available treatment regimens lack appropriate evidence of treatment effect from well-conducted clinical trials. In addition, due to the risk of CNS and organ

involvement, dosage regimens are often not established with attention to this nuance in the neonatal infection. Micafungin has been tested rigorously experimentally and PK bridging studies have established a dosage regimen that does account for the risk of CNS disease. However, the attempt to complete a clinical trial with this dosage was unsuccessful due to the low incidence of the disease (155). With the available clinical and PK data, an exposure-response analysis was performed. While the appropriate target exposure was achieved with the target dosage, the analysis did not find a significant difference between those infants that achieved the target exposure and those that did not. A larger sample size is needed in order to find the true relationship. The study is important as it emphasizes the limitations of small numbers, the need for well-characterized experimental models and PK bridging studies in the absence of large-scale clinical trials to establish efficacy and safety.

Chapter 8 provides the first population PK analysis of the investigational agent, VL-2397. This compound has demonstrated potent in vitro and in vivo activity against *Aspergillus* spp., including triazole-resistant pathogens. The pharmacokinetics of VL-2397 are complex. A non-linear saturable binding model provided the best fit to the data. The non-linearity appears to stem from non-linear protein binding. A better characterization of the mechanism of the non-linearity is important, particularly, for utilizing the PPK model for further dose identification in Phase II and III clinical studies. An in-depth understanding in protein binding in the preclinical models of invasive fungal infections will also be important to ensure bridging studies are appropriately performed and interpreted.

This thesis provides valuable insights into future research opportunities and areas of

further understanding. First, in the setting of invasive fungal disease, biomarkers have increased the ability to diagnosis infections. Experimentally these same biomarkers are utilized successfully to follow the course of an infection and response to antifungal therapy. These tools are desperately needed to provide a more objective guide to therapy in the clinic. Our data provides a path but requires further validation. This learning brings us closer to individualizing therapy to patients. Second, drug development of the next group of antifungal compounds will rely more and more on smaller databases. Therefore, a heightened emphasis on well-characterized *in vitro* and *in vivo* experiments that can be utilized to establish exposure thresholds from which PK bridging studies can be used from population PK models to ensure adequate dosing regimens. Finally, regulatory authorities are increasing their expertize in PK-PD and will continue to increasingly expect drug development programs include full PK-PD packages similar to those outlined in the EMA guidance.

In summary, invasive fungal infections result in significant morbidity and mortality even with the recent advances in the armamentarium. However, large-scale clinical trials to evaluate comparative efficacy and safety when completed do not always address questions pertaining to the heterogeneity of the populations in the clinical trials. Therefore, PK-PD techniques can assist in that effort. In addition, quite often these studies are not feasible due to the low incidence of the specific fungal infections; and therefore, evaluation of the antifungal agent in well-characterized *in vivo* and *in vitro* models followed by human PK bridging studies are essential in the optimization of these agents. Effectively combining these tools can be the difference between a successful or failed drug development program, or future failure post-market authorization due to

resistance development and failure reported in case series. Not to mention proper utilization of PK-PD techniques could eliminate some of the increased costs associated with the evaluation of multiple dosages in early proof of concept clinical trials.

Important questions about the appropriate use of antimicrobial therapies can be investigated using PK-PD techniques. Providing those that use these agents with an enhanced understanding of the amount and duration of a specific compound required to treat an infection. The result of these investigations should lead to better patient outcomes, decrease in the development of resistance pathogens, and minimizing the risk to antibiotic drug development programs due to better optimization of dosing regimens.

References

1. **Ambrose PG, Nightingale CH, Murakawa T.** 2009. Antimicrobial Pharmacodynamics in Theory and Clinical Practice. Antimicrobial Pharmacodynamics in Theory and Clinical Practice (Infectious Disease and Therapy). Taylor and Francis CRC ebook account. Kindle Edition, New York, NY.
2. **Rex JH, Eisenstein BI, Alder J, Goldberger M, Meyer R, Dane A, Friedland I, Knirsch C, Sanhai WR, Tomayko J, Lancaster C, Jackson J.** 2013. A comprehensive regulatory framework to address the unmet need for new antibacterial treatments. The Lancet Infectious Diseases **13:**269-275.
3. **Drusano G.** 2016. From lead optimization to NDA approval for a new antimicrobial: Use of pre-clinical effect models and pharmacokinetic/pharmacodynamic mathematical modeling. Bioorg Med Chem **24:**6401-6408.
4. **Hope W, Kruhlak M, Lyman C, Petraitiene R, Petraitis V, Francesconi A, Kasai A, Mickiene D, Sein T, Peter J, Kelaher A, Hughes J, Cotton M, Cotten C, Bacher J, Tripathi S, Bermudez L, Maugel T, Zerfas P, Wingard J, Drusano G, Walsh T.** 2007. Pathogenesis of *Aspergillus fumigatus* and the Kinetics of Galactomannan in an In Vitro Model of Early Invasive Pulmonary Aspergillosis: Implications for Antifungal Therapy. The Journal of Infectious Diseases **195:**455-466.
5. **Garnacho-Montero J, Olaechea P, Alvarez-Lerma F, Alvarez-Rocha L, Blanquer J, Galvan B, Rodriguez A, Zaragoza R, Aguado JM, Mensa J, Sole A, Barberan J.** 2013. Epidemiology, diagnosis and treatment of fungal respiratory infections in the critically ill patient. Rev Esp Quimioter **26:**173-188.
6. **Neofytos D, Treadway S, Ostrander D, Alonso CD, Dierberg KL, Nussenblatt V, Durand CM, Thompson CB, Marr KA.** 2013. Epidemiology, outcomes, and mortality predictors of invasive mold infections among transplant recipients: a 10-year, single-center experience. Transpl Infect Dis **15:**233-242.
7. **Lanternier F, Lortholary O.** 2008. Liposomal amphotericin B: what is its role in 2008? Clin Microbiol Infect **14:**71-83.
8. **Enoch D, Idris S, Aliyu S, Micallef C, Sule O, Karas J.** 2014. Micafungin for the treatment of invasive aspergillosis. Journal of Infection **68:**507-526.
9. **Herbrecht R, Maertens J, Baila L, Aoun M, Heinz W, Martino R, Schwartz S, Ullmann A, Meert L, Paesmans M, Marchetti O, Akan H, Ameye L, Shivaprakash M, Viscoli C.** 2010. Caspofungin first-line therapy for invasive aspergillosis in allogeneic hematopoietic stem cell transplant patients: an European Organisation for Research and Treatment of Cancer study. Bone Marrow Transplant **45:**1227-1233.
10. **Dolton M, McLachlan A.** 2014. Voriconazole pharmacokinetics and exposure-response relationships: assessing the links between exposure, efficacy and toxicity. Int J Antimicrob Agents **44:**183-193.
11. **Vermeulen E, Lagrou K, Verweij P.** 2013. Azole Resistance in *Aspergillus fumigatus*: a growing health concern. Curr Opin Infect Dis **26:**493-500.

12. **Latge J, Kobayashi, H,, Debeaupuis J, Diaquin M, Sarfati J, Wieruszeski J, Parra E, Bouchara J, Fournet B.** 1994. Chemical and Immunological Characterization of the Extracellular Galactomannan of *Aspergillus fumigatus*. Infection and Immunity **62:**5424-5433.
13. **Stynen D, Sarfati J, Goris A, Prevost MC, Lesourd M, Kamphuis H, Darras V, Latge JP.** 1992. Rat monoclonal antibodies against Aspergillus galactomannan. Infect Immun **60:**2237-2245.
14. **Jeans AR, Howard SJ, Al-Nakeeb Z, Goodwin J, Gregson L, Majithiya JB, Lass-Florl C, Cuenca-Estrella M, Arendrup MC, Warn PA, Hope WW.** 2012. Pharmacodynamics of voriconazole in a dynamic in vitro model of invasive pulmonary aspergillosis: implications for in vitro susceptibility breakpoints. J Infect Dis **206:**442-452.
15. **Petraitis V, Petraitiene R, Moradi P, Strauss G, Katragkou A, Kovanda L, Hope W, Walsh T.** 2016. Pharmacokinetics and Concentration-Dependent Efficacy of Isavuconazole for Treatment of Experimental Invasive Pulmonary Aspergillosis. Antimicrob Agents Chemother **60:**2718-2726.
16. **Al-Saigh R, Elefanti A, Velegraki A, Zerva L, Meletiadis J.** 2012. In vitro pharmacokinetic/pharmacodynamic modeling of voriconazole activity against Aspergillus species in a new in vitro dynamic model. Antimicrob Agents Chemother **56:**5321-5327.
17. **Pfeiffer C, Fine J, Safdar S.** 2006. Diagnosis of Invasive Aspergillosis Using a Galactomannan Assay: A Meta-Analysis. Clin Infect Dis **42:**1417-1427.
18. **Nouer SA, Nucci M, Kumar NS, Grazziutti M, Barlogie B, Anaissie E.** 2011. Earlier response assessment in invasive aspergillosis based on the kinetics of serum Aspergillus galactomannan: proposal for a new definition. Clin Infect Dis **53:**671-676.
19. **Woods G, Miceli M, Grazziutti M, Zhao W, Barlogie B, Anaissie E.** 2007. Serum *Aspergillus* Galactomannan Antigen Values Strongly Correlate With Outcome of Invasive Aspergillosis: A Study of 56 Patients With Hematologic Cancer. Cancer **110:**830-834.
20. **Miceli M, Grazziutti M, Woods G, Zhao W, Kocoglu M, Barlogie B, Anaissie A.** 2008. Strong Correlation between Serum *Aspergillus* Galactomannan Index and Outcome of Aspergillosis in Patients with Hematological Cancer: Clinical and Research Implications. Clinical Infectious Diseases **46:**1412-1422.
21. **Maertens J, Buve K, Theunissen K, Meersseman W, Verbeken E, Verhoef G, Van Eldere J, Lagrou K.** 2009. Galactomannan serves as a surrogate endpoint for outcome of pulmonary invasive aspergillosis in neutropenic hematology patients. Cancer **115:**355-362.
22. **Mikulska M, Furfaro E, Del B V, Gualandi F, Raiola A, Molinari M, Gritti P, Sanguinetti M, Posteraro B, Bacigalupo A, Viscoli C.** 2012. Galactomannan testing might be useful for early diagnosis of fusariosis. Microbiol Infect Dis **72:**367–369.
23. **Tortorano A, Esposto M, Prigitano A, Grancini A, Ossi C, Cavanna C, Cascio G.** 2012. Cross-reactivity of *Fusarium* spp. in the *Aspergillus* Galactomannan enzyme-linked immunosorbent assay. J Clin Microbiol **50:**1051–1053.

24. **Kauffmann-Lacroix C, Rodier M, Jacquemin J.** 2001. Detection of Galactomannan for Diagnosis of Fungal Rhinosinusitis. J Clin Microbiol **39:**4593–4594.
25. **Swanink C, Meis J, Rijs A, Donnelly J, Verweij P.** 1997. Specificity of a sandwich enzyme-linked immunosorbent assay for detecting *Aspergillus* galactomannan. J Clin Microbiol **35:**257-260.
26. **Huang Y, Hung C, Hsueh P.** Aspergillus galactomannan antigenemia in penicilliosis marneffei. AIDS **21:**1990–1991.
27. **Hope WW, Petraitis V, Petraitiene R, Aghamolla T, Bacher J, Walsh TJ.** 2010. The initial 96 hours of invasive pulmonary aspergillosis: histopathology, comparative kinetics of galactomannan and (1->3) beta-d-glucan and consequences of delayed antifungal therapy. Antimicrob Agents Chemother **54:**4879-4886.
28. **Bennett J, Friedman M, Dupont B.** 1987. Receptor-mediated clearance of *Aspergillus* galactomannan. J Infect Dis **155:**1005-1010.
29. **Duettmann W, Koidl C, Troppan K, Seeber K, Buzina W, Wolfler A, Wagner J, Krause R, Hoenigl M.** 2014. Serum and urine galactomannan testing for screening in patients with hematological malignancies. Medical Mycology **52:**647-652.
30. **Clemons K, Stevens D.** 2009. Conventional or Molecular Measurement of *Aspergillus* Load. Medical Mycology **47:**S132-S137.
31. **Thornton C.** 2008. Development of an Immunochromatographic Lateral-Flow Device for Rapid Serodiagnosis of Invasive Aspergillosis. Clinical and Vaccine Immunology **15:**1095-1105.
32. **de Heer K, van der Schee M, Zwinderman K, van den Berk I, Visser C, van Oers R, Sterk P.** 2013. Electronic Nose Technology for Detection of Invasive Pulmonary Aspergillosis in Prolonged Chemotherapy-Induced Neutropenia: a Proof-of-Principle Study. J Clin Microbiol **51:**1490-1495.
33. **Bretagne S, Marmorat-Khuong A, Kuentz M, Latge J, Bart-Delabesse E, Cordonnier C.** 1997. Serum *Aspergillus* Galactomannan Antigen Testing by Sandwich ELISA: Practical Use in Neutropenic Patients. Journal of Infection **35:**7-15.
34. **Machetti M, Zotti M, Veroni L, Mordini N, Van Lint M, Bacigalupo A, Paola D, Viscoli C.** 2000. Antigen detection in the diagnosis and management of a patient with probable cerebral aspergillosis treated with voriconazole. Transpl Infect Dis **2:**140-144.
35. **Mokaddas E, Burhamah M, Ahmad S, Khan Z.** 2010. Invasive pulmonary aspergillosis due to *Aspergillus terreus:* value of DNA, galactomannan and (1-3)-beta-D-glucan detection in serum samples as an adjunct to diagnosis. Journal of Medical Microbiology **59:**1519-1523.
36. **Weng TF, Wu KH, Wu HP, Peng CT, Chao YH.** 2016. Changes of serum aspergillus galactomannan during hematopoietic stem cell transplantation in children with prior invasive aspergillosis. Ital J Pediatr **42:**30.
37. **Koo S, Bryar J, Baden L, Marty F.** 2010. Prognostic Features of Galactomannan Antigenemia in Galactomannan-Positive Invasive Aspergillosis. J Clin Microbiol **48:**1255-1260.

38. **Boutboul F, Alberti C, Leblanc T, Sulahian A, Gluckman E, Derouin F, Ribaud P.** 2002. Invasive Aspergillosis in Allogeneic Stem Cell Transplant Recipients: Increasing Antigenemia Is Associated with Progressive Disease. Clinical Infectious Diseases **34:**939-943.
39. **Chai LY, Kullberg BJ, Earnest A, Johnson EM, Teerenstra S, Vonk AG, Schlamm HT, Herbrecht R, Netea MG, Troke PF.** 2014. Voriconazole or amphotericin B as primary therapy yields distinct early serum galactomannan trends related to outcomes in invasive aspergillosis. PLoS One **9:**e90176.
40. **Neofytos D, Railkar R, Mullane KM, Fredricks DN, Granwehr B, Marr KA, Almyroudis NG, Kontoyiannis DP, Maertens J, Fox R, Douglas C, Iannone R, Kauh E, Shire N.** 2015. Correlation between Circulating Fungal Biomarkers and Clinical Outcome in Invasive Aspergillosis. PLoS One **10:**e0129022.
41. **Petraitiene R, Petraitis V, Bacher JD, Finkelman MA, Walsh TJ.** 2015. Effects of host response and antifungal therapy on serum and BAL levels of galactomannan and (1-->3)-beta-D-glucan in experimental invasive pulmonary aspergillosis. Med Mycol **53:**558-568.
42. **Huureman L, Neely M, Veringa A, Perez F, Ramos-Martin V, Tissing W, Alffenaar J, Hope W.** 2016. Pharmacodynamics of Voriconazole in Children: Further Steps along the Path to True Individualized Therapy. Antimicrob Agents Chemother **60:**2336-2342.
43. **Astellas Pharma US I.** 2015. CRESEMBA™ (isavuconazonium sulfate) prescribing information. In: US FDA. http://www.astellas.us/docs/cresemba.pdf. Accessed
44. **Kovanda L, Desai A, Lu Q, Townsend R, Akhtar S, Bonate P, Hope W.** 2016. Isavuconazole Population Pharmacokinetic Analysis Using Non-Parametric Estimation in Patients with Invasive Fungal Disease: Results from the VITAL Study. Antimicrobial Agents and Chemotherapy doi:10.1128/AAC.00514-16.
45. **Schmitt-Hoffmann A, Roos B, Maares J, Heep M, Spickerman J, Weidekamm E, Brown T, Roehrle M.** 2006. Multiple-dose pharmacokinetics and safety of the new antifungal triazole BAL4815 after intravenous infusion and oral administration of its prodrug, BAL8557, in healthy volunteers. Antimicrob Agents Chemother **50:**286-293.
46. **Desai A, AH S-H, Mujais S, Townsend R.** 2016. Population Pharmacokinetics of Isavuconazole in Subjects with Mild and Moderate Hepatic Impairment. Antimicrob Agents Chemother **60:**3025-3031.
47. **Desai A, Kovanda L, Kowalski D, Lu Q, Townsend R, Bonate P.** 2016. Population Pharmacokinetics of Isavuconazole from Phase 1 and Phase 3 (SECURE) Trial in Adults and Target Attainment in Patients with Invasive Aspergillosis and Other Filamentous Fungi. Antimicrob Agents Chemother **60:**5483-5491.
48. **Maertens J, Raad I, Marr K, Patterson T, Kontoyiannis D, Cornely O, Bow E, Rahav G, Neofytos D, Aoun M, Baddley J, Giladi M, Heinz W, Herbrecht R, Hope W, Karthaus M, Lee D, Lortholary O, Morrison V, Oren I, Selleslag D, Shoham S, Thompson III G, Lee M, Maher R, Hortense Schmitt-Hoffmann A, Zeiher B, Ullmann A.** 2016. Isavuconazole versus voriconazole for primary treatment of invasive mould disease caused by *Aspergillus* and other

filamentous fungi (SECURE): a phase 3, randomised-controlled, non-inferiority trial. The Lancet **387:**760-769.

49. **Marty F, Ostrosky-Zeichner L, Cornely O, Mullane K, Perfect J, Thompson Gr, Alangaden G, Brown J, Fredricks D, Heinz W, Herbrecht R, Klimko N, Klyasova G, Maertens J, Melinkeri S, Oren I, Pappas P, Ráčil Z, Rahav G, Santos R, Schwartz S, Vehreschild J, Young J, Chetchotisakd P, Jaruratanasirikul S, Kanj S, Engelhardt M, Kaufhold A, Ito M, Lee M, Sasse C, Maher R, Zeiher B, Vehreschild M, Investigators VaFM.** 2016. Isavuconazole treatment for mucormycosis: a single-arm open-label trial and case-control analysis. Lancet Infect Dis doi:10.1016/S1473-3099(16)00071-2**:**pii: S1473-3099(1416)00071-00072.
50. **Thompson GR, 3rd, Wiederhold NP.** 2010. Isavuconazole: a comprehensive review of spectrum of activity of a new triazole. Mycopathologia **170:**291-313.
51. **Lepak AJ, Marchillo K, Vanhecker J, Andes DR.** 2013. Isavuconazole (BAL4815) pharmacodynamic target determination in an in vivo murine model of invasive pulmonary aspergillosis against wild-type and cyp51 mutant isolates of Aspergillus fumigatus. Antimicrob Agents Chemother **57:**6284-6289.
52. **Warn PA, Sharp A, Parmar A, Majithiya J, Denning DW, Hope WW.** 2009. Pharmacokinetics and pharmacodynamics of a novel triazole, isavuconazole: mathematical modeling, importance of tissue concentrations, and impact of immune status on antifungal effect. Antimicrob Agents Chemother **53:**3453-3461.
53. **Luo G, Gebremariam T, Lee. H, Edwards J, JE,, Kovanda L, Ibrahim A.** 2014. Isavuconazole Therapy Protects Immunosuppressed Mice from Mucormycosis. Antimicrob Agents Chemother **58:**2450-2453.
54. **Wiederhold N, Kovanda L, Najvar L, Bocanegra R, Olivo M, Kirkpatrick W, Patterson T.** 2016. Isavuconazole Is Effective for the Treatment of Experimental Cryptococcal Meningitis. Antimicrob Agents Chemother **60:**5600-5603.
55. **Mullane K, Aoun M, Franks B, Azie N, Mujais S, Kaufhold A, Maertens J.** 2015. Safety and outcomes in invasive aspergillosis patients with renal vs. no renal impairment treated with isavuconazole: experience from the SECURE (randomised) and VITAL Trials, abstr 25th European Congress of Clinical Microbiology and Infectious Diseases, Copenhagen, Denmark, April 25-28, 2015.
56. **Perfect J, Cornely O, Ostrosky-Zeichner L.** 2015. Outcomes, safety, and tolerability of isavuconazole for the treatment of invasive fungal disease (phase 3 VITAL trial), abstr 19th Congress of the International Society for Human and Animal Mycology, Melbourne, Australia, May 4-8, 2015.
57. **Thompson Gr, Rendon A, Ribeiro Dos Santos R, Queiroz-Telles F, Ostrosky-Zeichner L, Azie N, Maher R, Lee M, Kovanda L, Engelhardt M, Vazquez J, Cornely O, Perfect J.** 2016. Isavuconazole Treatment of Cryptococcosis and Dimorphic Mycoses. Clinical Infectious Diseases **63:**356-362.
58. **Rahav G, Oren I, Mullane K, Maher R, Lee M, Zeihner B, Schmitt-Hoffmann AH, Giladi M.** 2015. An open-label phase 3 study of isavuconazole (VITAL): focus on patients with mixed fungal infections, abstr 25th Annual European Conference on Clinical Microbiology and Infectious Diseases, Copenhagen, Denmark, April 25-28, 2015.

59. **Cornely OA, Ostrosky-Zeichner L., Rahav G.** 2014. Outcomes in patients with invasive mold disease caused by *Fusarium* or *Scedosporium* spp. treated with isavuconazole: experience from the VITAL and SECURE trials, abstr 54th Interscience Conference on Antimicrobial Agents and Chemotherapy, Washington, DC, USA, September 5-9, 2014.
60. **Manzoni P, Mostert M, Castagnola E.** 2015. Update on the management of Candida infections in preterm neonates. Arch Dis Child Fetal Neonatal Ed **100:**F454-459.
61. **Arsenault A, Bliss J.** 2015 Neonatal Candidiasis: New Insights into an Old Problem at a Unique Host-Pathogen Interface. Curr Fung Infect Rep **9:**246-252.
62. **Smith P, Steinbach W, Benjamin D, Jr.** 2005. Neonatal Candidiasis. Infect Dis Clin North Am **19:**603-615.
63. **Benjamin D, DeLong E, Cotten C, Garges H, Steinbach W, Clark R.** 2004. Mortality following blood culture in premature infants: increased with Gram-negative bacteremia and candidemia, but not Gram-positive bacteremia. J Perinatol **24:**175-180.
64. **Watt K, Cohen-Wolkowiez M, Ward R, Benjamin D.** 2012. Pediatric antifungal drug development: lessons learned and recommendations for the future. Pediatric Infectious Disease Journal **31:**635-637.
65. **Stoll B, Hansen N, Adams-Chapman I, Fanaroff A, Hintz S, Vohr B.** 2004. Neurodevelopmental and Growth Impairment Among Extremely Low-Birth-Weight Infants With Neonatal Infection. JAMA **292:**2357-2365.
66. **Benjamin D, Jr, , Stoll B, Fanaroff A, McDonald S, Oh W, Higgins R, Duara S, Poole K, Laptook A, Goldberg R, Network NIoCHaHDNR.** 2006. Neonatal candidiasis among extremely low birth weight infants: risk factors, mortality rates, and neurodevelopmental outcomes at 18 to 22 months. Pediatrics **117:**84-92.
67. **Pappas P, Kauffman C, Andes D, Clancy C, Marr K, Ostrosky-Zeichner L, Reboli A, Schuster M, Vazquez J, Walsh T, Zaoutis T, Sobel J.** 2016. Clinical Practice Guideline for the Management of Candidiasis: 2016 Update by the Infectious Diseases Society of America. Clin Infect Dis doi:10.1093/cid/civ933.
68. **Cornely O, Pappas P, Young J, Maddison P, Ullmann A.** 2011. Accumulated safety data of micafungin in therapy and prophylaxis in fungal diseases. Expert Opin Drug Saf **10:**171-183.
69. **Arrieta A, Maddison P, Groll A.** 2011. Safety of micafungin in pediatric clinical trials. Pediatr Infect Dis J **30:**e97-e102.
70. **Hope W, Mickiene D, Petraitis V, Petraitiene R, Kelaher A, Hughes J, Cotton M, Bacher J, Keirns J, Buell D, Heresi G, Benjamin D, Jr, , Groll A, Drusano G, Walsh T.** 2008. The pharmacokinetics and pharmacodynamics of micafungin in experimental hematogenous *Candida* meningoencephalitis: implications for echinocandin therapy in neonates. J Infect Dis **197:**163-171.
71. **Hope W, Smith P, Arrieta A, Buell D, Roy M, Kaibara A, Walsh T, Cohen-Wolkowiez M, Benjamin DJ.** 2010. Population pharmacokinetics of micafungin in neonates and young infants. Antimicrob Agents Chemother **54:**2633-2637.
72. **Benjamin D, Jr, , Smith P, Arrieta A, Castro L, Sánchez P, Kaufman D, Arnold L, Kovanda L, Sawamoto T, Buell D, Hope W, Walsh T.** 2010. Safety

and pharmacokinetics of repeat-dose micafungin in young infants. Clin Pharmacol Ther **87:**93-99.

73. **Nakamura I, Kanasaki R, Yoshikawa K, Furukawa S, Fujie A, Hamamoto H, Sekimizu K.** 2017. Discovery of a new antifungal agent ASP2397 using a silkworm model of *Aspergillus fumigatu*s infection. The Journal of Antibiotics **70:**41-44.
74. **Nakamura I, Yoshimura S, Masaki T, Takase S, Ohsumi K, Hashimoto M, Furukawa S, Fujie A.** 2017. ASP2397: a novel antifungal agent produced by *Acremonium persicinum* MF-347833. The Journal of Antibiotics **70:**45-51.
75. **Nakamura I, Ohsumi K, Yoshikawa K, Kanasaki R, Masaki T, Takase S, Hashimoto M, Fujie A, Nakai T, Matsumoto S, Takeda S, Akamatsu S, Uchida S, Maki K.** ASP2397: A Novel Natural Product with Potent Fungicidal Activity against *Aspergillus* spp. A New Mode of Action and *In Vitro* Activity, p. *In* (ed),
76. **Nakamura I, Nakai T, Matsumoto S, Takeda S, Akamatsu S, Uchida S, Koide Y, Mitori H, Noto T, Maki K.** ASP2397: A Novel Natural Product with Potent Fungicidal Activity against *Aspergillus* spp. (2)- *In Vivo* Activity against *A. fumigatus*, p. *In* (ed),
77. **Neely MN, van Guilder MG, Yamada WM, Schumitzky A, Jelliffe RW.** 2012. Accurate detection of outliers and subpopulations with Pmetrics, a nonparametric and parametric pharmacometric modeling and simulation package for R. Ther Drug Monit **34:**467-476.
78. **Astellas Pharma US Inc.** 2015. CRESEMBA® (isavuconazonium sulfate) prescribing information. http://www.astellas.us/docs/cresemba.pdf. Accessed
79. **Rex JH, Eisenstein BI, Alder J, Goldberger M, Meyer R, Dane A, Friedland I, Knirsch C, Sanhai WR, Tomayko J, Lancaster C, Jackson J.** 2013. A comprehensive regulatory framework to address the unmet need for new antibacterial treatments. Lancet Infect Dis **13:**269–275.
80. **Petraitis V, Petraitiene R, Sarafandi AA, Kelaher AM, Lyman CA, Casler HE, Sein T, Groll AH, Bacher J, Avila NA, Walsh TJ.** 2003. Combination therapy in treatment of experimental pulmonary aspergillosis: synergistic interaction between an antifungal triazole and an echinocandin. J Infect Dis **187:**1834–1843.
81. **CLSI.** 2008. Reference method for broth dilution antifungal susceptibility testing of filamentous fungi; Approved Standard. M38-A2; Second Edition. Wayne, PA, USA: Clinical and Laboratory Standards Institute; 2008.
82. **Espinel-Ingroff A, Chowdhary A, Gonzalez GM, Lass-Florl C, Martin-Mazuelos E, Meis J, Pelaez T, Pfaller MA, Turnidge J.** 2013. Multicenter study of isavuconazole MIC distributions and epidemiological cutoff values for Aspergillus spp. for the CLSI M38-A2 broth microdilution method. Antimicrob Agents Chemother **57:**3823-3828.
83. **Seyedmousavi S, Bruggemann RJ, Meis JF, Melchers WJ, Verweij PE, Mouton JW.** 2015. Pharmacodynamics of isavuconazole in an Aspergillus fumigatus mouse infection model. Antimicrob Agents Chemother **59:**2855-2866.
84. **Box H, Livermore J, Johnson A, McEntee L, Felton TW, Whalley S, Goodwin J, Hope WW.** 2015. Pharmacodynamics of Isavuconazole in a

Dynamic In Vitro Model of Invasive Pulmonary Aspergillosis. Antimicrob Agents Chemother **60:**278-287.

85. **Marr K, Balajee S, McLaughlin L, Tabouret M, Bentsen C, Walsh T.** 2004. Detection of galactomannan antigenemia by enzyme immunoassay for the diagnosis of invasive aspergillosis: variables that affect performance. J Infect Dis **190:**641–649.
86. **Guigue N, Lardeux S, Alanio A, Hamane S, Tabouret M, Bretagne S.** 2015. Importance of Operational Factors in the Reproducibility of *Aspergillus* Galactomannan Enzyme Immune Assay. PLoS One **10:**1-10.
87. **Schmiedel Y, Zimmerli S.** 2016. Common invasive fungal diseases: an overview of invasive candidiasis, aspergillosis, cryptococcosis, and Pneumocystis pneumonia. Swiss Medical Weekly **146**.
88. **Patterson T, Thompson Gr, Denning D, Fishman J, Hadley S, Herbrecht R, Kontoyiannis D, Marr K, Morrison V, Nguyen M, Segal B, Steinbach W, Stevens D, Walsh T, Wingard J, Young J, Bennett J.** 2016. Practice Guidelines for the Diagnosis and Management of Aspergillosis: 2016 Update by the Infectious Diseases Society of America. Clinical Infectious Diseases **63:**e1-e60.
89. **Leroux S, Ullmann A.** 2013. Management and diagnostic guidelines for fungal diseases in infectious diseases and clinical microbiology: critical appraisal. Clin Microbiol Infect **19:**1115-1121.
90. **Al-Nakeeb Z, Petraitis V, Goodwin J, Petraitiene R, Walsh TJ, Hope WW.** 2015. Pharmacodynamics of amphotericin B deoxycholate, amphotericin B lipid complex, and liposomal amphotericin B against Aspergillus fumigatus. Antimicrob Agents Chemother **59:**2735-2745.
91. **Henderson R, Diggle P, Dobson A.** 2000. Joint modelling of longitudinal measurements and event time data. Biostatistics **1:**465-480.
92. **Ibrahim J, Chu H, Chen L.** 2010. Basic concepts and methods for joint models of longitudinal and survival data. Journal of Clinical Oncology **28:**2796-2801.
93. **Asar Ö, Ritchie J, Kalra P, Diggle P.** 2015. Joint modelling of repeated measurement and time-to-event data:an introductory tutorial. International Journal of Epidemiology **44:**334-344.
94. **Desai A, Kovanda L, Hope W, Mouton J, Andes D, Kowalski D, Townsend R, Bonate P.** 2015. Exposure–Response Analysis of Isavuconazole in Patients with Disease Caused by Aspergillus Species or Other Filamentous Fungi, abstr ECCMID, Copenhagen, Denmark, April, 2015.
95. **Chai LY, Kullberg BJ, Johnson EM, Teerenstra S, Khin LW, Vonk AG, Maertens J, Lortholary O, Donnelly PJ, Schlamm HT, Troke PF, Netea MG, Herbrecht R.** 2012. Early serum galactomannan trend as a predictor of outcome of invasive aspergillosis. J Clin Microbiol **50:**2330-2336.
96. **Desai A, Kovanda L, Kowalski D, Townsend R, Mujais S, Bonate P.** 2015. Exposure-Safety Analysis of Isavuconazole in Patients from SECURE Study with Disease Caused by *Aspergillus* Species or Other Filamentous Fungi, abstr 55th Annual Interscience Conference on Antimicrobial Agents and Chemotherapy, San Diego, CA, USA,

97. **Luo G, Gebremariam T, Lee H, Edwards JE, Jr., Kovanda L, Ibrahim AS.** 2014. Isavuconazole therapy protects immunosuppressed mice from mucormycosis. Antimicrob Agents Chemother **58:**2450–2453.
98. **Vehreschild M, Vehreschild JJ, Marty FM.** 2014. Primary treatment of invasive mucormycosis (IM) with isavuconazole (VITAL study) or amphotericin formulations (FungiScope™): case-matched analysis, abstr 56th American Society of Hematology Annual Meeting and Exposition, San Francisco, CA, USA, December 6-9, 2014.
99. **Desai A, Kovanda L, Kowalski D, Lu Q, Townsend R.** 2014. Isavuconazole (ISA) population pharmacokinetic modeling from phase 1 and phase 3 clinical trials and target attainment analysis, abstr 54th Interscience Conference on Antimicrobial Agents and Chemotherapy, Washington, DC, USA, September 5-9, 2014.
100. **Seyedmousavi S, Bruggemann RJ, Meis JF, Melchers WJ, Verweij PE, Mouton JW.** 2015. Pharmacodynamics of isavuconazole in an Aspergillus fumigatus mouse infection model. Antimicrobial Agents and Chemotherapy **59:**2855-2866.
101. **Lepak AJ, Marchillo K, VanHecker J, Diekema D, Andes DR.** 2013. Isavuconazole pharmacodynamic target determination for Candida species in an in vivo murine disseminated candidiasis model. Antimicrob Agents Chemother **57:**5642-5648.
102. **Warn PA, Sharp A, Denning DW.** 2006. In vitro activity of a new triazole BAL4815, the active component of BAL8557 (the water-soluble prodrug), against Aspergillus spp. J Antimicrob Chemother **57:**135-138.
103. **Ghannoum M, Isham N.** 2005. Antifungal activity of BAL4815, a novel azole against dermatophytes and emerging non-dermatophyte fungi including Zygomycetes, abstr 45th Interscience Conference on Antimicrobial Agents and Chemotherapy, Washington, DC, USA, December 16-19, 2005.
104. **Warn P, Denning D, Heep M, Isham N, Ghannoum M.** 2005. *In vitro* activity of a new triazole BAL4815 against *Candida* isolates with decreased fluconazole susceptibility, abstr 45th Interscience Conference on Antimicrobial Agents and Chemotherapy, Washington, DC, USA, December 16-19, 2005.
105. **Mouton J, Verweij P, Warn P, Denning D, Heep M, Isham N, Ghannoum M.** 2005. *In vitro* activity of a new triazole BAL4815 against *Candida* isolates with decreased fluconazole susceptibility, abstr 2nd Trends in Medical Mycology, Berlin, Germany, October 23-26, 2005.
106. **Seifert H, Aurbach U, Stefanik D, Cornely O.** 2007. In vitro activities of isavuconazole and other antifungal agents against Candida bloodstream isolates. Antimicrob Agents Chemother **51:**1818-1821.
107. **Wheat L, Connolly P, Smedema M, Durkin M, Goldman M.** 2006. *In vitro* activity of a new triazole, BAL8557, against *Histoplasma* capsulatum isolates from patients who failed fluconazole therapy, abstr 16th Congress of the International Society for Human and Animal Mycology, Paris, France, June 25-29, 2006.
108. **Martin de la Escalera C, Aller A, López-Oviedo E, Martos A, Romero A, Castro C, Cantón E, Martín-Mazuelos E.** 2006. *In vitro* activity of BAL4815 (a

new azole) against filamentous fungi, abstr 16th Congress of the International Society for Human and Animal Mycology, Paris, France, June 25-29, 2006.
109. **Heep M, Grover P, Brown N, Sahm D, Jones M.** 2007. Evaluation of isavuconazole (BAL8557/BAL4815) Etest compared to broth microdilution antifungal susceptibility testing against quality control strains and fluconazole susceptible clinical *Candida* isolates abstr 17th European Congress of Clinical Microbiology and Infectious Diseases, Munich, Germany, March 31-April 4, 2007.
110. **Curfs-Breuker I, Mouton J, Debets-Ossenkopp Y, Endtz H, Verweij P, Meis J.** 2007. In vitro activity of isavuconazole (BAL4815) compared with seven other antifungal agents against 309 prospectively collected clinical *Candida* isolates from The Netherlands, abstr 17th European Congress of Clinical Microbiology and Infectious Diseases, Munich, Germany, March 31-April 4, 2007.
111. **Guinea J, Peláez T, Recio S, Torres-Narbona M, Bouza E.** 2008. In vitro antifungal activities of isavuconazole (BAL4815), voriconazole, and fluconazole against 1,007 isolates of zygomycete, *Candida*, *Aspergillus*, *Fusarium*, and *Scedosporium* species. Antimicrob Agents Chemother **52:**1396–1400.
112. **Viljoen J, Mitha I, Heep M, Ghannoum M.** 2005. Efficacy, safety, and tolerability of three different dosing regimens of BAL8557 vs. fluconazole in a double-blind, randomized, multicenter trial for the treatment of esophageal candidiasis (EC) in immunocompromised adults, abstr 45th Interscience Conference on Antimicrobial Agents and Chemotherapy, Washington, DC, USA, December 16-19, 2005.
113. **Ostrosky-Zeichner L, Inurria N, Rodreguez J, Chen E, Paetznick V.** 2009. Comparative *in vitro* activity of isavuconazole (ISA) against medically important yeasts and moulds abstr 49th Interscience Conference on Antimicrobial Agents and Chemotherapy, San Francisco, CA, USA, September 12-15, 2009.
114. **Howard S, Lass-Florl C, Cuenca-Estrella M, Gomez-Lopez A, Arendrup M.** 2013. Determination of isavuconazole susceptibility of *Aspergillus* and *Candida* species by the EUCAST method. Antimicrob Agents Chemother **57:**5426-5431.
115. **Testing ECoAST-SoAS.** 2012. Posaconazole and *Aspergillus* spp.: Rationale for the clinical breakpoints, version 1.0. http://www.eucast.org.
116. **Testing ECoAST-SoAS.** 2012. Voriconazole and *Aspergillus* spp.: Rationale for the clinical breakpoints, version 1.0, http://www.eucast.org.
117. **Kullberg B-J, GR T, Pappas P, Vasques J, Viscoli C, L. O-Z, Rotstein C, Sobel J, Herbrecht R, G R, Van Wijngaerden E, De Waele J, Jaruratanasirikul S, Chetchotisakd P, Kovanda L, Lademacher C, Lee M, Engelhardt M.** Isavuconazole versus caspofungin in the treatment of Candidaemia and other invasive *Candida* infections: the ACTIVE trial, abstr 26th European Congress of Clinical Microbiology and Infectious Diseases (ECCMID), Amsterdam, Netherlands, 9-12 April 2016
118. **Blijlevens N, Donnelly J, de Pauw B.** 2001. Empirical therapy of febrile neutropenic patients with mucositis: challenge of risk-based therapy. Clin Microbiol Infect **7:**47-52.

119. **Lipp H.** 2010. Clinical pharmacodynamics and pharmacokinetics of the antifungal extended-spectrum triazole posaconazole: an overview. Br J Clin Pharmacol **70:**471–480.
120. **EMA.** 2015. European Medicines Agency Cresemba (isavuconazonium sulfate) Product Information. http://www.ema.europa.eu/ema/index.jsp?curl=pages/medicines/human/medicines/002734/human_med_001907.jsp&mid=WC0b01ac058001d124. Accessed
121. **Schmitt-Hoffmann A, Desai A, Kowalski D, Pearlman H, Yamazaki T, Townsend R.** 2016. Isavuconazole absorption following oral administration in healthy subjects is comparable to intravenous dosing, and is not affected by food, or drugs that alter stomach pH. Int J Clin Pharmacol Ther **54:**572-580.
122. **Pfizer I.** 2014. DIFLUCAN® (Fluconazole Tablets) (Fluconazole for Oral Suspension). In: US FDA. http://labeling.pfizer.com/ShowLabeling.aspx?id=575. Accessed
123. **Krishna G, Moton A, Ma L, Medlock M, McLeod J.** 2009. Pharmacokinetics and Absorption of Posaconazole Oral Suspension under Various Gastric Conditions in Healthy Volunteers. Antimicrobial Agents and Chemotherapy **53:**958-966.
124. **Merck C, Inc.** 2016. NOXAFIL™ (posaconazole) prescribing information. In: US FDA. https://www.merck.com/product/usa/pi_circulars/n/noxafil/noxafil_pi.pdf. Accessed
125. **Janssen Pharmaceutical I.** 2014. Sporanox™ (itraconazole capsules) prescribing information. In: US FDA. http://www.janssen.com/us/sites/www_janssen_com_usa/files/products-documents/pi-sporanoxcapsules.pdf. Accessed
126. **Kraft W, Chang P, van Iersel M, Waskin H, Krishna G, Kersemaekersb W.** 2014. Posaconazole Tablet Pharmacokinetics: Lack of Effect of Concomitant Medications Altering Gastric pH and Gastric Motility in Healthy Subjects. Antimicrobial Agents and Chemotherapy **58:**4020-4025.
127. **Lewis R.** 2011. Pharmacokinetic-pharmacodynamic optimization of triazole antifungal therapy. Current Opinion in Infectious Diseases **24:**S14-S29.
128. **Krishna G, AbuTarif M, Xuan F, Martinho M, Angulo D, Cornely O.** 2008. Pharmacokinetics of Oral Posaconazole in Neutropenic Patients Receiving Chemotherapy for Acute Myelogenous Leukemia or Myelodysplastic Syndrome. Pharmacotherapy: The Journal of Human Pharmacology and Drug Therapy **28:**1223-1232.
129. **Ezzet F, Wexler D, Courtney R, Krishna G, Lim J, Laughlin M.** 2005. Oral Bioavailability of Posaconazole in Fasted Healthy Subjects: Comparison Between Three Regimens and Basis for Clinical Dosage Recommendations. Clinical Pharmacokinetics **44:**211-220.
130. **Krishna G, Ma L, Martinho M, O'Mara E.** 2012. Single-dose phase I study to evaluate the pharmacokinetics of posaconazole in new tablet and capsule formulations relative to oral suspension. Antimicrob Agents Chemother **56:**4196-4201.

131. **Wood N, Tan K, Purkins L, Layton G, Hamlin J, Kleinermans D, Nichols D.** 2003. Effect of omeprazole on the steady-state pharmacokinetics of voriconazole. Br J Clin Pharmacol **56:**56-61.
132. **Purkins L, Wood N, Kleinermans D, Nichols D.** 2003. Histamine H2-receptor antagonists have no clinically significant effect on the steady-state pharmacokinetics of voriconazole. Br J Clin Pharmacol **56:**51–55.
133. **Han K, Capitano B, Bies R, Potoski B, Husain S, Gilbert S, Paterson D, McCurry K, Venkataramanan R.** 2010. Bioavailability and Population Pharmacokinetics of Voriconazole in Lung Transplant Recipients. Antimicrobial Agents and Chemotherapy **54:**4424–4431.
134. **Pfizer I.** 2015. VFEND™ (voriconazole) prescribing information. In: US FDA. http://labeling.pfizer.com/ShowLabeling.aspx?id=618. Accessed
135. **Liu P, Mould DR.** 2014. Population Pharmacokinetic Analysis of Voriconazole and Anidulafungin in Adult Patients with Invasive Aspergillosis. Antimicrob Agents Chemother **58:**4718–4726.
136. **Gubbins P, Krishna G, Sansone-Parsons S, Penzak S, Dong L, Martinho M, Anaissie E.** 2006. Pharmacokinetics and Safety of Oral Posaconazole in Neutropenic Stem Cell Transplant Recipients. Antimicrobial Agents and Chemotherapy **50:**1993-1999.
137. **Park W, Cho J, Park S, Kim E, Yoon S, Yoon S, Lee J, Koh Y, Song K, Choe P, Yu K, Kim E, Bang S, Kim N, Kim I, Oh M, Kim H, Song S.** 2016. Effectiveness of increasing the frequency of posaconazole syrup administration to achieve optimal plasma concentrations in patients with haematological malignancy. International Journal of Antimicrobial Agents **48:**106-110.
138. **Sansone-Parsons A, Krishna G, Simon J, Soni P, Kantesaria B, Herron J, Stoltz R.** 2007. Effects of Age, Gender, and Race/Ethnicity on the Pharmacokinetics of Posaconazole in Healthy Volunteers. Antimicrobial Agents and Chemotherapy **51:**495-502.
139. **Vanstraelen K, Prattes J, Maertens J, Lagrou K, Schoemans H, Peersman N, Vermeersch P, Theunissen K, Mols R, Augustijns P, Annaert P, Hoenigl M, Spriet I.** 2016. Posaconazole plasma exposure correlated to intestinal mucositis in allogeneic stem cell transplant patients. European Journal of Clinical Pharmacology **72:**953-963.
140. **Ullmann A, Akova M, Herbrecht R, Viscoli C, Arendrup M, Arikan-Akdagli S, Bassetti M, Bille J, Calandra T, Castagnola E, Cornely O, Donnelly J, Garbino J, Groll A, Hope W, Jensen H, Kullberg B, Lass-Flörl C, Lortholary O, Meersseman W, Petrikkos G, Richardson M, Roilides E, Verweij P, Cuenca-Estrella M, Group EFIS.** 2012. ESCMID* guideline for the diagnosis and management of *Candida* diseases 2012: adults with haematological malignancies and after haematopoietic stem cell transplantation (HCT). Clin Microbiol Infect **18:**53-67.
141. **Cornely O, Bassetti M, Calandra T, Garbino J, Kullberg B, Lortholary O, Meersseman W, Akova M, Arendrup M, Arikan-Akdagli S, Bille J, Castagnola E, Cuenca-Estrella M, Donnelly J, Groll A, Herbrecht R, Hope W, Jensen H, Lass-Flörl C, Petrikkos G, Richardson M, Roilides E, Verweij P, Viscoli C, Ullmann A, Group EFIS.** 2012. ESCMID* guideline for the

diagnosis and management of *Candida* diseases 2012: non-neutropenic adult patients. Clin Microbiol Infect **18:**19-37.

142. **Hope W, Castagnola E, Groll A, Roilides E, Akova M, Arendrup M, Arikan-Akdagli S, Bassetti M, Bille J, Cornely O, Cuenca-Estrella M, Donnelly J, Garbino J, Herbrecht R, Jensen H, Kullberg B, Lass-Florl C, Lortholary O, Meersseman W, Petrikkos G, Richardson M, Verweij P, Viscoli C, Ullmann A, Group EFIS.** 2012. ESCMID* guideline for the diagnosis and management of Candida diseases 2012: prevention and management of invasive infections in neonates and children caused by *Candida* spp. Clinical Microbiology and Infection **18 Suppl 7:**38-52.
143. **Astellas Pharma US I.** 2016. MYCAMINE® (micafungin sodium) prescribing information. https://www.mycamine.com. Accessed
144. **Benjamin D, Jr,, Kaufman D, Hope W, Smith P, Arrieta A, Manzoni P, Kovanda L, Lademacher C, Isaacson B, Jednachowski D, Wu C, Walsh T.** 2015. Micafungin versus Conventional Amphotericin B in the Treatment of Invasive Candidiasis in Infants, abstr Interscience Conference on Antimicrobial Agents and Chemotherapy, San Diego, CA, USA,
145. **Heresi G, Gerstmann D, Reed M, van den Anker J, Blumer J, Kovanda L, Keirns J, Buell D, Kearns G.** 2006. The pharmacokinetics and safety of micafungin, a novel echinocandin, in premature infants. Pediatr Infect Dis J **25:**1110-1115.
146. **Undre N, Stevenson P, Freire A, Arrieta A.** 2012. Pharmacokinetics of micafungin in pediatric patients with invasive candidiasis and candidemia. Pediatr Infect Dis J **31:**630-632.
147. **Queiroz-Telles F, Berezin E, Leverger G, Freire A, van der Vyver A, Chotpitayasunondh T, Konja J, Diekmann-Berndt H, Koblinger S, Groll A, Arrieta A, Group MICS.** 2008. Micafungin versus liposomal amphotericin B for pediatric patients with invasive candidiasis: substudy of a randomized double-blind trial. Pediatr Infect Dis J **27:**820-826.
148. **Hope WW, Kaibara A, Roy M, Arrieta A, Azie N, Kovanda LL, Benjamin DK, Jr.** 2015. Population pharmacokinetics of micafungin and its metabolites M1 and M5 in children and adolescents. Antimicrob Agents Chemother **59:**905-913.
149. **Berenguer J, Buck M, Witebsky F, Stock F, Pizzo P, Walsh T.** 1993. Lysis-centrifugation blood cultures in the detection of tissue-proven invasive candidiasis. Disseminated versus single-organ infection. Diagnostic microbiology and infectious disease **17:**103–109.
150. **Kelly M, Benjamin D, Smith P.** 2015. The Epidemiology and Diagnosis of Invasive Candidiasis Among Premature Infants. Clin Perinatol **42:**105–117.
151. **Fanaroff A, Korones S, Wright L, Verter J, Poland R, Bauer C, Tyson J, Philips Jr, Edwards W, Lucey J, Catz C, Shankaran S, Oh W.** 1998. Incidence, presenting features, risk factors and significance of late onset septicemia in very low birth weight infants. Pediatr Infect Dis J **17:**593-598.
152. **Salvatore C, Chen T, Toussi S, DeLaMora P, Petraitiene R, Finkelman M, Walsh T.** 2016. (1→3)- β -D-glucan in cerebrospinal fluid as a biomarker for Candida and Aspergillus infections of the central nervous system in pediatric patients. J Pediatr Infect Dis Soc **5:**277-286.

153. **Salvatore C, Petraitiene R, Sitaras L, Hammad H, Leimena P, Toussi S, Finkelman M, Walsh T.** Prospective study and analytical performance of serum (1->3)-β-D-glucan in pediatric patients, p. *In* (ed),
154. **Benjamin DJ, Stoll B, Gantz M, Walsh M, Sánchez P, Das A, Shankaran S, Higgins R, Auten K, Miller N, Walsh T, Laptook A, Carlo W, Kennedy K, Finer N, Duara S, Schibler K, Chapman R, Van Meurs K, Frantz Ir, Phelps D, Poindexter B, Bell E, O'Shea T, Watterberg K, Goldberg R, NICHD N.** 2010. Neonatal candidiasis: epidemiology, risk factors, and clinical judgment. Pediatrics **126:**e865-873.
155. **Aliaga S, Clark R, Laughon M, Walsh T, Hope W, Benjamin D, Kaufman D, Arrieta A, Benjamin DJ, Smith P.** 2014. Changes in the Incidence of Candidiasis in Neonatal Intensive Care Units. Pediatrics **133:**236-242.
156. **Hope W, Drusano G, Rex J.** 2016. Pharmacodynamics for antifungal drug development: an approach for acceleration, risk minimization and demonstration of causality. J Antimicrob Chemother **71:**3008-3019.
157. **Cadena J, Thompson Gr, Patterson T.** 2016. Invasive Aspergillosis: Current Strategies for Diagnosis and Management. Infect Dis Clin North Am **30:**125-142.
158. **Nett J, Andes D.** 2016. Antifungal Agents: Spectrum of Activity, Pharmacology, and Clinical Indications. Infect Dis Clin North Am **30:**51-83.
159. **Peyton L, Gallagher S, M H.** 2015. Triazole antifungals: a review. Drugs Today (Barc) **51:**705-718.
160. **Hsiang T, Baillie D.** 2005. Comparison of the yeast proteome to other fungal genomes to find core fungal genes. J Mol Evol **60:**475-483.
161. **Cox S, Matthews P.** 2002. Exponential Time Differencing for Stiff Systems. Journal of Computational Physics **176:**430-455.
162. **Hassan I, Waheed A, Yadav S, Singh T, Ahmad F.** 2008. Zinc α2-glycoprotein: A Multidisciplinary Protein. Mol Cancer Res **6:**892-906.
163. **Gibiansky L, Gibiansky E.** 2009. Target-mediated drug disposition model: approximations, identifiability of model parameters and applications to the population pharmacokinetic–pharmacodynamic modeling of biologics. Expert Opin Drug Metab Toxicol **5:**803-812.